ČESKÉ VYSOKÉ
UČENÍ TECHNICKÉ
V PRAZE

FAKULTA
STROJNÍ

DIPLOMOVÁ PRÁCE

2020

MICHAL
CIHLÁŘ

ZADÁNÍ DIPLOMOVÉ PRÁCE

I. OSOBNÍ A STUDIJNÍ ÚDAJE

Příjmení: **Cihlář** Jméno: **Michal** Osobní číslo: **422725**

Fakulta/ústav: **Fakulta strojní**

Zadávající katedra/ústav: **Ústav energetiky**

Studijní program: **Jaderná energetická zařízení**

Studijní obor: **Jaderná energetická zařízení**

II. ÚDAJE K DIPLOMOVÉ PRÁCI

Název diplomové práce:

Technologie solných reaktorů a testování materiálů sekundárního okruhu reaktoru Energy-Well

Název diplomové práce anglicky:

The technology of Molten Salt Reactors and Energy-Well secondary loop material testing

Pokyny pro vypracování:

1) Proveďte rešerši solných reaktorů
2) Seznamte se s historií solných reaktorů
3) Seznamte se s koncepty solných reaktorů v současnosti
4) Popište jednotlivé používané soli, využívané materiály a způsoby koroze materiálů v solích
5) Připravte a proveďte korozní testy vybraných materiálů předpokládaných v sekundárním okruhu reaktoru Energy-Well v soli NaBF4
6) V závislosti na experimentálních možnostech proveďte více typů testů (různé teploty, různé doby trvání korozního experimentu)
7) Diskutujte výsledky testů
8) Vše přehledně zpracujte do diplomové práce

Seznam doporučené literatury:

T. J. Dolan: Molten Salt Reactors and Thorium Energy. 2017
P. Yvon: Structural materials for generation IV nuclear reactors.2017

Jméno a pracoviště vedoucí(ho) diplomové práce:

Ing. Jan Prehradný, Ph.D., ústav energetiky FS

Jméno a pracoviště druhé(ho) vedoucí(ho) nebo konzultanta(ky) diplomové práce:

Ing. Martin Mareček, Centrum výzkumu Řež s.r.o.

Datum zadání diplomové práce: **24.04.2020** Termín odevzdání diplomové práce: **26.06.2020**

Platnost zadání diplomové práce: **31.12.2021**

Ing. Jan Prehradný, Ph.D. podpis vedoucí(ho) práce	podpis vedoucí(ho) ústavu/katedry	prof. Ing. Michael Valášek, DrSc. podpis děkana(ky)

III. PŘEVZETÍ ZADÁNÍ

Diplomant bere na vědomí, že je povinen vypracovat diplomovou práci samostatně, bez cizí pomoci, s výjimkou poskytnutých konzultací. Seznam použité literatury, jiných pramenů a jmen konzultantů je třeba uvést v diplomové práci.

8.6.2020 Datum převzetí zadání	 Podpis studenta

Čestné prohlášení

Prohlašuji, že jsem diplomovou práci vypracoval samostatně, že jsem řádně citoval všechny použité prameny a literaturu, a že práce nebyla využita v rámci jiného vysokoškolského studia či k získání jiného nebo stejného titulu.

Nemám závažný důvod proti použití tohoto školního díla ve smyslu § 60 Zákona č. 121/2000 Sb. o právu autorském, o právech souvisejících s právem autorským a o změně některých zákonů (autorský zákon).

V Praze dne 24. 7. 2020 .....

Bc. Michal Cihlář

Autor: Bc. Michal Cihlář

Název práce: Technologie solných reaktorů a testování materiálů sekundárního okruhu reaktoru Energy-Well

Druh práce: Diplomová práce

Vedoucí práce: Ing. Jan Prehradný, Ph.D. Ústav energetiky, Fakulta strojní, České vysoké učení technické v Praze

Konzultanti: Ing. Martin Mareček, Ing. Jan Uhlíř, CSc. oddělení Jaderného palivového cyklu, Centrum výzkumu Řež s.r.o.

Bibliografické údaje: Počet stran: 69
Počet obrázků: 45
Počet tabulek: 7
Počet příloh: 7

Abstrakt: První jaderný reaktor s tekutým palivem byl navržen již ve druhé polovině čtyřicátých let dvacátého století jakožto jedna z možností rozvoje jaderné energetiky. V návaznosti byly v průběhu padesátých a šedesátých let intenzivně studovány roztavené sole a technologie solných reaktorů (MSR) v Národních laboratořích Oak Ridge ve Spojených státech. Tato technologie se v minulém století neuplatnila kvůli její náročnosti, ale na začátku nového tisíciletí byl MSR vybrán jako jeden z perspektivních konceptů reaktorů čtvrté generace. A i proto nyní probíhá výzkum a vývoj technologie MSR v řadě vědeckých institucích i soukromých společnostech po celém světě. Asi největší výzvou je životnost konstrukčních materiálů, která je značně omezována vysokou korozivitou roztavených solí. Právě korozní chování konstrukčních materiálu v prostředí tekutých solí je i hlavním tématem této práce v rámci které byly provedeny tři testy nerezových ocelí (316L, EUROFER 97) a niklových slitin (Incoloy 800HT, Inconel 600 and 625, MoNiCr, HN80MTY) v tekuté soli NaF – $NaBF_4$. Testy probíhaly po dobu 30 a 90 dní při teplotách 550 °C a 700 °C, které odpovídají pracovním teplotám solných reaktorů. Hmotnostní úbytky testovaných ocelí a slitin byly změřeny. Navíc byly provedeny analýzy chemického složení a povrchu s pomocí energeticky disperzního spektroskopu a skenovacího elektronového mikroskopu. Na jejich základě byla určena hloubka korozní vrstvy a úbytek chromu v povrchové vrstvě.

Klíčová slova: solné reaktory, roztavené soli, korozní testy, niklové slitiny, NaF-NaBF4

Author: Bc. Michal Cihlář

Title: The technology of Molten Salt Reactors and Energy-Well secondary loop material testing

Thesis type: Master's thesis

Thesis advisor: Ing. Jan Prehradný, Ph.D. Department of Energy Engineering, Faculty of Mechanical Engineering, Czech Technical University in Prague

Consultants: Ing. Martin Mareček, Ing. Jan Uhlíř, CSc. Nuclear Fuel Cycle Department, Research Centre Řež

Bibliographical notes: Number of pages: 69
Number of figures: 45
Number of tables: 7
Number of appendices: 7

Abstract: The idea of a nuclear reactor with a liquid fuel has been proposed since the 1940s as one of the ways for the nuclear energy industry. For this purpose, molten salts and Molten Salt Reactors (MSR) were researched extensively in Oak Ridge National Laboratory in the 1950s and 1960s. This challenging technology has not succeeded in the previous century; however, at the beginning of the new millennia, MSR technology has been chosen as one of Generation IV nuclear reactor designs; therefore, the research and development of MSR is nowadays ongoing all around the world. The main challenge of the MSR is the lifetime of construction material due to the high corrosiveness of molten salts. This corrosion resistance aspect is the main focus of this Master's thesis. Therefore, three tests of stainless steels (316L, EUROFER 97) and nickel alloys (Incoloy 800HT, Inconel 600 and 625, MoNiCr, HN80MTY) within NaF – $NaBF_4$ molten salt were performed. The tests were ongoing for either 30 or 90 days at the temperatures of 550 °C and 700 °C, which correspond to operating temperatures of MSR. The mass losses of specimens were determined. Moreover, chemical composition analysis and surface analysis were performed using Energy Dispersive X-ray Spectroscopy (XRF) and Scanning Electron Microscope (SEM). Based on all these measurements, the depth of the corrosion layer and chromium depletion rate were determined.

Keywords: molten salt reactors, molten salts, corrosion tests, NaF-NaBF4, nickel alloys

Acknowledgment

I wish to express my sincere appreciation to my supervisor, Ing. Jan Prehradný, Ph.D. for the opportunity, all the advice, and willingness to help at any time. Moreover, I would like to thank Ing. Martin Mareček for the help to prepare and conclude corrosion tests and Ing. Jan Uhlíř, CSc. for his advice regarding molten salts and molten salt reactors. Furthermore, I would like to acknowledge Mr. Roman Janura, Bc. Erika Tomášková, and Ms. Lenka Riezsová for the help with sample preparation, Ing. Klára Řezanková, Ph.D. and Mgr. Kristína Sihelská for the help with XRF analysis, and Ing. Alica Fedoriková, Ph.D. for the help with SEM analysis. Big thanks also belong to my family for ongoing support during the time of writing this Master's thesis and during my entire studies.

Lastly, I wish to show my gratitude to Centrum výzkumu Řež s.r.o. for providing all the experimental equipment and for financial support by TAČR projects *TH02020113 (Výzkum a vývoj technologie jaderných reaktorů chlazených fluoridovými solemi)* and *TK0230125 (Energy Well – projektové řešení demonstrační jednotky malého modulárního reaktoru chlazeného fluoridovými solemi)* and MŠMT project *Research for SUSEN, JPC (R4S).*

Bc. Michal Cihlář

Table of contents

0. The list of abbreviations

ADS	Accelerator-driven system
ANP	Aircraft Nuclear Propulsion program
AMSTER	Actinides Molten Salt TransmutER
ARE	Aircraft Reactor Experiment
ARIS	Advanced Reactors Information System
BWR	Boiling water reactor
CA	Copenhagen Atomics
CANDU	Canada Deuterium Uranium (pressurized heavy-water reactor design)
CAS	Chinese Academy of Sciences
CAWB	Copenhagen Atomics Waste Burner
CEA	French Alternative Energies and Atomic Energy Commission
CMSR	Compact Molten Salt Reactor
CNRS	French National Centre for Scientific Research
CNSC	Canadian Nuclear Safety Commission
CTAH	Coiled tube air heater
CVŘ	Research Centre Řež
DMSR	Denatured molten salt reactor
EdF	Électricité de France
Euratom	European Atomic Energy Community
FHR	Fluoride-salt cooled high-temperature reactor
FLiBe	LiF-BeF salt
FLiNaK	LiF-NaF-KF salt
FP	Fission product
Gen	Nuclear reactor generation
GFR	Gas-cooled fast reactor
GIF	Generation IV International Forum
IAEA	International Atomic Energy Agency
IMSR	Integral Molten Salt Reactor
IPyC	Inner pyrolytic carbon layer
ITMSF	International Thorium Molten-Salt Forum
KP	Kairos Power
KP-FHR	Kairos Power fluoride salt-cooled high temperature reactor
LFR	Lead-cooled fast reactor
LFTR	Liquid-fluoride thorium reactor
LWR	Light water reactor (PWRs and BWRs together)
MA	Minor Actinide
MIT	Massachusetts Institute of Technology
Mk1 PB-FHR	Mark-1 Pebble-bed fluoride-salt-cooled, high-temperature reactor
MSBR	Molten Salt Breeder Reactor
MSFR	Molten Salt Fast Reactor
MSR	Molten salt reactor
MSRE	Molten-Salt Reactor Experiment
NACC	Nuclear air-Brayton combined cycle
NGNP/NHI	Next Generation Nuclear Plant to the Nuclear Hydrogen Initiative
NPP	Nuclear power plant

NRC	US Nuclear Regulatory Commission
OPyC	Outer pyrolytic carbon layer
ORNL	Oak Ridge National Laboratory
PBMR	Pebble bed modular reactor
PR&PP	Proliferation resistance and physical protection
PRIS	Power Reactor Information System
PWAR-1	Pratt and Whitney Aircraft Reactor
PWR	Pressurized water reactor
sCO2	Supercritical CO2
SCRAM	Safety control rod actuator mechanism
SCWR	Supercritical-water-cooled reactor
SEM	Scanning electron microscope
SFR	Sodium-cooled fast reactor
SINAP	Shanghai Institute of Applied Physics
SNF	Spent nuclear fuel
SS	Stainless steel
SSR-TS	Stable Salt Reactor – Thermal Spectrum
SSR-W	Stable Salt Reactor – Wasteburner
THTR	Thorium High-temperature Reactor
TMSR	Thorium Molten Salt Reactor
TMSR-LF	Thorium Molten Salt Reactor – Liquid fuel
TMSR-SF	Thorium Molten Salt Reactor – Solid fuel
TRISO	Tristructural-isotropic (a form of solid fuel)
UCB	University of California, Berkley
VHTR	Very-high-temperature reactor
XRF	X-ray Fluorescence analysis
720 h / 550 °C	720 hours long test at the temperature of 550 °C
720 h / 700 °C	720 hours long test at the temperature of 700 °C
2160 h / 550 °C	2160 hours long test at the temperature of 550 °C

1. Future of Nuclear Energy

Perception of electricity production and the whole electricity market is changing rapidly in the last several years with the rise of renewable sources, the development of Africa and Asia, and environmental movements all around the world. One of the changes is the decline of coal power plants, and potentially also gas power plants, while its place is overtaken mainly by renewables. However, it cannot be done only by wind, solar, and hydro, because of their intermittence. There needs to be a stable source of baseload, and capacity to balance electricity demand and production. There are many different ideas on how to do it. One of the proven technologies is nuclear power.

1.1. Current Energy Status Regarding Nuclear Power

Worldwide, nuclear power shared 4.44 % of primary energy consumption in 2015 (renewables 9.57 %, fossil fuels 85.99 %). The comparison between the years 2005, 2010, and 2015 is shown in Figure 1 (Schiffer, 2016). At the end of the year 2019, there are 449 operational (or long-term shutdown) reactors in the world, and 52 reactors are under construction (International Atomic Energy Agency's Power Reactor Information System, n.d.). Total installed NET electrical capacity of nuclear power accounts of 398887 MW and those 52 under-construction reactors are supposed to add 52659 MW of total installed NET electrical capacity in the future (IAEA's PRIS, n.d.). Most of the currently operating reactors are either light water – pressurized water reactors (PWRs) and boiling water reactors (BWRs), or heavy water reactors for example Canada Deuterium Uranium (CANDU) of Generation II and III.

Figure 1

"Comparative graph of primary energy consumption over the past 15 years." Adapted from Schiffer (2016), p. 4.

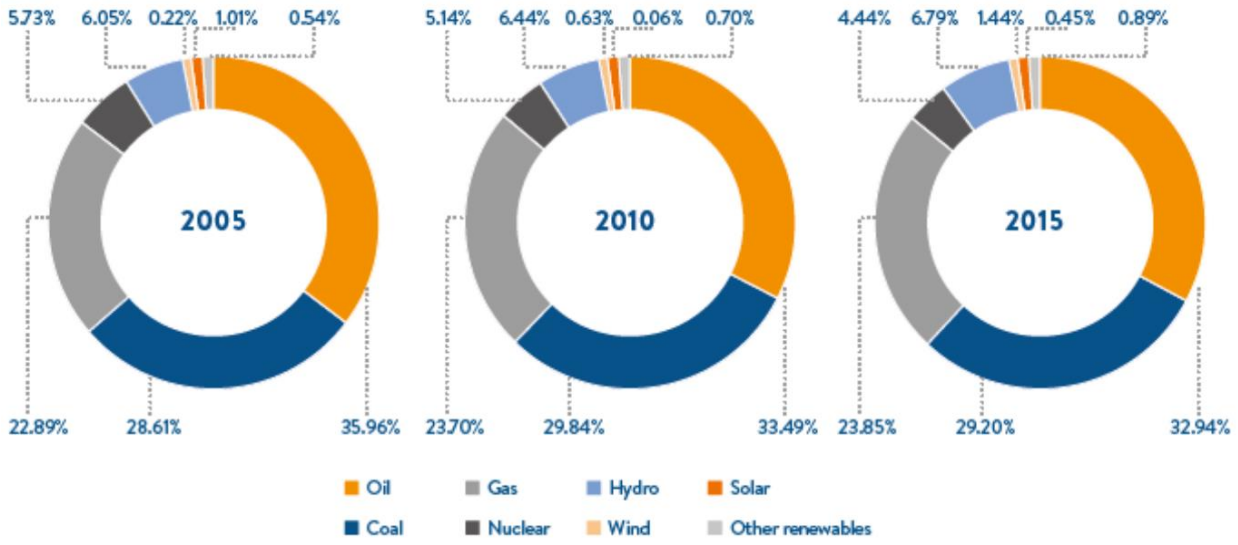

The main advantages of nuclear power are the low cost of uranium fuel, which leads to the fact that nuclear power is the lowest-cost baseload electricity supply option in many markets (Schiffer, 2016); reliability; and low environmental impact, either measured by carbon emissions or by required area. However, there are more advantages to come with new Generation IV nuclear reactor designs.

1.2. Generation IV

Nuclear reactor designs are divided according to Generations. First nuclear power plants - early prototypes of nuclear reactors - generating electricity for a power grid were labeled as Gen I. Followed by commercial power reactors with revisited and upgraded designs of Gen II. Reactors built between 1995 and 2010 with increased efficiency are referred to as Gen III. Gen III+ reactors with further improved parameters are being built now. Overview of nuclear reactors generations with power plant examples is given in Figure 2.

Figure 2

An infographic showing examples of Nuclear Power Plants throughout the different generations. Adapted from "Generations of nuclear reactors" (2018), edited.

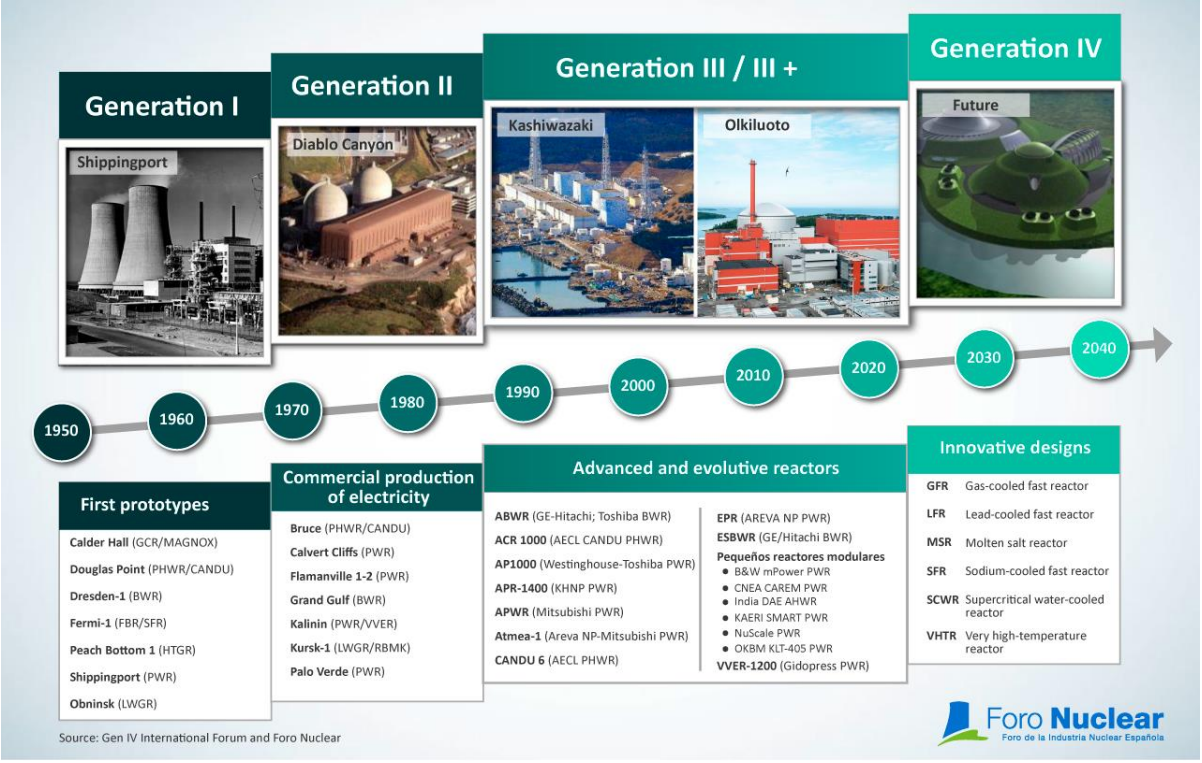

In 2001, the founding document of Generation IV International Forum (GIF) had been signed by nine countries (Argentina, Brazil, Canada, France, Japan, the Republic of Korea, the Republic of South Africa, the United Kingdom, and the United States) with the Russian Federation, the People's Republic of China, Switzerland, and Euratom joining later followed by Australia. The Czech Republic is not a direct member of GIF; however, it is active through Euratom in many branches of research and development for Gen IV technologies with the priority put on MSR technologies. The main purpose of GIF is to develop nuclear system designs with the following goals: reduction in radioactive waste, particularly long-lived high-level waste; high safety; good economics; sustainability; and increased proliferation resistance (Duarte et al., 2013).

GIF has selected six reactor designs to be further developed with promising expectations to fulfill prior mentioned goals. These designs are Very-high-temperature reactor (VHTR), Supercritical-water-cooled reactor (SCWR), Gas-cooled fast reactor (GFR), Sodium-cooled fast reactor (SFR), Lead-cooled fast reactor (LFR) and Molten salt reactor (MSR) (Duarte et al., 2013). The basic schematic layouts of these six reactor designs are in Figure 3.

Figure 3

Schematic representations of six Gen IV nuclear reactor concepts. Adapted from "The Generation IV International Forum" (n.d.).

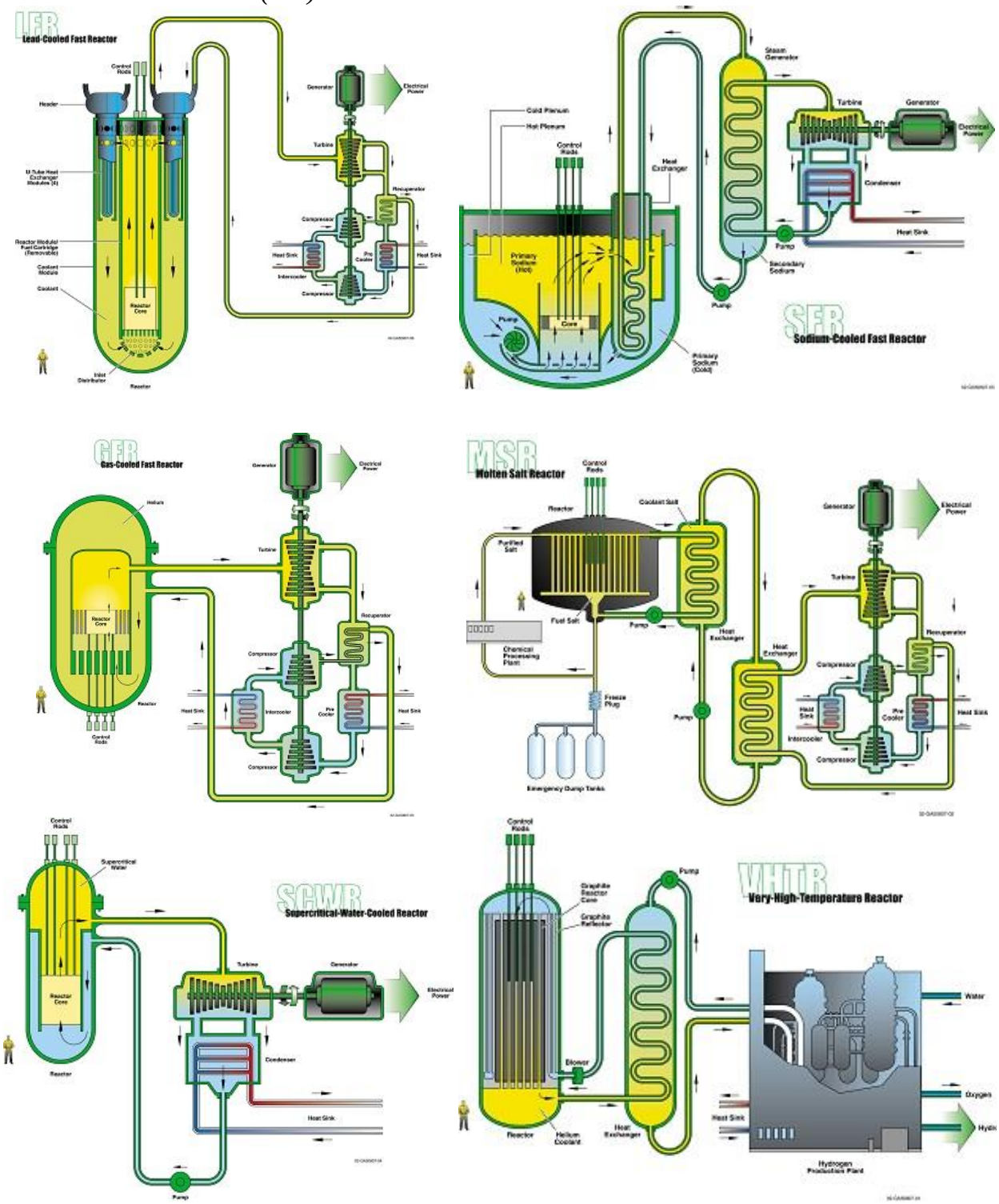

2. Molten Salt Reactors

Molten Salt Reactors (MSRs) are nuclear reactors that use, as the name suggests, molten salts within their core as coolant or fuel carrier. This idea stands far away from current designs of PWR, BWR, CANDU, and actually all the energetic reactors using water as a coolant and solid ceramic form of fuel. Even though the concept of the molten salt reactor was overlooked during past years, it has significant advantages: low-pressure primary loop; higher efficiency due to higher outlet temperature; possible continuous refueling and fission products removing; no fuel fabrication; possible breeding capacity; and more (Small Nuclear Power Reactors, 2019).

Some of the MSR designs exploit the breeding capacity in order to use the thorium cycle, which produce fission ^{233}U from ^{232}Th. The use of the thorium might be the reason why there was a significant drop in the research conducted after the initial interest. As the 1984 Nobel Prize laureate for physics Carlo Rubbia suggests, the lack of interest and funding have deep roots in the fact that thorium bred ^{233}U is difficult to turn into a weapon due to its' contamination of other uranium isotopes (^{232}U and ^{234}U) leading into a high proliferation resistance and physical protection (PR&PP) (Rubbia, 2010). Nonetheless, this strong PR&PP is a great advantage nowadays. Moreover, the Th-U fuel cycle reduces the production of minor actinides (MA) and consequently significantly decreases the requirements for long-time nuclear waste storage.

2.1. History of Molten Salt Reactors

The first idea of a nuclear reactor with fuel in liquid form came in the 1940s when Eugene Wigner and Alvin Weinberg introduced a design of a reactor with ^{233}U-Th fuel dissolved in aqueous water in 1945. This idea was later realized in 1953 as the Homogeneous Reactor Experiment with light water and power output of 150 kWe in 1953.

Figure 4

"Elevative section of the Aircraft Reactor Experiment." Adapted from Bettis & Ergen (1958), p. 675.

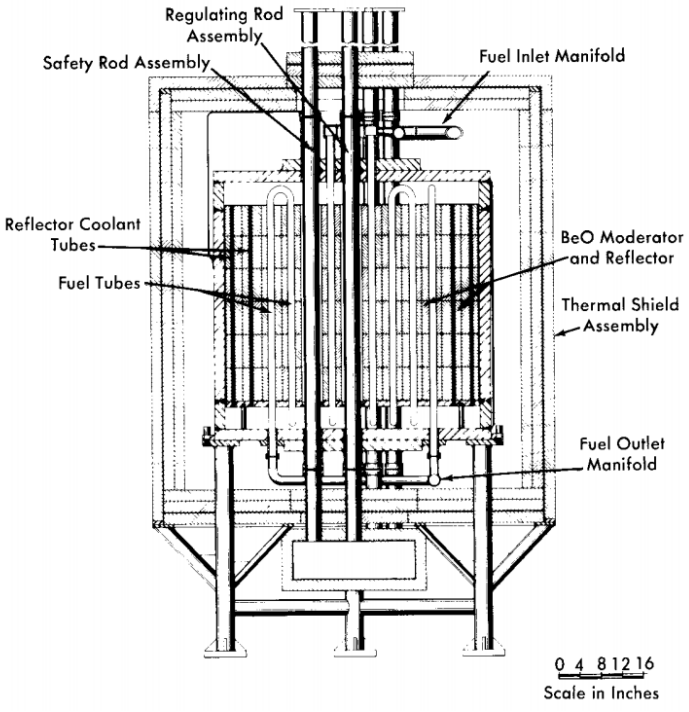

The idea to use a molten fluoride salt instead of water comes from Raymond Briant, and the research of molten salt reactors started with the U.S. Aircraft Nuclear Propulsion (ANP) program in the 1950s. The ANP program resulted in the aircraft reactor experiment (ARE) in 1954 at Oak Ridge National Laboratory (ORNL), Tennessee. Its schematic layout is in Figure 4. The ARE was operated for more than 100 hours, with its' outlet temperatures rising as high as 860 °C and the power up to 2.5 MWt. As a fuel, the ARE used molten fluoride salt NaF-ZrF_4-UF_4 with 53-41-6 mol% concentrations flowing through fuel tubes. Neutrons were moderated by beryllium oxide (BeO), and the reactor core was cooled by liquid sodium. As a secondary loop coolant helium was used. The main structural material used in the ARE was Inconel 600 alloy. The ARE experiment showed two important results. First, that molten salt fuel reactor has a strong negative reactivity coefficient with temperature and that the xenon gas could be removed from the molten salt.

During the same time as ARE, another experimental reactor for potential aircraft propulsion called Pratt and Whitney Aircraft Reactor (PWAR-1), was developed. The design of the PWAR-1 core (Figure 5) was rather simple - NaF-ZrF_4-UF_4 fuel salt within fuel annulus surrounded by beryllium reflector-moderator and with inner control rod in the middle of core's annulus. The main purpose of the PWAR-1 experiment was mainly to get data. Therefore, the operating temperature of 677 °C and basically zero power were sufficient in order to perform the criticality experiment in 1957.

Figure 5

"Cross-section of PWAR-1 core." Adapted from Dolan (2017), p. 287.

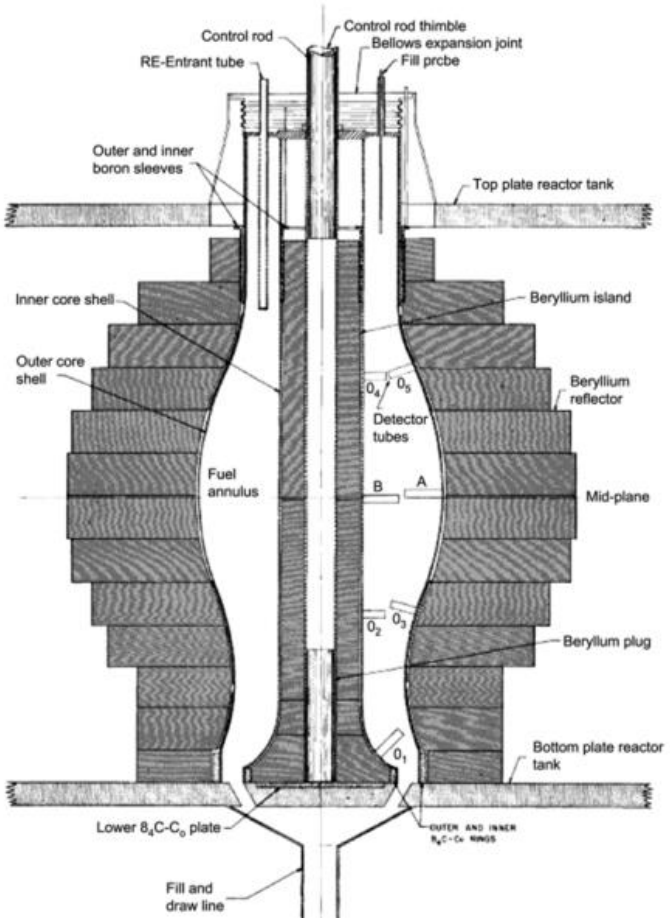

After the end of ARE and PWAR-1 operations, researchers and engineers at ORNL come up with many different ideas and designs for molten salt reactors. Some of these designs were breeding reactors with two fluid graphite-moderated core. A concept of fast-spectrum two-fluid molten-salt breeder reactor from 1958 is in Figure 6. Even though the advantages of two fluid design; as better neutron economy, higher breeding ratio, easier protactinium extraction, simpler removal of rare earth fission products, and many more; cannot be disputed, the complexity of such a design changed the focus of scientists to one fluid design.

Figure 6

"An 1958 concept for a two-fluid molten-salt breeder reactor." Adapted from Sorensen (n.d.a), edited.

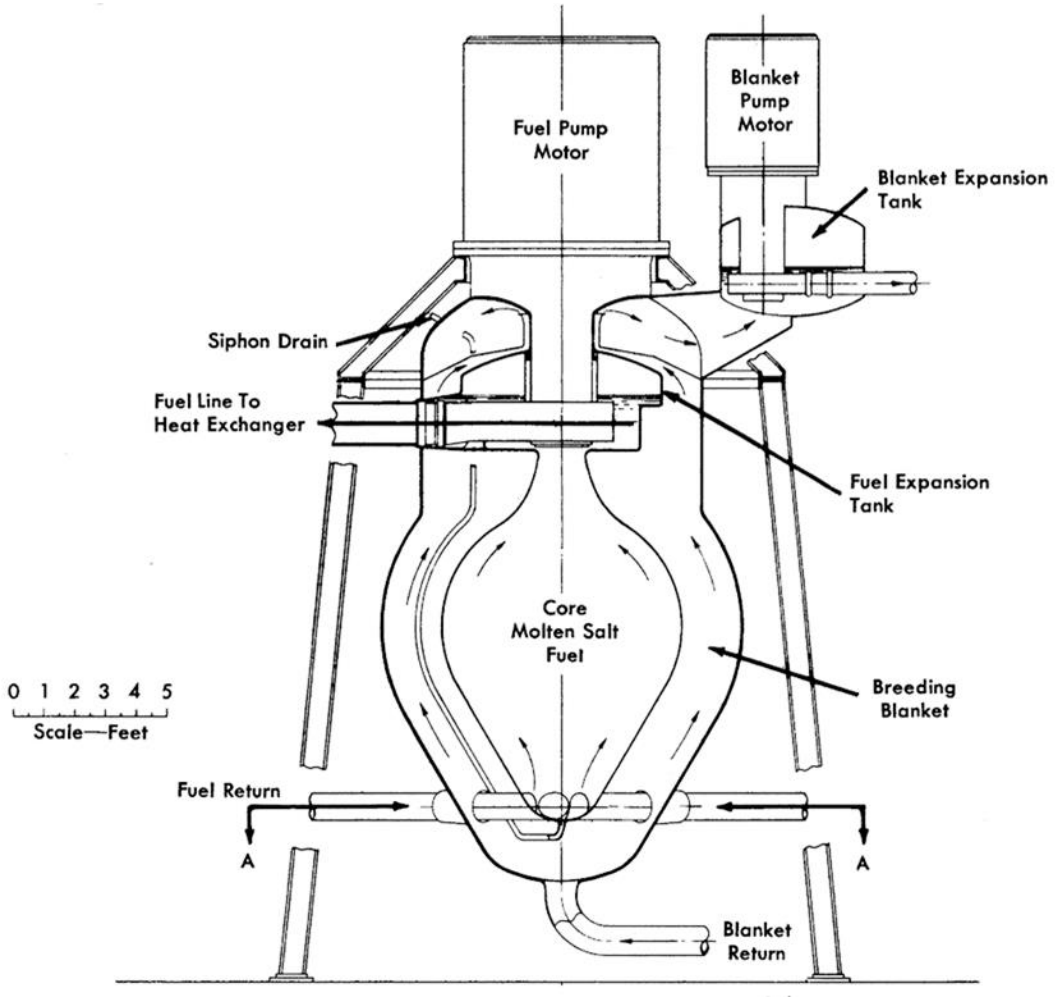

This focus on one fluid design resulted in the Molten-Salt Reactor Experiment (MSRE), which become critical in 1965 at ORNL (Figure 7 and Figure 8). The MSRE was operated for 4.5 years with three different fissile fuel materials: ^{233}U, ^{235}U, and ^{239}Pu. This thermal neutron spectrum reactor used LiF-BeF_2-ZrF_4-UF_4 with 65-29-5-1 mol% fuel salt. Neutrons were moderated by pyrolytic graphite, and the reactor core was cooled by molten 2LiF-BeF_2 salt mixture as a secondary loop coolant. The main structural material used in the MSRE was INOR-8 alloy (later called Hastelloy-N). INOR-8 nickel-based alloy was developed after evaluation of data obtained during ARE to overcome corrosion problems of Inconel 600 alloy.

Figure 7

"MSRE reactor vessel." Adapted from Robertson (1965), p. 11, edited.

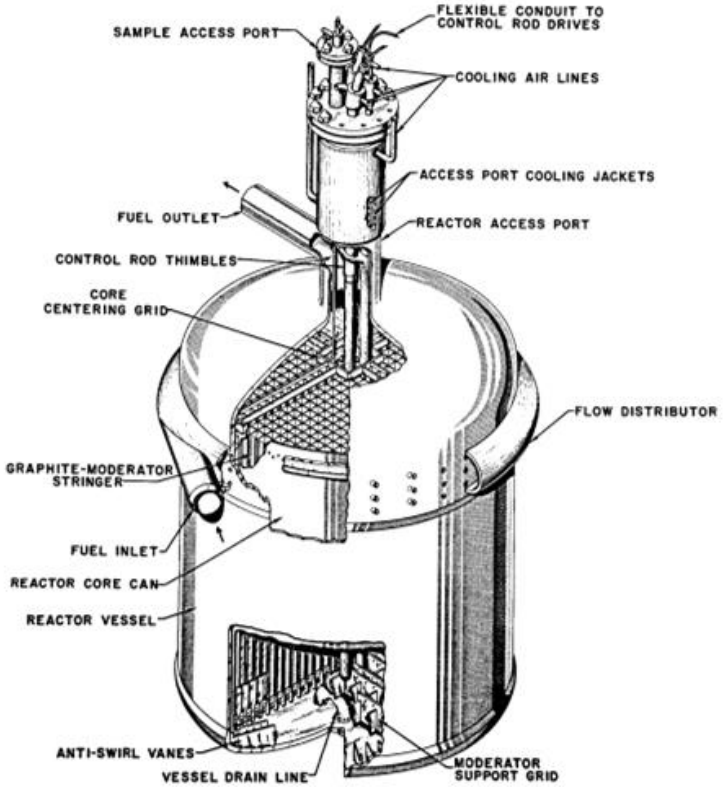

Figure 8

"MSRE Flow diagram." Adapted from Robertson (1965), p. 10.

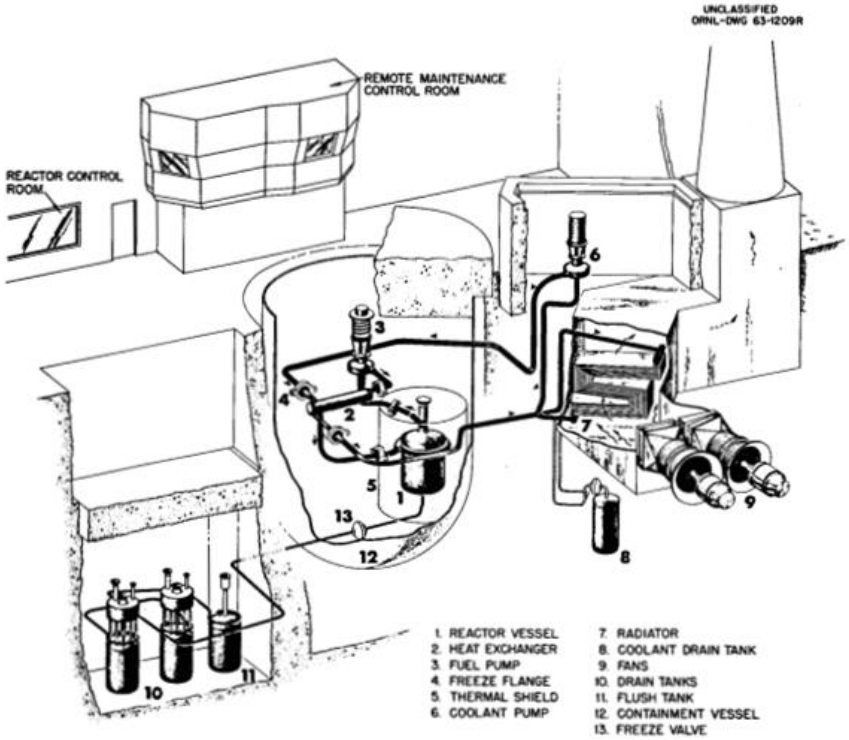

The great success of MSRE and ARE led to the concept of a breeder reactor. This concept of a breeder reactor, named Molten Salt Breeder Reactor (MSBR), was to utilize the thorium fuel cycle. The sectional elevation of the MSBR is shown in Figure 9. The following parameters were proposed for MSBR: LiF-BeF_2-ThF_4-UF_4 with 72-16-12-0.4 mol% as fuel salt, NaF-$NaBF_4$ with 8-92 mol% as the secondary coolant, and power output 1000 MWe (2250 MWt). The design report was written; however, all the further work was terminated due to a focus on light water reactor technology (Sorensen, n.d.b).

The small hint of revived interest in molten salt reactors came at the end of the 1970s with the US administration decision to abandon commercial reprocessing of spent fuels. MSBR and molten salt reactors generally were thought to have proliferation resistance, and therefore a new project of Denatured molten salt reactor (DMSR) started. DMSR was based on the MSBR concept with the shift from breeder to converter design; reduction of online reprocessing to remove only gaseous FP and noble metals; containment containing full fuel load for 30-year operation period; and flattened and lowered power density to allow 30-year graphite moderator lifetime. Nonetheless, even this project ended as a design only, and with its termination, the molten salt reactors were mostly abandoned for several decades (Macpherson, 1985; Serp et al., 2014; Uhlíř, 2007).

Figure 9

"Sectional Elevation of MSBR Vessel." Adapted from Rosenthal et al. (1969), p. 56.

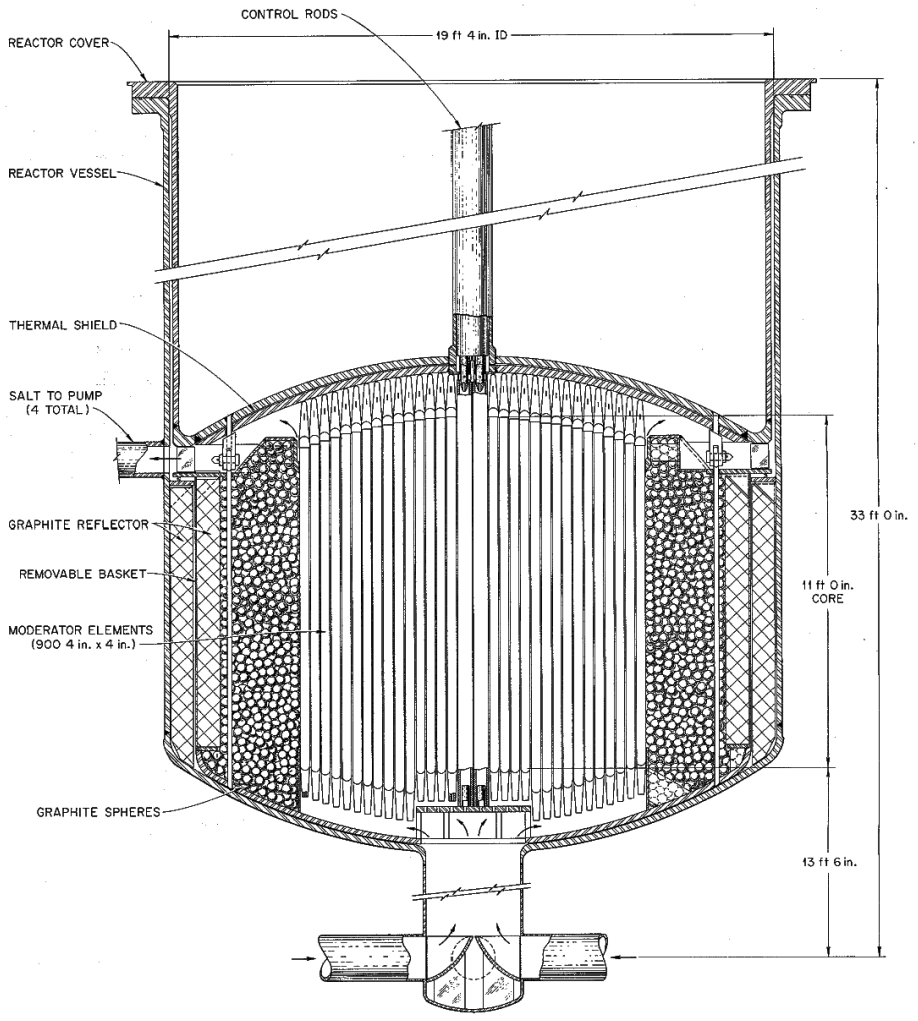

Despite the US' decision to move away from MSRs, there were several countries with smaller or larger research. In France, CEA (French Alternative Energies and Atomic Energy Commission) and EdF (Électricité de France) continued their research and development based on the MSBR project in the 1970s. French interest in molten salt reactors continued with some interruptions and resulted in the AMSTER (Actinides Molten Salt TransmutER) concept and the MSFR (Molten Salt Fast Reactor) design. The AMSTER was supposed to be a graphite-moderated molten salt reactor with continuous refueling using either ^{238}U or ^{232}Th (Vergnes et al., 2000). The description of the MSFR is given in chapter 2.3.8.

At the same time, China and Shanghai Institute of Applied Physics (SINAP), which is a part of the Chinese Academy of Sciences, built a zero – power MSR. During the first half of the 1970s, about 400 scientists and engineers in SINAP worked on the goal of building 25 MWe Thorium Molten Salt Reactor (TMSR). However, in the second half of the 1970s, the focus has been changed to LWRs and on building Qinshan NPP - I 300 MWe power plant (Xu, 2017).

Another ongoing research is in the Czech Republic as a part of many projects, such as SPHINX project, Fluoride reprocessing project, and others. These projects have many focuses: theoretical and experimental physics, molten salt thermohydraulics, structural material development, fuel salt chemistry, and more. Many interesting experiments have been done, and a lot of significant results have been obtained, for example: reactor physics experiments with inserted molten salt zones in research reactors, verification of molten salt fuel processing, electrochemical separation of actinides from fission products for online reprocessing, development of computational codes for the composition evolution during the burnout of liquid fuel, and development of MoNiCr nickel-based superalloy (more about that in chapter 4.8).

2.2.Molten Salt Reactors Types

There are many different types and versions of MSRs. They can be divided by the configuration of the fuel they use, by neutron spectrum, or other criteria. However, fuel configuration and the shape of the neutron spectrum are the most important features and have a significant impact on the whole reactor design, its complexity, safety features, core volume, and more.

2.2.1. Fuel Configurations of Molten Salt Reactors

At the beginning of molten salt research, only fuel dissolved into molten salt coolant was considered; however, in the past few years, another two different ideas were thought of. Those two new ideas are fuel dissolved in molten salt, but kept in static fuel pins; and solid fuel, usually in the form of TRISO fuel particles, within a graphite matrix. All three configurations have their pros and cons, which are described in the following paragraphs.

Molten Salt Fuel. Molten salt fuel is the only molten salt reactor type that has already been proven experimentally. In this case, the fuel itself is dissolved within primary coolant salt. It allows for continuous fission products removal; online refueling, which leads to longer campaign than LWRs and higher safety due to lower reactivity reserve; higher operational temperatures and lower pressures; no fuel fabrication; no need for burnable absorbers; and more. On the other hand, dissolved fuel irradiates the whole primary loop by delayed neutrons; the primary loop has bigger fuel inventory due to the circulation of fuel out of core; and the whole primary loop system is rather complex. As an example, the reactor vessel cross-section of MSRE is shown in Figure 10.

Figure 10
MSRE reactor vessel cross-section. Adapted from Robertson (1965), p. 76.

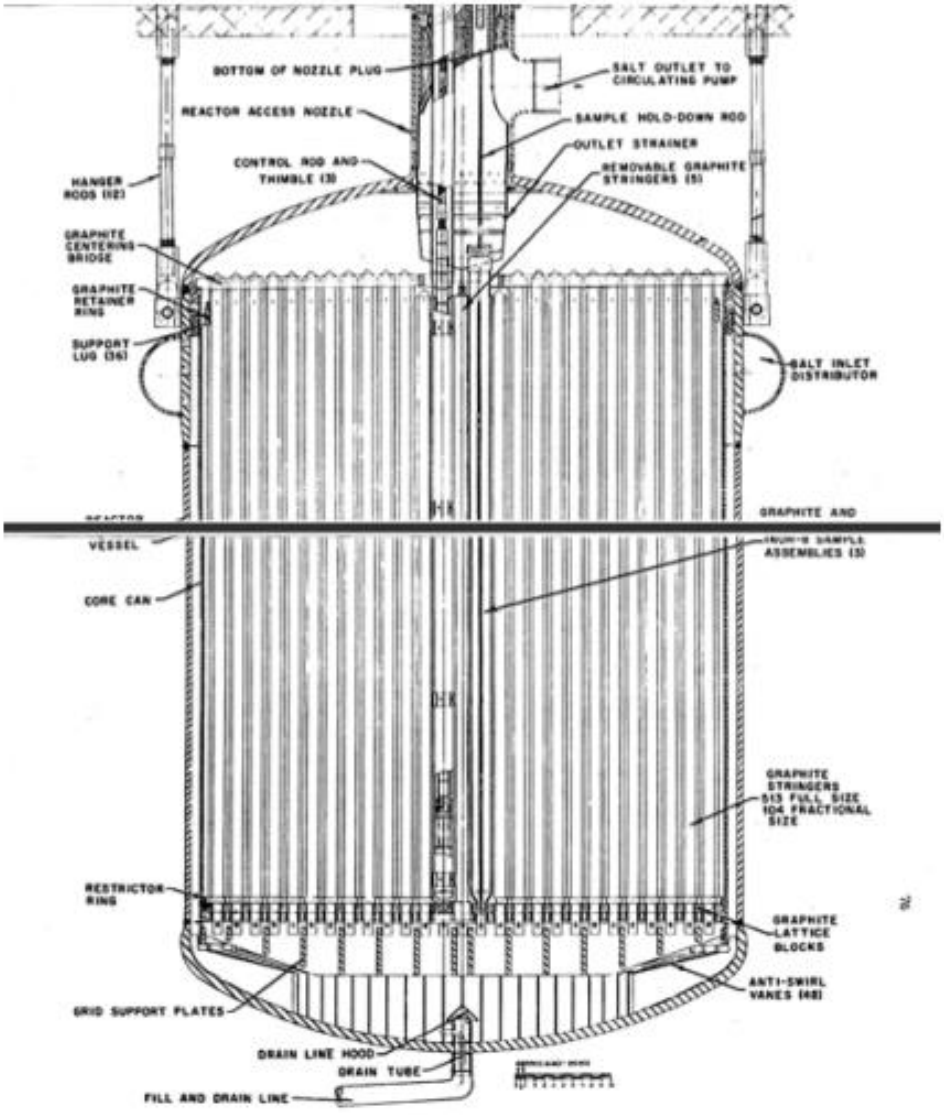

Static Molten Salt Fuel. Static molten salt fuel is in the form of molten salt contained within tubes or pins resembling regular LWR pins. It has similar chemistry as regular molten salt fuel; however, it avoids many of its disadvantages, such as out-of-core irradiation and activation, out-of-core decay heat production, and it might also add another barrier for fission products. Unfortunately, it also loses many advantages connected to fuel being dissolved in coolant circulating in the first loop: continuous fission products removing, online refueling, and small reactivity reserve.

Even within the concepts of static molten salt fuel reactors, some differences could be found. The fuel tube could be either vented or not. A vented tube, in Figure 11, releases gaseous fission products into the coolant salt and, therefore, to the gas space in the reactor. The sealed tubes accumulate all the FPs within the tube. This accumulation leads to high pressure and increased tube rupture risk. Heat transfer from static fuel pins to molten salt coolant, and general fuel pin behavior, need to be further investigated.

Figure 11

"Vented molten salt tube." Adapted from Dolan, (2017), p. 487, edited.

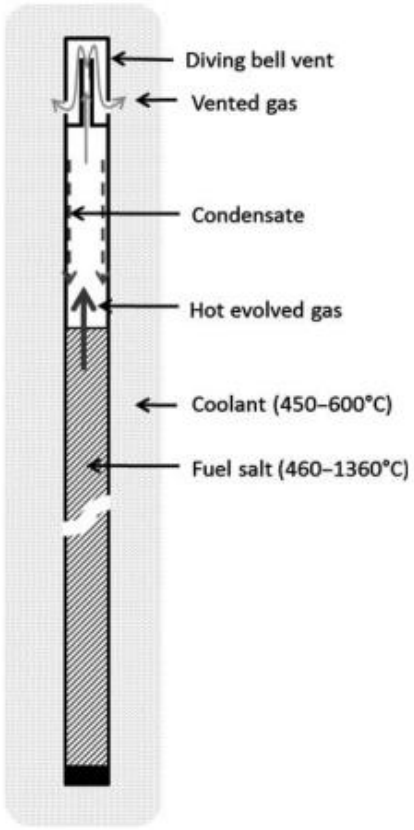

Solid Fuel. Solid fuel reactors cooled by molten salts, in the USA termed fluoride-salt cooled high-temperature reactors (FHRs), are now being developed by research institutions, universities, and private companies all around the world. The main idea behind this effort is to take advantage of fuel, which was previously developed for High-temperature gas-cooled reactors and molten salt coolant of Molten salt reactors. Thanks to this fuel-coolant combination, proposed designs have low pressure, high temperature, high efficiency, small reactor vessel, and small containment. Moreover, the solid fuel is in the form of TRISO (Tristructural-isotropic) particles within a graphite matrix, and therefore it serves as another safety barrier against FP release.

TRISO fuel particle is a sphere with approximately 0.92 mm in diameter. It is made up of five different parts with five different purposes. Every particle starts as a fuel sphere with approx. 0.5 mm in diameter, called kernel, made from UO_2. Around the kernel, there is the first coating layer of porous carbon, called a buffer layer. This layer is 0.095 mm wide and provides space for gaseous fission products released during fuel irradiation. The second coating layer is pyrolytic carbon with high density (IPyC). The main purpose of this layer is to provide structural strength and support. It is also critical during manufacturing, because it prevents chlorine, used during deposition of the next layer, to react with the kernel or buffer layer. The width of the IPyC layer is approx. 0.04 mm. Over the IPyC layer is deposited 0.035 mm wide silicon carbide layer (SiC). Because of high strength and chemical resistance, the SiC layer behaves as containment for gaseous and metallic fissions products. A final layer is made of pyrolytic carbon (OPyC). The thickness of the last layer is 0.04 mm. It provides support for the SiC layer and also the bonding surface necessary for making fuel compacts (Cul et al., 2002).

Figure 12

Schematics of TRISO Pebble bed fuel elements. Adapted from IAEA's ARIS (2011), p. 8, edited.

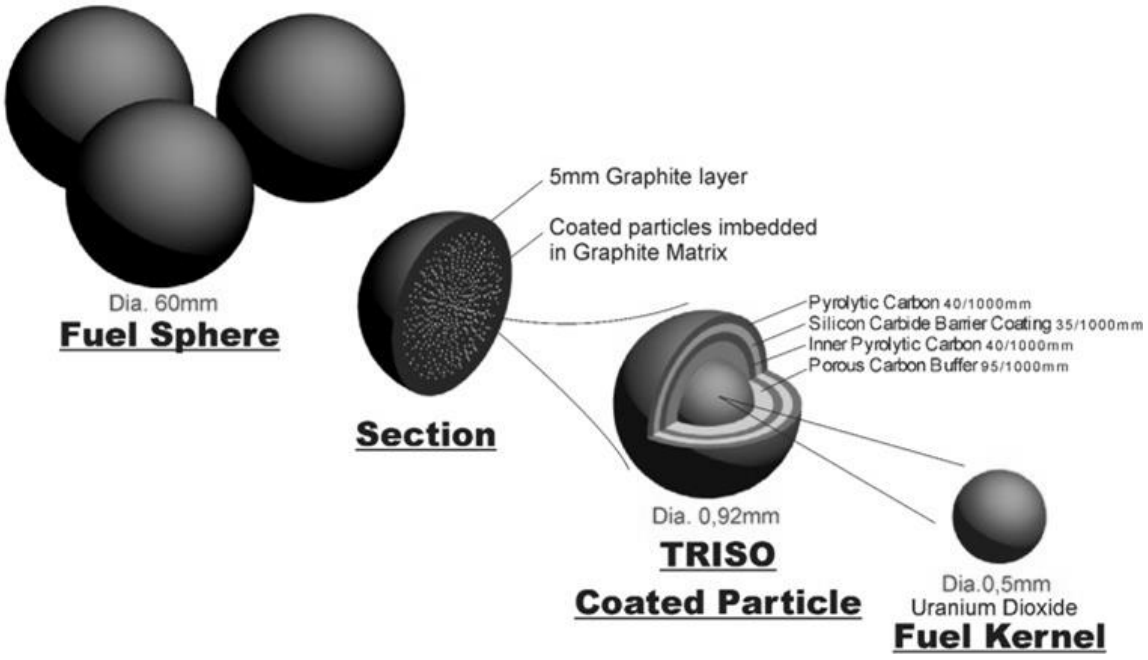

Many TRISO fuel particles are mixed with carbon mastic, as can be seen in Figure 12. The mixture is then shaped into short right-circular cylinders, spheres, or any other shape, according to the type of reactor. In the case of pebble-bed reactors, spheres might contain about 12000 TRISO particles. They have a diameter of 60 mm, including a 5 mm thick surface graphite layer without TRISO particles. All given dimensions are specific for THTR and PBMR, and they might vary for other designs (Brähler et al., 2008; International Atomic Energy Agency's Advanced Reactors Information System, 2011).

There are two typical reactor configurations of the FHR concept, the pebble bed type and the prismatic block type. In a prismatic core, reflectors and fuel blocks create a hexagonal matrix. They are usually arranged to form an inner graphite reflector, an annular active fuel core, and an outer reflector. The disposition of the second – pebble bed – design is similar to the former one. In the middle, there might be an inner graphite reflector surrounded by an annular active fuel core and encased by the outer graphite reflector. One of the representative designs without the inner graphite reflector is the TMSR-SF1 reactor, which schematic layout is in Figure 13. In the pebble bed reactors, an annular active fuel core is made of fuel pebbles with an approximate size of 60 mm. During the reactor operation, these pebbles continue to circulate down through the core. This circulation is driven only by gravity, and there is no artificial mechanism to force pebbles to circulate through the core. Once a pebble reaches the bottom of the core, it is removed, and its properties, namely burnup and safety (leaking of fission products), are measured. After these measurements, it is decided whether a pebble is returned to the top of the core or disposed to the storage. This fuel handling system increases the costs of the pebble bed design, but on the other hand, it allows online refueling during the reactor operation. Both reactor designs use control rods for reactivity control and shutdown. Besides, small absorber pebbles can be inserted into the core of the pebble-bed design during an emergency shutdown.

Figure 13

"TMSR-SF1 schematic layout." Adapted from Xu (2017), p. 17.

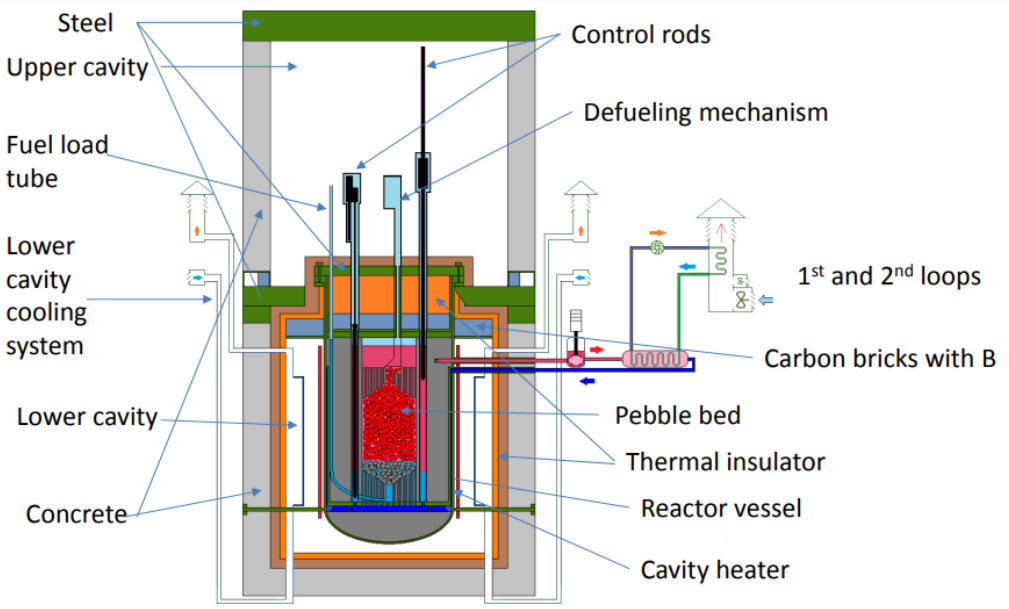

2.2.2. Molten Salt Reactors Neutron Spectra

As it is mentioned above, the neutron spectrum is an important characterization for any nuclear reactor, which MSRs are not an exception. The spectrum chosen for a specific reactor has major consequences to the design, such as the need for materials that can withstand hard neutron spectrum in the case of fast neutrons or large core volume, and therefore a large reactor vessel, in order to incorporate moderator to slow down neutrons. Apart from common nuclear reactors working at criticality, there is a possibility to utilize MSRs with subcritical assemblies that would be supported by a neutron source, which are referred to as accelerator-driven reactors.

Fast. Molten salt reactors with fast neutron spectrum (MSFR) can use ^{232}Th or ^{238}U as fuel and utilize fast fission neutrons; therefore, there is no need for a moderator in the reactor core, which is the main lifetime limiting factor if graphite is used. As a result, the reactor core and the whole reactor vessel is smaller than a reactor vessel of reactors with a thermal neutron spectrum. Moreover, MSFRs have a high negative reactivity temperature coefficient, and consequently, they regulate reactor thermal power output by themselves. Another advantage of MSFRs is the possibility for long-lived nuclear waste incineration and nuclear fuel breeding. The use of fast neutron spectrum has its drawbacks too; one of them is considerable damage induced in structural materials by high fast-neutron flow.

Thermal. Molten salt reactors with thermal neutron spectrum can use ^{233}U, ^{235}U, or ^{239}Pu as fuel and require a moderator in order to slow down the fission neutrons. In most cases, the graphite is used as the moderator; however, designs including regular or heavy water moderator are proposed too. In the use of graphite, high priority needs to be given to its manufacturing process. Any impurity could have devastating effects inducing faster corrosion of construction materials of the reactor vessel or decreasing the reactor's neutron efficiency if neutron absorbers are present. A high density of the material is necessary to slow down neutrons efficiently, whereas increased porosity rapidly accelerates the degradation process of graphite induced by molten salt coolant. Even with high manufacturing standards, graphite has a limited lifetime inside the reactor core, and this fact needs to be taken into account during the design process of the reactor.

Accelerator-driven Systems. Accelerator-driven systems (ADS) are subcritical assemblies, where a self-sustaining chain reaction does not occur. It commonly consists of a high-energy (~ 1 GeV) high-intensity proton accelerator; a spallation target, where incident protons cause a spallation reaction, which emits tens of neutrons; and a blanket region, where incident neutrons from the spallation reaction cause either fission or transformation of breeding material into fission material. Fission also produces heat, which could be converted to an electricity output; nonetheless, the main causes for the use of ADS are breeding fission material for other reactors and incineration of the SNF and particularly the MA. A schematic representation of an accelerator-driven system is in Figure 14.

Figure 14

Basic schematics of Accelerator-driven system (ADS). Adapted from Dolan (2017), p. 496, edited.

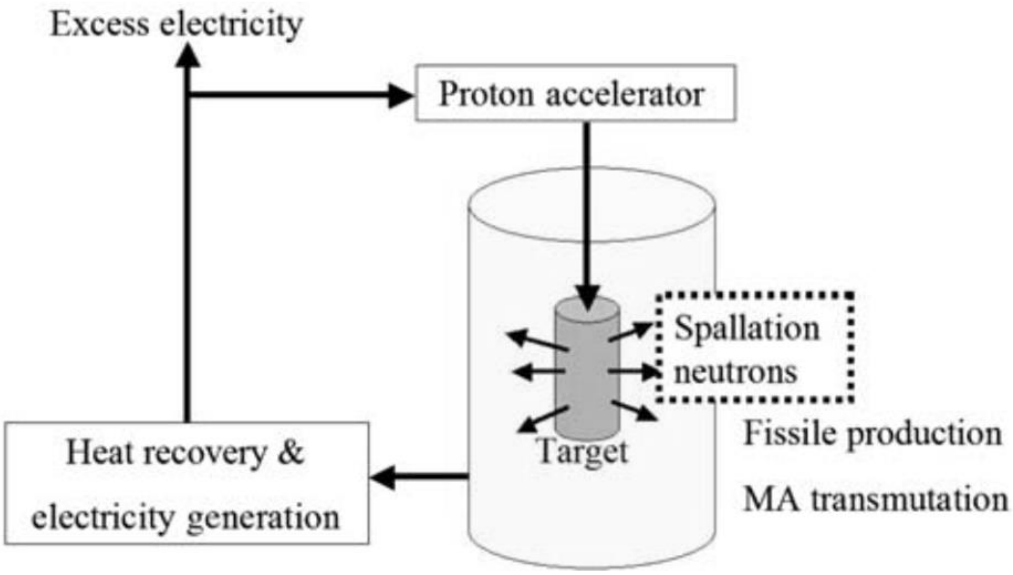

2.3. Currently Proposed Designs of Molten Salt Reactors

As it was mentioned above, the history of MSRs has two peaks of interest. The first peak was in the 1950s and 1960s during the research lead by ORNL and the second one after the inclusion of MSRs into promising designs of Gen IV. This raised interest, and consequently, all the research and development done in the past 15 to 20 years, results in almost industry-ready technology. This technological readiness could not have been overlooked by private companies anymore; therefore, these companies have come up with many different proposals. They use different fuel configurations with its benefits and drawbacks, and also incorporate their ideas, solutions, and design changes.

Several MSR designs in different stages of development are presented on the following pages. Some of the designs are backed mainly by research institutions, and the others are fully commercial projects; however, all of these projects use molten salts, aim to help fight climate change, and want to build the first prototypes in this decade. Summary of main parameters of discussed designs is shown in Table 1.

Note that most of the available information about currently proposed designs are directly from institutions and companies themselves or the Advanced Reactors Information System (ARIS) of the International Atomic Energy Agency (IAEA). These documents, such as IAEA's ARIS (2018), have not been peer-reviewed and are not independent studies.

Table 1

Basic parameters of some currently proposed molten salt reactor designs.

Company name	Reactor design	Reactor thermal power	Fuel enrichment	Reactor operating pressure	Reactor coolant outlet temperature	Reactor coolant inlet temperature	Reactor coolant flow rate	Type of cycle	Power output	NET efficiency	Main turbine temperature	Main steam pressure
		MWt	%	MPa	°C	°C	kg/s	-	MWe	%	°C	MPa
SINAP	TMSR SF1	10	17	0.5	650	600	84	-	-	-	-	-
UCB	Mk1 PB-FHR	236	19.9	0.3	700	600	976	Brayton	100	42.5	670	18.85[a]
Terrestrial Energy	IMSR-400	400	<5	<0.4	670-700	625-660	5400	Rankine	190	47.5	585	19
Flibe Energy	LFTR	600	-	0.1	650	500	-	Brayton	250	41.7	550	20[a]
ITMSF	MSR-FUJI	450	2	0.5	704	565	2400	Rankine	200	44.4	538	-
Seaborg Technologies	CMSR	250	Re-processed SNF	1	700/900	600/700	-	Rankine	100-115	40-46	-	-
Copenhagen Atomics	CA Waste Burner	50	-	-	-	-	-	Brayton	20	40	-	-
CNRS (EU)	MSFR	3000	-	0.1	750	650	4.5 m3/s	-	1300	-	-	-
Moltex Energy	SSR-W	750	Reactor grade plutonium	0.1	630	500	5700	Rankine	300	40	538	26
ThorCon International	ThorCon	557	19.7	1.2	704	565	3000	Supercritical Rankine	250	44.9	538	26
Kairos Power	KP-FHR	320	19.75	<0.2	650	550	1200-1400	-	140	45	585	19
Research Centre Řež	Energy Well	20	15	0.1	700	650	186	Brayton	8,4	42	621	21[a]

[a]gas CO_2 cycle

2.3.1. TMSR SF1/LF1 (SINAP CAS, China)

Thorium Molten Salt Reactor Project (TMSR) of the Chinese Academy of Sciences aims to "Develop Th-Energy, Non-electric application of Nuclear Energy based on TMSR during coming 20-30 years." As a part of this project, there are two separate designs, namely TMSR SF1 with solid fuel and TMSR LF1, in Figure 15, with liquid fuel. Both designs are developed at the same time; however, with different plans and timetables.

In 2019, the construction of the TMSR-SF1 simulate reactor called TMSR-SF0 was finished. This mock-up reactor with electrically heated core (370 kWt) has a 1:3 size ratio to TMSR-SF1 and will operate with LiF-NaF-KF (FLiNaK) molten salt. During its operation, TMSR-SF0 is supposed to provide design verification (passive heat removal capability, integrate and separate hydraulics information, thermal insulation data, and more), simulation research of various events, benchmarking, training, and scaling analysis.

Figure 15

Schematic layout of the TMSR-LF1 reactor. Adapted from Xu (2017), p. 24.

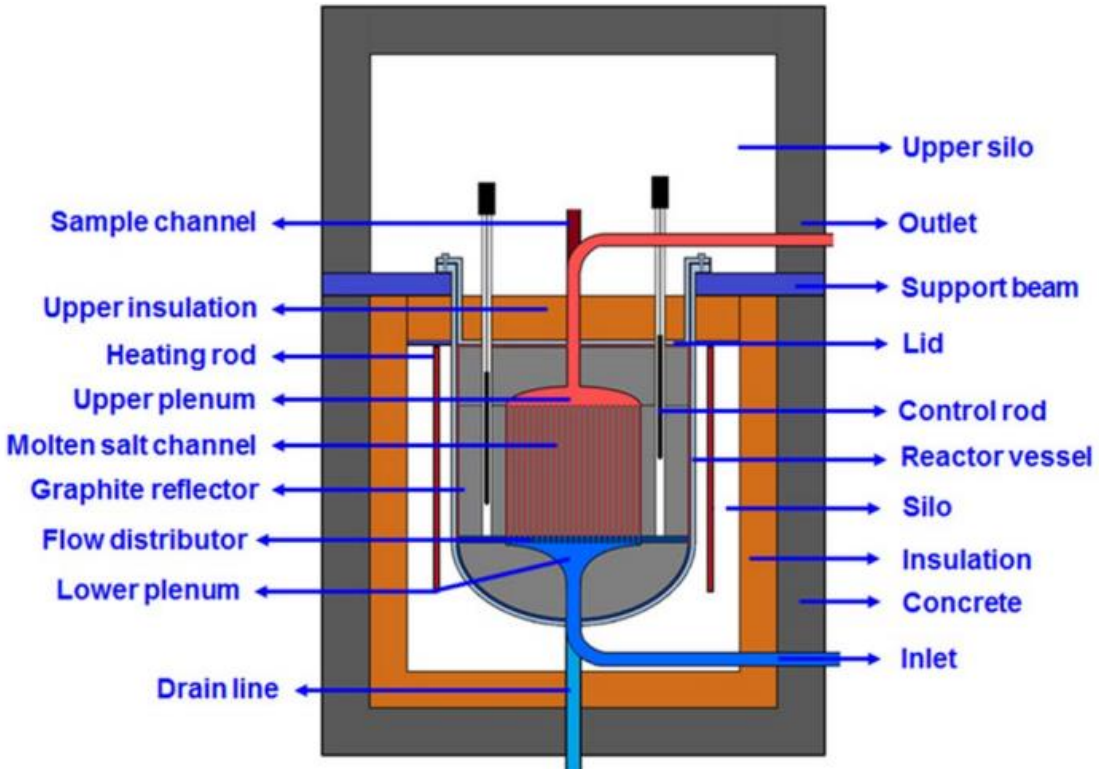

At the end of 2019, the TMSR-SF part of SINAP's program is proceeding with preliminary engineering design aiming to finish the TMSR-SF1 10 MWt prototype as soon as 2025. This prototype should be followed by the TMSR-SF2 and the TMSR-SF3, which are a 100 MWt demonstration pebble bed plant and a 1 GW demonstration plant, respectively.

The TMSR-SF1 is planned to have 60 mm TRISO fuel pebbles and an output coolant temperature of 650 °C. The core of the TMSR-SF1 is designed to have a height of 3 m and a diameter of 2.85 m contained in a 7.8 m high-pressure vessel. ^{7}Li enriched FLiBe molten salt will be used as primary coolant and FLiNaK as a secondary coolant. Passive residual heat removal is ensured by cavity cooling.

The TMSR-LF1 is the conceptual design with the power of 2 MWt and a mixed thorium – uranium fuel inventory with enriched ^{235}U to less than 20 %. The TMSR part of the research and development is optimized for thorium utilization and better sustainability with closed Th-U fuel cycle; however, it presents greater technical challenges. The TMSR-LF1 will use a combination of online and offline salt processing with continuous treatment of the molten salt and discharging it after around six years of use. The basic flow schematic of TMSR-LF1 is shown in Figure 16. Similarly to TMSR-SF1, ^{7}Li enriched FLiBe molten salt will be used as a primary coolant. After the TMSR-LF1, the 2 MWt pilot plant, which is now being built in Wuwei, Gansu province and should be finished by the end of 2020, SINAP plans to follow up with a TMSR-LF2 (10 MWt experimental reactor) by 2025, and TMSR-LF3 (100 MWt demonstration plant) ("Shanghai Institute Of Applied Physics," n.d.; "Thorium Molten Salt Reactor," n.d.; Xu, 2017; Zou, 2019).

Figure 16

"TMSR-LF1 flow schematic." Adapted from Zou (2019), p. 19, edited.

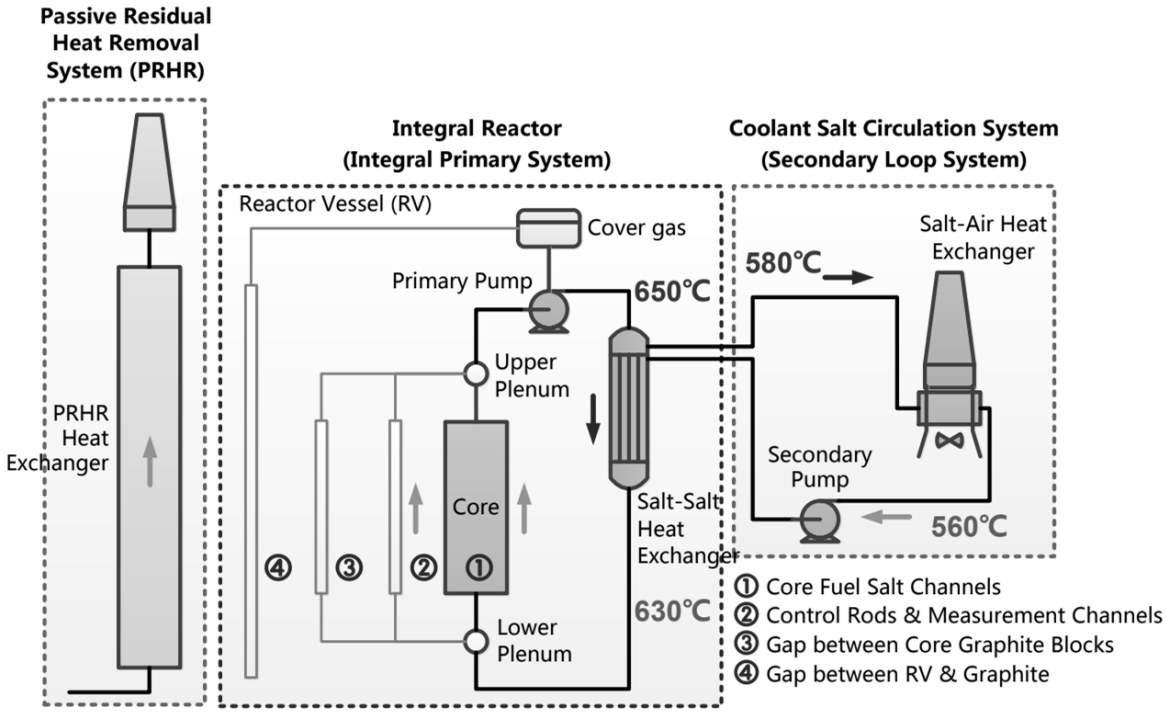

2.3.2. Mk1 PB-FHR (University of California in Berkeley, USA)

The University of California, Berkeley is researching and developing molten salt cooled pebble bed reactor with a Nuclear air-Brayton combined cycle (NACC) called Mark-1 Pebble-bed fluoride-salt-cooled, high-temperature reactor (Mk1 PB-FHR). Thanks to the NACC, the Mk1 PB-FHR can operate in two different modes. The first mode is the baseload mode, where a gas turbine is propelled solely by the nuclear reactor itself, producing 100 MWe. The second mode is the peak demand mode. In this mode, natural gas is cofired with high efficiency in order to deliver a peak power of 241 MWe.

All components of Mk1 PB-FHR are made to be transported by train. With its modular nature, it is proposed to be built as several units powerplant. The reference configuration contains twelve units on one site. This reference configuration could deliver 1200 MWe in baseload mode and 2900 MWe in peaks.

As almost all of the other molten salt reactors, the Mk1 PB-FHR uses FLiBe molten salt as a primary coolant. Primary coolant salt is cooled in the inhouse developed Coiled tube air heater (CTAH), where it heats compressed air. Compressed air is later utilized by a gas turbine in the open Brayton cycle. The reactor core vessel of Mk1 PB-FHR design is shown in Figure 17. As mentioned above, the design uses TRISO fuel in the form of pebble beds. These pebbles are smaller than those proposed for HTGRs (PBMR), have a different design with low-density graphite nucleus, the fuel annulus, and uranium enrichment of 19.9 wt% of ^{235}U. The safety of the Mk1 PB-FHR reactor is assured by negative fuel, moderator, and coolant temperature reactivity feedbacks; buoyant control rod system; shutdown blades; passive natural-circulation-driven heat transport; and many many more (Andreades et al., 2014, 2016; IAEA's ARIS, 2016a; "The Mark 1 Pebble-Bed Fluoride High Temperature Reactor," n.d.).

Figure 17

"The Mk1 PB-FHR reactor vessel." Adapted from Andreades et al. (2014), p. 16.

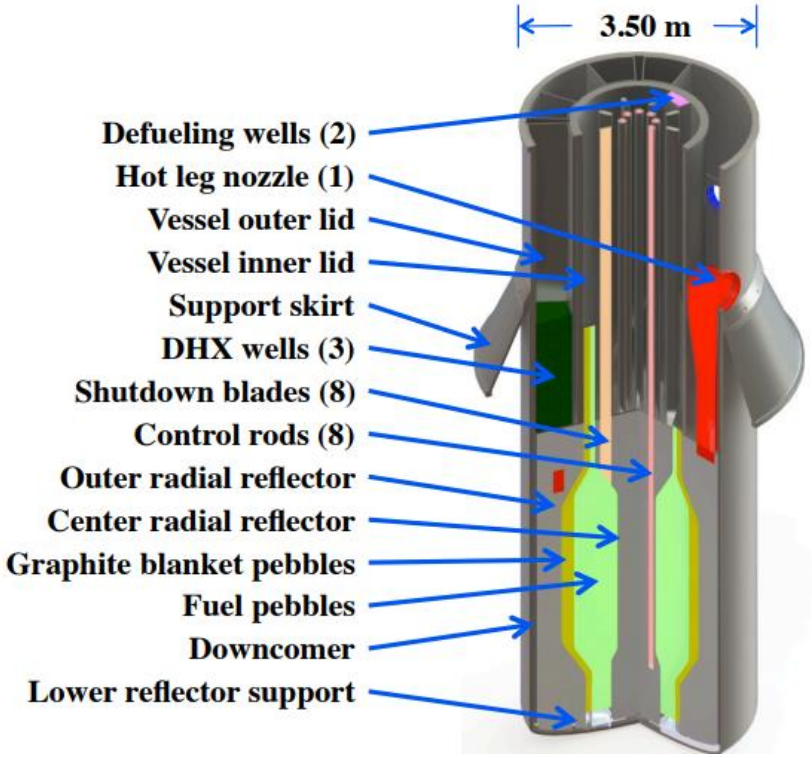

2.3.3. IMSR-400 (Terrestrial Energy, Canada)

Canadian company Terrestrial Energy is developing a molten-fuel salt-cooled reactor with an integral design called IMSR-400 (Figure 18). The company was established in 2013 and is based on the previous research of molten salt reactors at ORNL. The Terrestrial Energy completed Phase 1 of the Canadian Nuclear Safety Commission's (CNSC) Vendor Design Review in November 2017 and is now focusing on siting work at Canadian National Laboratories and discussion with US Nuclear Regulatory Commission (NRC) ("Terrestrial Energy Inc," n.d.).

Figure 18

"Rendering of the IMSR Core-unit." Adapted from "Terrestrial Energy Inc." (n.d.).

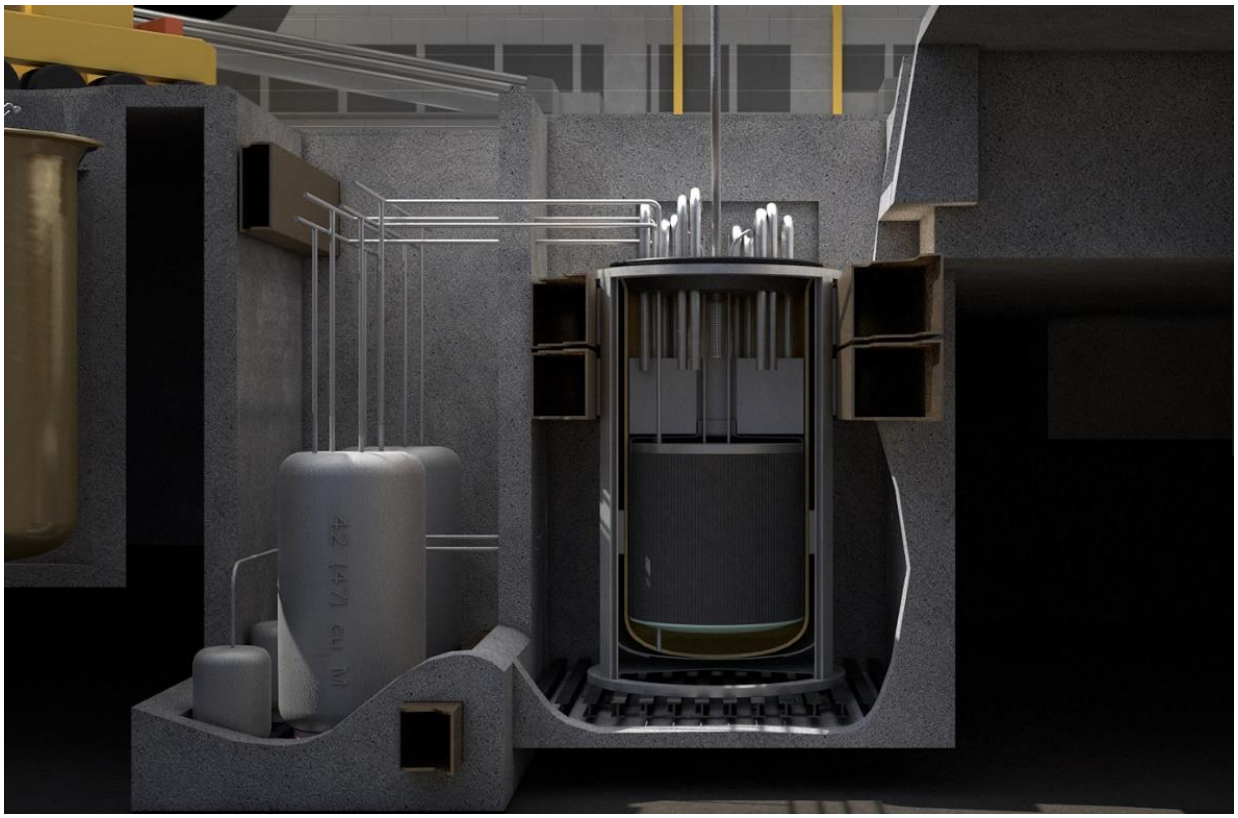

The Integral Molten Salt Reactor – 400 Megawatts-thermal (IMSR-400) is a small modular reactor with molten salt fuel. IMSR-400 uses a graphite moderator in order to achieve a thermal neutron spectrum. This concept has four different coolant loops. First is the reactor-vessel-only fuel loop with fluoride salt, then secondary coolant loop with fuel-free fluoride salt, connected to the intermediate loop of solar salt, and finally regular steam loop with a turbine. Figure 19 describes how the IMSR works and how the heat produced could be used.

The main characteristics of this reactor design are shown in Table 1. The safety of the reactor is assured by multiple safety mechanisms such as chemical stability of the fluoride salts containing fuel and fission products, passive heat removal, negative temperature feedback, and more. The main advantage of the IMSR-400 is its integral design. Integral design with a sealed reactor vessel allows to operate a power plant for seven years without refueling and other fuel/primary loop operations. After this period, the sealed vessel is taken back to the central facility for refurbishing or recycling. As it is mentioned in the IAEA Status report, "This sealed, integral reactor architecture ... allows the actual power plant site to always operate in a clean, simple environment without risk of facility contamination." (IAEA's ARIS, 2016b).

Figure 19

"IMSR: how it works diagram." Adapted from "Terrestrial Energy Inc." (n.d.).

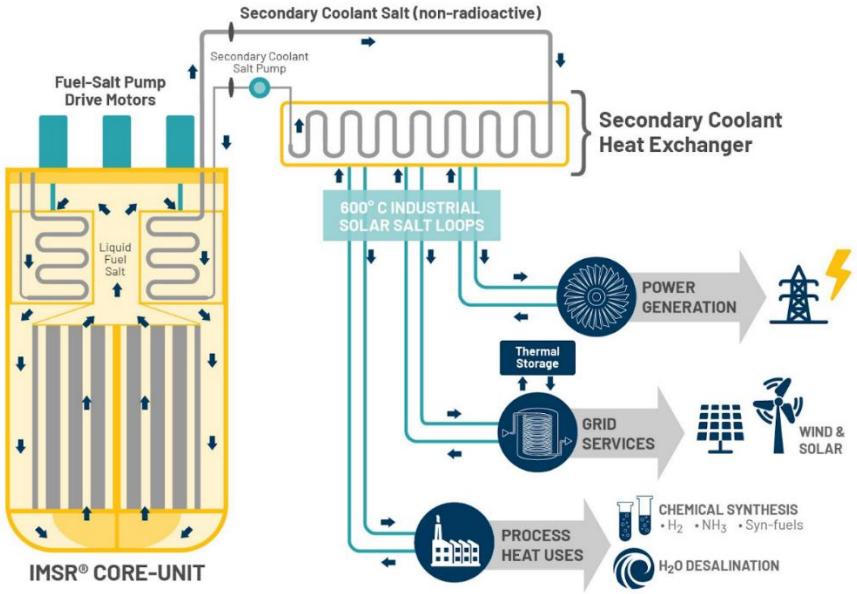

2.3.4. LFTR (Flibe Energy, USA)

The USA based company Flibe Energy was founded in 2011. Since then, it is developing a unique reactor concept named the liquid-fluoride thorium reactor (LFTR) and it is shown in Figure 20. LFTR utilizes the thorium fuel cycle with a highly neutron-efficient two-flow reactor core design. It operates in a thermal neutron spectrum, where graphite is the moderator. For power conversion, LFTR uses a closed supercritical CO_2 Brayton-cycle.

The basic characteristics of the LFTR design can be found in Table 1. As it was mentioned above, LFTR uses thorium fuel, which is one of the biggest advantages. Thorium is four times more abundant element in the Earth's crust than uranium, and it is usually a waste by-product of rare earth mining. The inherent safety of the reactor is based on low operational pressure, passive cooling, high-margins, and online fuel reprocessing ("Flibe Energy, Inc.," n.d.; IAEA's ARIS, 2016c; "Program on Technology Innovation," 2015).

Figure 20

"LFTR power plant concept rendering." Adapted from "Flibe Energy, Inc." (n.d.).

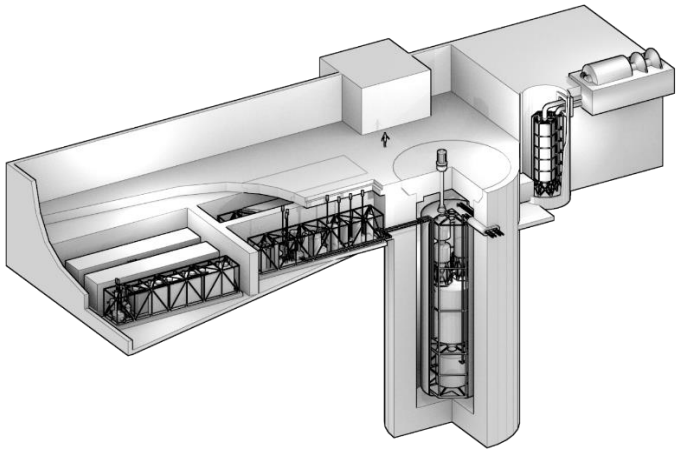

2.3.5. MSR-FUJI (International Thorium Molten-Salt Forum: ITMSF, Japan)

MSR-FUJI, in its version FUJI-U3, is a successor design of the Japanese MSR research originating in the 1980s and its previous designs mini-FUJI, super-FUJI, and FUJI-Pu. The MSR-FUJI design, in Figure 21, is developed under the umbrella of the International Thorium Molten-Salt Forum: ITMSF. The reactor itself operates in a thermal neutron spectrum and uses graphite as a moderator. Fuel, thorium and initial uranium, is dissolved in molten salt. This choice, together with the correct design, ensures the breeding capability of MSR-FUJI. The projected power output is 200 MWe (450 MWt).

Primary and secondary molten salts are FLiBe and NaF-$NaBF_4$, respectively. As the main construction material was chosen Hastelloy N. The safety of the reactor has several levels: shut-down control rods and graphite power control rod, fuel salt flow control system, fuel salt drain system, and fuel salt concentration adjusting system. Moreover, the power of the MSR-FUJI could be changed by temperature control by the turbine (IAEA's ARIS, 2016d).

Figure 21

"Schematic diagram of MSR-FUJI." Adapted from IAEA's ARIS (2016d), edited.

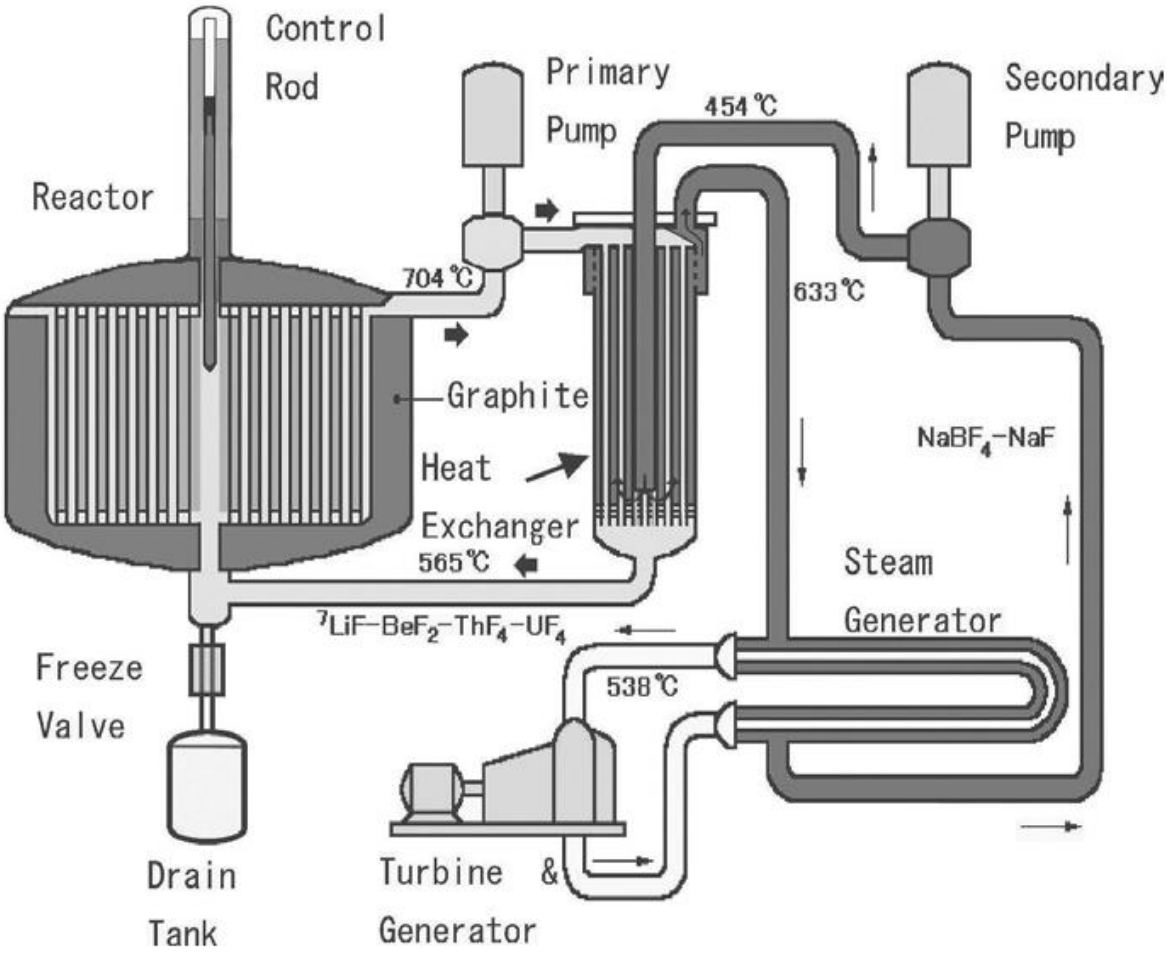

2.3.6. CMSR (Seaborg Technologies, Denmark)

The Danish company Seaborg Technologies is developing Compact Molten Salt Reactor (CMSR) design with a thermal neutron spectrum. CMSR (Figure 22) has single molten salt design and uses a combination of thorium and SNF as a fuel.

Similar to many other proposed molten salt designs of Gen IV, CMSR takes advantage of modular approach and mass production; off-site recycling; and SNF burning. It operates according to the optimal configuration principle, which results in either shutdown or coming back to a stable operating point after any disruption. Other safety mechanisms involve a freeze plug, active fuel chemistry, SCRAM system, and passive and active cooling systems.

In the CMSR, neutrons are moderated by the graphite. Graphite blocks are coated with a metal to reduce corrosion. CMSR design uses eutectic Sodium-actinide fluoride salt mixture. For reactivity control, there is a series of moderation rods around the edge of the reactor core. These rods are able to adjust the temperature within 200 °C (IAEA's ARIS, 2016e; "Seaborg Technologies," n.d.).

Figure 22

An early model of the CSMR underground cave. Adapted from Dolan (2017), p. 611.

2.3.7. Copenhagen Atomics Waste Burner (Copenhagen Atomics, Denmark)

Another Danish company, Copenhagen Atomics, entered the field of MSRs with its' project of Copenhagen Atomics Waste Burner (CAWB). CAWB is a single fluid molten fluoride salt thermal spectrum breeding reactor moderated by heavy water. This design differs greatly from other concepts introduced in this section. The difference is heavy water used as a moderator, instead of the commonly proposed graphite. The use of heavy water has many advantages and trade-offs, e.g., simple reactivity control, unlimited moderator lifetime, but also a potential for steam explosion.

Figure 23

"Illustration of the CA Waste Burner concept fitting into a 40-ft. container." Adapted from Dolan (2017), p. 602, edited.

However, similarly to other MSR designs, CAWB is supposed to be small and modular. As can be seen in Figure 23, it can be contained in a standard 40-foot shipping container. It also introduces some novel ideas such as reactivity control by heavy water moderator level adjustments; continuous passive draining and active pumping of the moderator as well as fuel salt; passive geothermal cooling (Figure 24); and a frozen thorium salt blanket shielding.

Copenhagen Atomics promotes fast technology cycles and rapid prototyping. Therefore parameters, functions, and the design as a whole might be changed heavily in the future ("Engineering the Future of Energy," n.d.).

Figure 24

"CA Waste Burner underground with decay heat removal pipes." Adapted from Dolan (2017), p. 603.

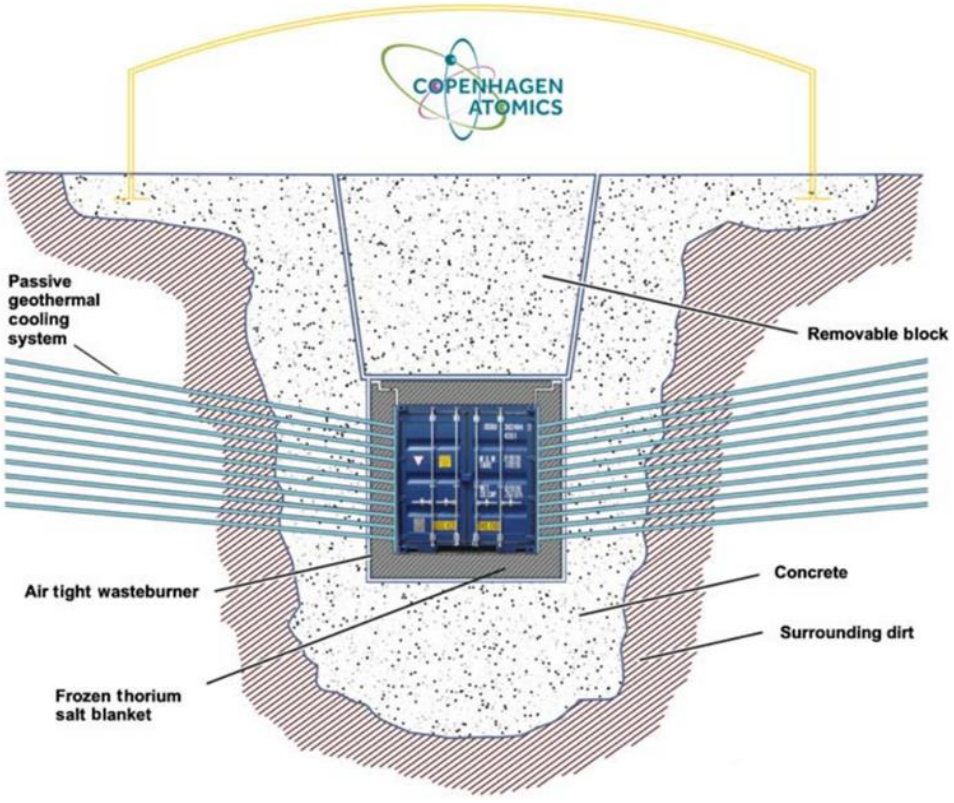

2.3.8. MSFR (CNRS, France)

One molten salt reactor design with a fast neutron spectrum comes from France, more specifically, it is proposed and developed by the National Centre for Scientific Research (CNRS) and is called Molten Salt Fast Reactor (MSFR). This research is supported by the Euratom's projects (MOST, ALISIA, and EVOL). The fast neutron spectrum of the reactor allows designers to avoid the use of graphite, the main lifetime limiting factor of other MSR designs.

The MSFR reactor (Figure 25) will operate in the thorium fuel cycle breeder regime with breeding salt contained in the reactor blanket, which will increase the breeding ratio. The MSFR is designed for the power output of 3000 MWt at the output temperature of 750 °C.

It is noteworthy that there are no structural components in the center of the reactor core – where the neutron flow is the highest. This design feature improves the reactor structural components lifetime expectancy and makes the whole reactor design simpler.

The safety of the MSFR is based on a passive salt draining system, a low core reactivity inventory, and the large negative feedback coefficients. Interestingly, no control rods are necessary for regular operation or accidents mitigation. Moreover, the freeze plug uses active cooling provided by a small electric fan. This fan is directly powered by the electricity produced by the reactor; therefore, the plug melts and let the salt drains into a subcritical tank whenever the reactor fails to provide electricity. (Heuer et al., 2014; Mathieu et al., 2006 & 2009, "MSFR - Laboratory of Subatomic Physics & Cosmology," 2019).

Figure 25

Schematic drawing of the MSFR reactor design. Adapted from Pioro (2016), p. 159.

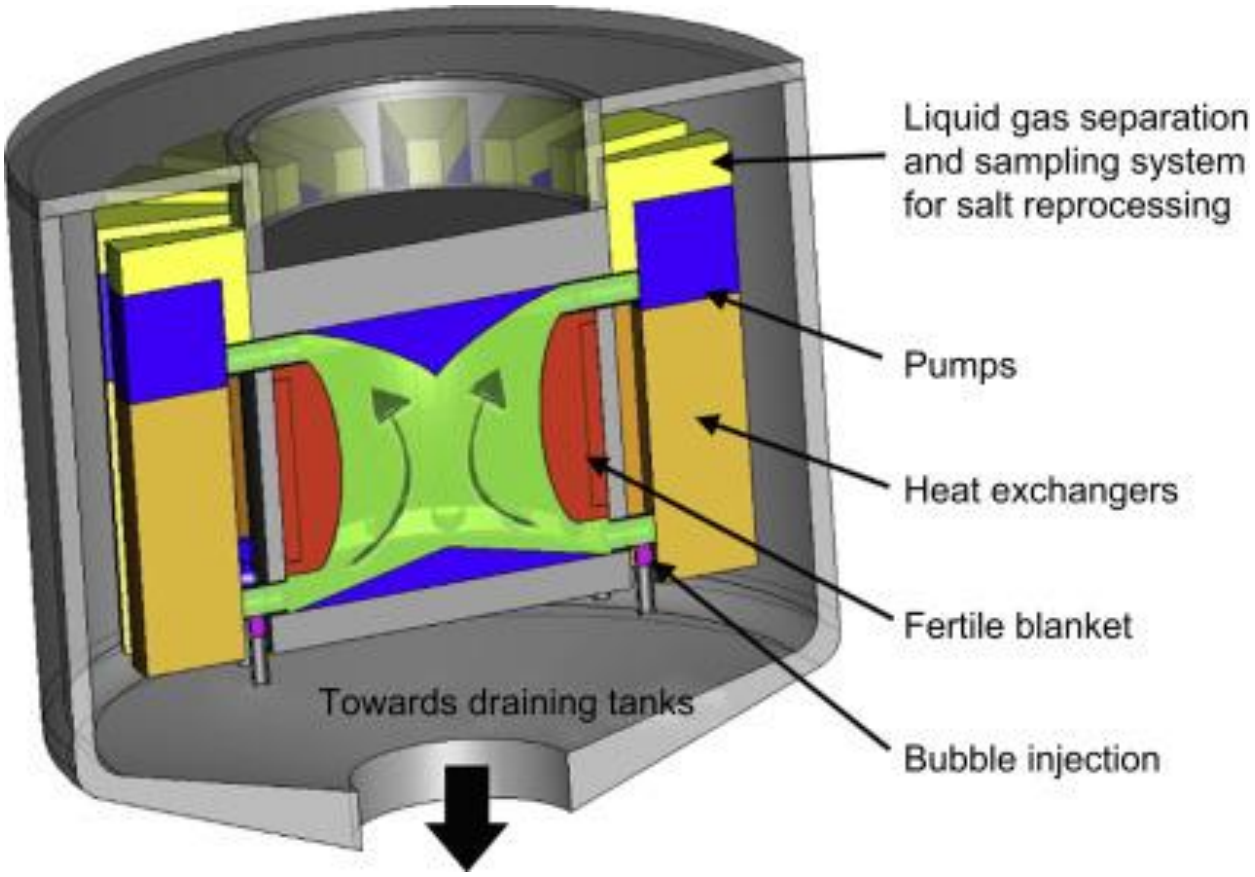

2.3.9. SSR-W/TS (Moltex Energy, United Kingdom)

Another molten salt reactor design with a fast neutron spectrum comes from UK based company Moltex Energy and is called Stable Salt Reactor - Wasteburner (SSR-W), shown in Figure 26. The fast neutron spectrum of the reactor allows designers to avoid the use of graphite, the main lifetime limiting factor of other MSR designs. It is proposed together with Stable Salt Reactor - Thermal Spectrum (SSR-TS) in order to achieve high electricity production with possible thorium cycle, and also to reduce the long-lived actinides in the SNF. As the name suggests, SSR-TS operates in a thermal neutron spectrum that is achieved with a graphite moderator. However, the use of graphite moderator is not a limiting factor in this case, due to the fact that graphite moderator is included in fuel assemblies themselves.

Another advantage of both Moltex Energy SSR designs is the use of static fuel form. This ensures safety, similar to all molten salt reactors, without the need for managing a mobile liquid fuel. Because of the use of static fuel, fuel assemblies might be operated as regular PWR assemblies. However, thanks to the fact that both SSR-W and SSR-TS, operate at the atmospheric pressure, online refueling can be done.

SSRs use NaCl-$PuCl_3$-UCl_3 fuel salt contained in fuel tubes and sodium potassium zirconium fluoride salt as primary and secondary coolant. The tertiary coolant is sodium potassium nitrate salt ("solar salt"). The tertiary coolant system has storage tanks that might be used to balance the power plant output with the grid. This storage-balance system makes SSRs a great partner for renewable sources (Moltex Energy, 2018; "Moltex Energy," 2020).

Figure 26

"Section through the SSR-W module." Adapted from Moltex Energy (2018), p. 11, edited.

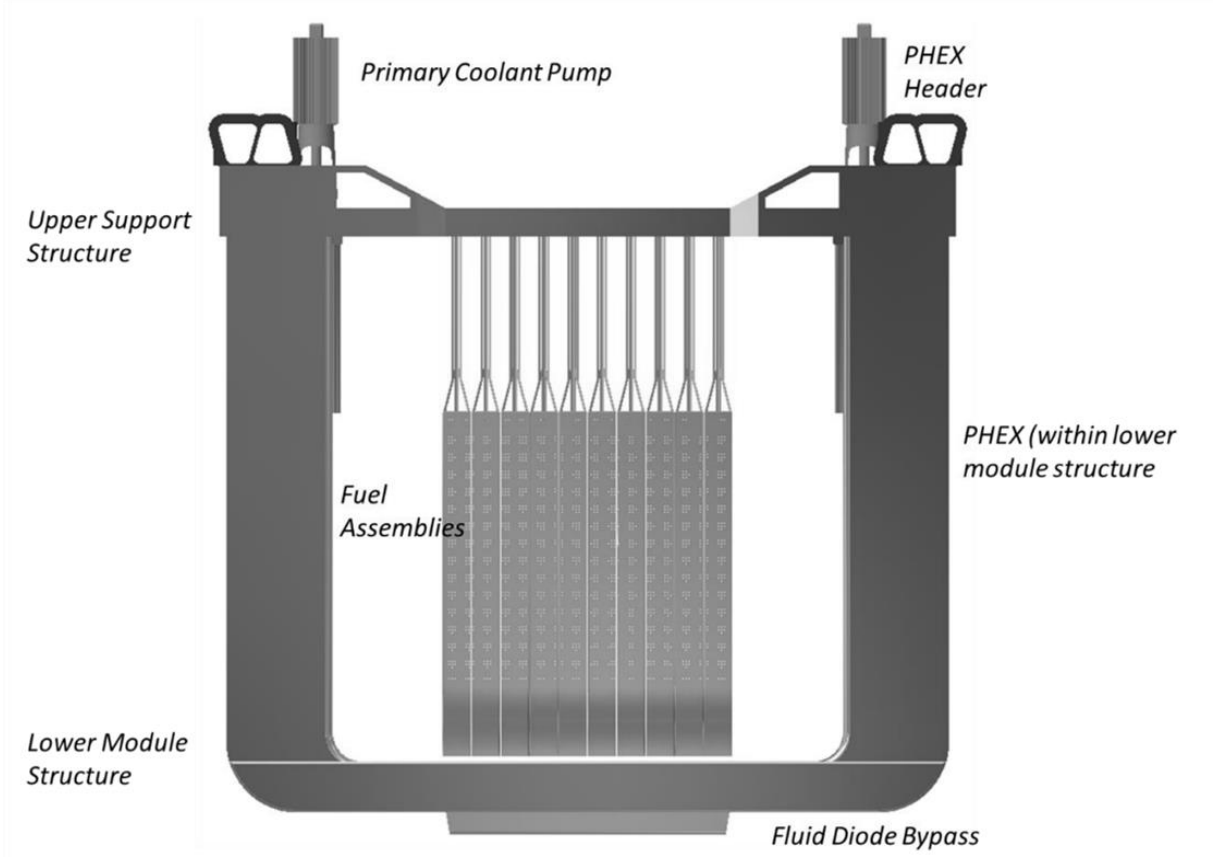

2.3.10. ThorCon (ThorCon Power, USA)

ThorCon design (Figure 27) by ThorCon Power is a regular molten salt small modular reactor with liquid fuel based on a combination of Th-bred ^{233}U and low-enriched (less than 20 %) U-235 within sodium – beryllium fluorides. The whole primary loop, including the reactor vessel called Pot, header tank, the primary loop pump, and the primary loop heat exchanger, is encapsulated in a larger Can container. The Can serves many purposes such as on- and off-site transporting before and after 4+4 years fuel cycle; radioactive release barrier; partial passive decay heat removal; and more.

The main advantages of ThorCon design are its black start capability and decay heat removal system. The black start capability is ensured by a 15 MW Sentry turbogenerator (TG). This TG is able to deliver power during reactor start-up, and also to ensure safety during station blackout. During a station blackout, the Sentry TG will be supplied by decay heat steam long enough to maintain coolant circulation until the auxiliary boiler is brought to the operation.

Decay heat removal is secured by the decay heat removal system using a pond and silo-cooling wall. This system allows to reject the heat via Can silo wall and the off-gas system during both regular operations and in the event of a shutdown. During normal operation, pond water is pumped to sprayers in the cooling towers. In the case of a station blackout, the cooling towers will operate by natural convection (IAEA's ARIS, 2016f, "Powering up our world," n.d.).

Figure 27

"Cutaway view of two module Silo Hall." Adapted from The ThorCon Team (2018), p. 6.

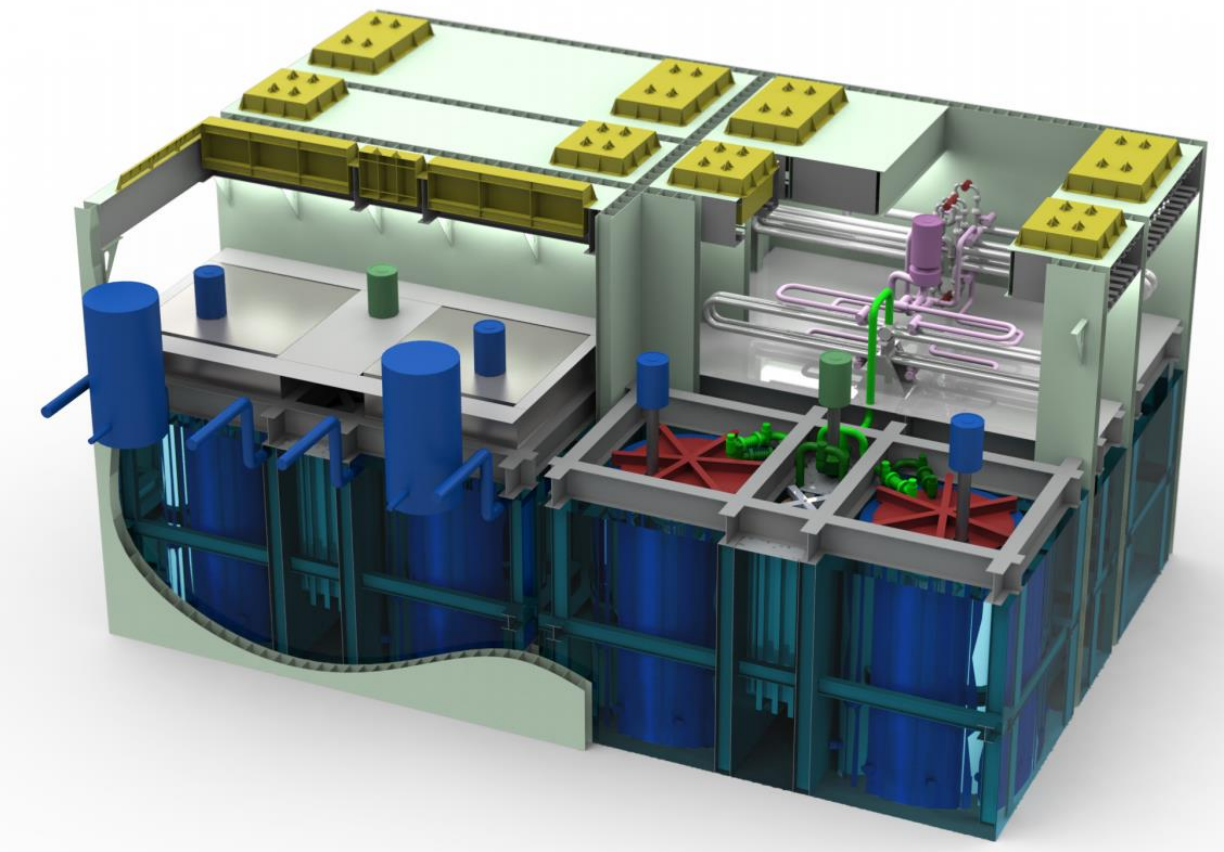

2.3.11. KP-FHR (Kairos Power, USA)

The Kairos Power, a California based startup company, claims to aim to "enable the world's transition to clean energy, with the ultimate goal of dramatically improving people's quality of life while protecting the environment." ("The Future of Nuclear Power," n.d.) It was founded by nuclear experts from UCB building upon knowledge gained by the research of the Fluoride High-temperature Reactor (FHR) concept and Mark1 PB-FHR. UCB has been working on these concepts in cooperation with MIT and the University of Wisconsin-Madison since 2011. In November 2018, the Kairos Power started pre-application interactions with US NRC.

The Kairos Power fluoride salt-cooled high temperature reactor (KP-FHR) shows similar features as UCB's Mk1 PB-FHR, such as thermal neutron spectrum, Pebble-bed TRISO fuel, molten salt coolant, and passive safety mechanisms; however, in contrary it uses nitrate salt as an intermediate coolant and readily-available steam turbine. The reactor vessel, primary, secondary, and tertiary loops are shown in Figure 28.

The proposed parameters of KP-FHR are shown in Table 1. It uses FLiBe primary salt, TRISO Pebble-bed fuel with an innovative design of small buoyant pebbles, and $NaNO_3$-KNO_3 (60-40 wt%) intermediate "solar" salt. The concept allows for online refueling. As a main reactor structural material will be used stainless steel 316 ("The Future of Nuclear Power," n.d., Hastings, 2018).

Figure 28

Picture of KP-FHT. Adapted from "The Future of Nuclear Power" (n.d.), edited.

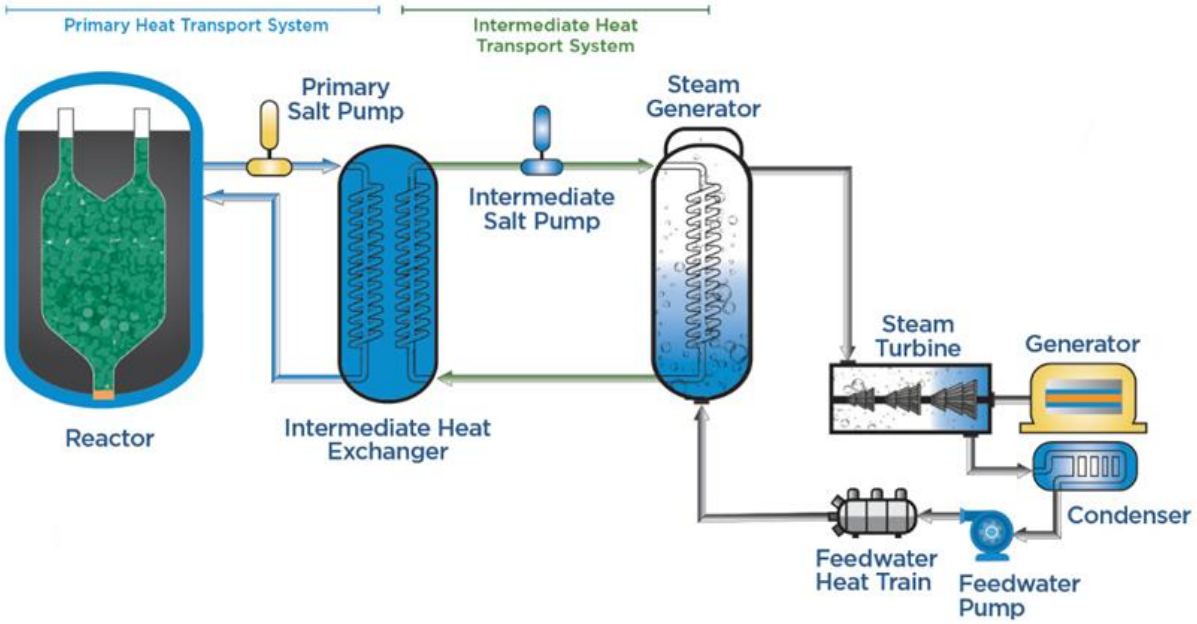

2.3.12. Energy Well (Research Centre Řež, Czech Republic)

Energy Well is a design of a small modular reactor with prismatic TRISO fuel cooled by FLiBe molten salt. This project is developed by Research Centre Řež, a company based in the Czech Republic. The idea was revealed during the SMR 2018 (Small Modular Reactors) conference in Prague, Czech Republic.

The primary loop is cooled by a secondary – intermediate – loop of NaF-$NaBF_4$ molten salt. For electricity generation is responsible a supercritical CO_2 Ericson-Brayton cycle, either simple or with regeneration or recompression. For the safety of the reactor, there are various passive and active systems, such as control and safety rods, passive shutdown capsules, natural convection heat removal accident system, strong negative reactivity change in case of cooling salt leakage to the primary loop, and more. The passive shutdown capsule is an innovative feature. It is located within the primary circuit and melts down when a threshold temperature is reached while releasing $NaBF_4$ absorber to the core. Currently, researchers and engineers are preparing a design for the mock-up test facility with a longer-term plan for a demonstration unit and a first of a kind reactor (Centrum výzkumu Řež, n.d.; Kolektiv ÚJV Řež a.s. a CVŘ, 2018; Ruscak, M., 2019, 2020).

Fuel assemblies and reactor core. Energy Well fuel assemblies (Figure 29) have hexagonal shape divided by graphite support structure into three segments. In each segment, there are layers of fuel plates and coolant channels. Moreover, coolant flows not only in coolant channels within fuel assemblies but also between the fuel assemblies themselves.

The reactivity is controlled by control rods with B_4C absorbers. In the Energy Well design, there are two types of control rods, regulation and safety rods. Regulation rods are situated within each fuel assembly; whereas, safety rods are situated within the radial reflector. During the regular operations, safety rods are fully pulled out - ready to fall down and stop the reaction.

Primary circuit. Energy Well is a pool-type reactor, and the primary cooling circuit consists of these main parts: reactor core, reactor vessel, graphite reflector, and heat exchangers. The FLiBe molten salt flows upward through the core and enters the heat exchangers located above the core. From there, the molten salt is pushed downward by the main circulation pumps, which are placed above each heat exchanger. The primary circuit is encapsulated within a container that can be shipped on a road or rails.

Secondary circuit. The main purpose of the intermediate secondary circuit is to create a barrier between the primary and tertiary circuit. The secondary circuit includes salt/salt heat exchanger, salt/sCO_2 heat exchanger, circulation pump, and auxiliary systems. The main criteria for choosing a secondary circuit medium is solidification temperature because lower solidification temperature results in higher thermal efficiency. When the main and other criteria are applied, NaF-$NaBF_4$ molten salt seems like the best option. However, this salt has not been studied as extensively as FLiBe and other salts.

Figure 29

Partial cross-sectional view on Energy Well fuel assembly. Adapted from Losa et al. (2017), pg. 3, edited.

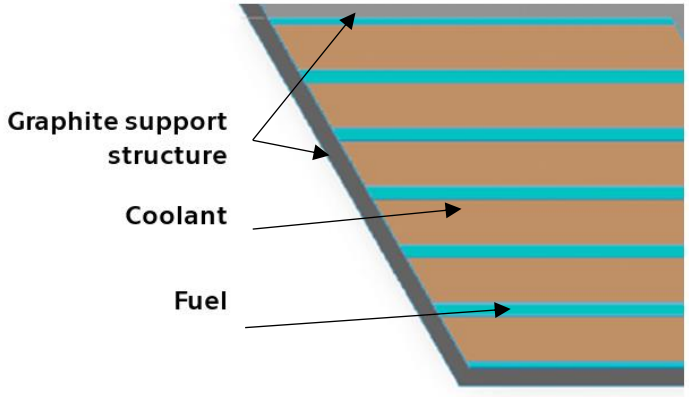

3. Molten Salts

One of the key parts of molten salt reactor designs are fuel and cooling salts. Salts generally are chemical compounds made of acid and alkali. At room temperature, salts are commonly in transparent crystalline form, and in the liquid, transparent form at high temperatures (Figure 30) (Holcomb & Cetiner, 2010). Many different salts exist based on a combination of acid and alkali.

For potential candidates, many important properties are required; among others they are high boiling point, low vapor pressure, high thermal conductivity, high density at low pressures, and low price. There is a long history of molten salt research (Kelmers et al., 1976; Williams, 2006a; Williams, 2006b). Most of it was done by ORNL during the 1960s and the 1970s when the research of ARE, MSRE, and MSBR was ongoing (more in the chapter 2.1).

There are three main types of molten salts that are considered for use in molten salt reactors: fluoride, chloride, and nitrate salts. This paper focuses mainly on fluoroboric-fluoride salts as the main candidates for the secondary loop coolant salts at this time, and the comparison with fluoride salts, which are of the highest interest for the primary loop (Cantor et al., 1968).

Figure 30

FLiBe fuel salt in a solid and liquid form. Adapted from Sorensen (2018), p. 6.

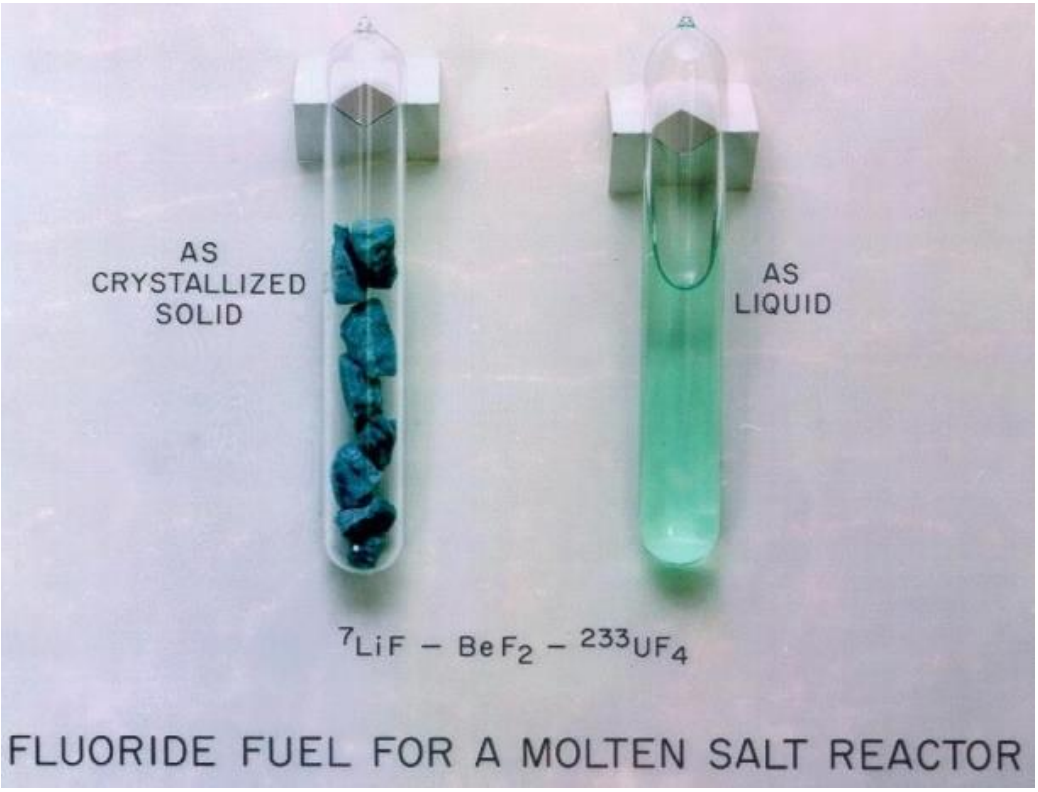

3.1.NaF-NaBF4

The first salt described in this paper is a eutectic mixture of sodium tetrafluoroborate and sodium fluoride. The eutectic composition for NaF-$NaBF_4$ is 8-92 mol%, with a eutectic temperature of 384 °C. A phase diagram showing melting temperatures could be seen in Figure 31. The biggest advantages of this eutectic mixture are low freezing point, high heat capacity, low viscosity, and low cost. All the important physical properties are summarized and compared with other salts in Table 2.

NaF-$NaBF_4$ molten salt was considered as a prime candidate for NGNP/NHI Heat-Transfer Loop. However, due to its main disadvantage, high decomposition pressure at 900 °C, it was recommended to be ruled out. In the case of this thesis, targeted temperatures are 550 °C and 700 °C. It allows us to reconsider the potential of NaF-$NaBF_4$ within these scenarios, and make a suggestion for these mid to mid-high temperatures (Williams, 2006b).

Figure 31

"Binary phase diagram of NaF-$NaBF_4$ system." Adapted from Williams (2006b), p. 4.

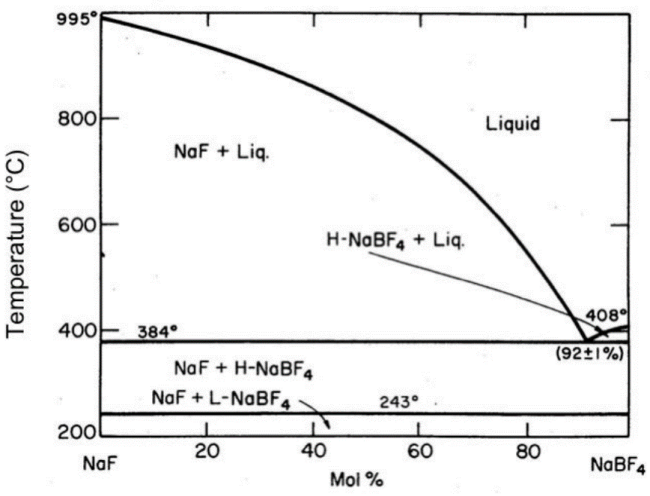

3.2.KF-KBF_4

The biggest competitor for NaF-$NaBF_4$ within secondary loop coolant salts, appear to be KF-KBF_4. The eutectic composition for KF-KBF_4 is 25.5-74.5 mol%, with a eutectic temperature of 460 °C. Even though it has a higher freezing point and a lower heat capacity, KF-KBF_4 is highly superior to NaF-$NaBF_4$, with almost a hundred times lower vapor pressure at 900 °C. The binary phase diagram of the KF-KBF_4 system is shown in Figure 32.

Figure 32

"Binary phase diagram of KF-KBF_4 system." Adapted from Williams (2006b), p. 4.

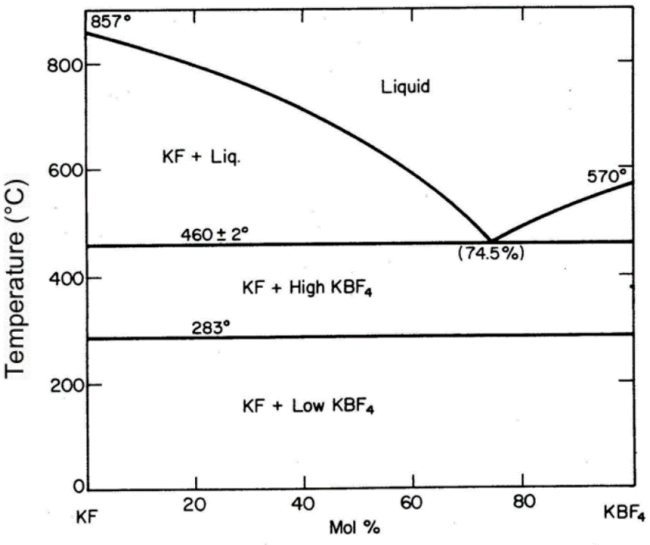

3.3.FLiBe

Arguably, the most researched and the most promising salt for nuclear application is the eutectic composition of LiF-BeF_2 (66-34 mol%), often called FLiBe. It has been used in the first molten salt reactor experiments at ORNL, as mentioned in the chapter 2.1. Its eutectic temperature lies at 459 °C.

Properties that predetermine FLiBe molten salt to be the main focus for molten salt reactor research are high heat capacity, high thermal conductivity coefficient, high boiling point, and great neutron moderation ability.

Natural lithium consists of two stable isotopes ^{6}Li (7.59 %) and ^{7}Li (92.41 %). ^{6}Li isotope has a quite high microscopic cross-section of neutron reaction versus ^{7}Li. The total neutron cross-section of ^{6}Li is 150 barns for the energy of 1 eV and 1 barn for ^{7}Li at the same energy of 1 eV (The Nuclear Energy Agency, n.d.). Therefore, ^{7}Li enrichment is important for primary loops in order to lower neutron interactions, mainly the tritium production. However, this fact is unimportant for secondary loops where no enrichment is required.

Cons of FLiBe are a higher melting point with comparison to NaF-$NaBF_4$, higher price, and beryllium toxicity (Stefaniak, 2011; Strupp, 2011a; & Strupp, 2011b).

3.4.FLiNaK

In the beginning, this mixture of LiF-NaF-KF (46.5-11.5-42 mol%), often referred to as FLiNaK, was developed as primary loop salt. However, because of her poor neutronic properties, it was dismissed as primary loop salt and is only researched as secondary loop salt. Most of its properties are similar or worse than FLiBe.

Table 2

Physical properties of NaF-$NaBF_4$, KF-KBF_4, FLiBe, and FLiNaK salts (Cornwell, 1971; Petroski, 2006; Sohal et al., 2013; & Williams, 2006b).

		NaF-$NaBF_4$	KF-KBF_4	FLiBe	FLiNaK
Composition	mol %	8-92	25.5 - 74.5	66-34	46.5 - 11.5 - 42
Composition	wt %	3-97	13-87	53-47	29-12-59
Melting Point	°C	385	460	460	454
Density	g/cm^3	1.754	1.696	1.940	2.020
Heat capacity	cal/g-°C	0.360	0.312	0.577	0.48
Volumetric heat capacity	cal/cm^3-°C	0.632	0.529	1.16	0.96
Viscosity	cP	0.90	0.90	5.6	2.9
Thermal conductivity	W/m-°C	0.40	0.38	1.0	0.92
900 °C vapor pressure	mm Hg	9500	100	-	0.5

4. Materials

Molten salt, with its corrosiveness and high temperature, is a challenging environment. Common stainless steels are usually not a good choice for fluoride-based molten salts. Stainless steel cannot produce a passivation layer within the molten salt environment to stop or slow down corrosion. Thus, special construction materials must be chosen carefully. One of the purposely designed materials is Hastelloy N. Hastelloy N was developed during the pioneering beginnings of MSR research at ORNL. It is based on nickel with molybdenum and chromium, as well as most of the other promising materials. However, some stainless steels with higher concentrations of nickel might prove themselves useful. For further read about MSR construction materials, please refer to Yvon (2017).

4.1.Stainless Steel 316L

Stainless steel 316L (UNS S31603, W. Nr. 1.4404) is molybdenum-bearing austenitic stainless steel with a high content of chromium and nickel. SS 316L has excellent weldability and high-temperature resistance, as well as good strength, creep resistance, and corrosion resistance.

Common applications of SS 316L include automotive and aerospace industry, chemical processing equipment, marine constructions, medical implants, and pollution control equipment ("316/316L Stainless Steel," n.d.; Bell, 2019; "Stainless 316, 316L, 317, 317L," n.d.).

4.2.Stainless Steel EUROFER 97

EUROFER 97 – the European reference material for the first wall of a DEMO fusion reactor – stainless steel is the result of more than two decades of research and development (Rieth et al., 2003). It began as the research of Nb-free steel, Martensite (steel) for the Next European Torus project, and continued as the low activation steels research (OPTIFER, F82H-mod).

The main purpose of EUROFER 97 (Figure 33) is its use as a material for the first wall of a DEMO fusion reactor. Because of this specific targeted use, EUROFER 97 has a very low concentration of Nb, Ni, and other elements, which would result in high activity. Thanks to this composition, it can be considered as low-level radioactive waste after the use in a fusion reactor (Rieth et al., 2003).

Figure 33

"Blocks of Eurofer97 alloy steel." Adapted from "NRG irradiates steel alloy for use in ITER" (2019).

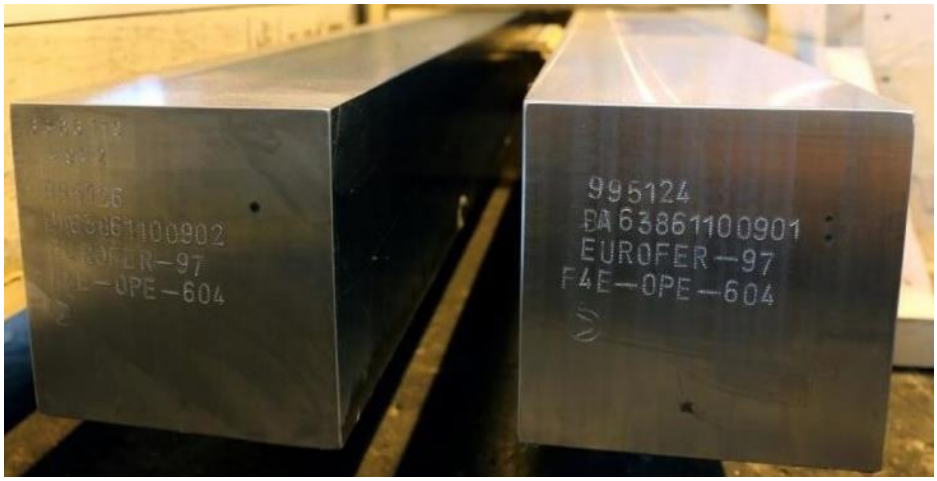

4.3.Monel Alloy 400

Alloy 400 (UNS N04400, W. Nr. 2.4360) is a nickel-copper alloy with manganese and iron. It possesses a slight magneticity at room temperature. Alloy 400 has good strength, toughness, and general corrosion resistance. However, it shows excellent resistance in flowing salt and brackish water, and also in an environment of hydrochloric and hydrofluoric acids. Alloy 400 can be hardened only by cold working.

Common applications of Alloy 400 includes crude oil distillation towers, marine components such as propellers and pumps, salt production, the nuclear industry (manufacture of shaft refining and isotope separation), eyeglass industry, chemical plants, gasoline and water tanks, and deaerating heaters ("Alloy 400 Tech Data," n.d.; "Monel 400 - UNS N04400." n.d.; "Monel alloy 400," n.d.; "Monel Alloy 400 Nickel Alloy," n.d.).

4.4. Incoloy 800HT

Incoloy 800HT (UNS N08811, W. Nr. 1.4959) is an iron-nickel-chromium alloy gradually developed since the 1960s for high-temperature use. Incoloy 800HT has high creep rupture strength and can be easily cold-worked and welded. Incoloy 800HT is sometimes referred to as Ferrochronin 800, Nickelvac 800, or Nicrofer 3220.

As it was mentioned above, Incoloy 800HT finds its various uses throughout many high-temperature applications. Specifically, it includes ethylene pyrolysis, hydrocarbon cracking, petrochemical industry, heat exchangers, chemical plants, heat treatment furnaces and valves, fittings, and other components in a high-temperature corrosive environment ("Alloy 800H/HT," n.d.; "Incoloy 800 Advanced Nickel Alloy," n.d.; "Incoloy 800H/HT," n.d.; "Super Alloy Incoloy 800HT," 2012).

Table 3

Mechanical properties of chosen alloys (Ignatiev & Surenkov, 2013; Ignatiev et al., 2008; "Inconel alloy 600," n.d.; "Inconel alloy 625," n.d.; Koukolikova et al., 2018; Mergia & Boukos, 2008; "Monel alloy 400," n.d.; "Monel Alloy 400 Nickel Alloy," n.d.; Rieth et al., 2003; "Specification Sheet: Alloy 800H/800HT," n.d.; "Stainless 316, 316L, 317, 317L," n.d.; "Super Alloy Incoloy 800HT (UNS N08811)," 2012).

Property	Unit	316L	EUROFER 97	Incoloy 800HT	Inconel 600	Inconel 625	MoNiCr	HN80MTY
Density	g/cm3	6.1	6.1	6.1	7.1	7.1	-	-
Mean Coefficient of Thermal Expansion	m/m*K *10^{-6}	16.5	12.23	14.4	10.4	12.8	-	-
at temperature	*°C*	*20 - 100*	*20 - 100*	*20 - 100*	*20*	*93*	-	-
Thermal Conductivity	W/m*K	14.6	27.1	11.5	14.9	9.8	-	-
at temperature	*°C*	*20 - 100*	*22*	*20 - 100*	*20*	*21*	-	-
Modulus of Elasticity (Young)	GPa	18.7	-	196.5	1.8	25.7	-	-
at temperature	*°C*	*20*	-	*100*	*22*	*21*	-	-
Tensile Strenght (Ultimate Stress)	MPa	29.5[a]	1.11[b]	13.7[b]	550 – 725[c]	827 – 1034[d]	29.1[e]	10.3[b]
Yield Strenght (0.2 % Offset)	MPa	23.7[a]	21.7[b]	6.9[b]	203 – 345[c]	414 – 655[d]	24.5[e]	25.3[b]
Hardness	-	217[a, f]	13.3 HV30[b,g]	30.3[h]	65 – 85[c,f]	145 – 220[d, h]	139 HV10[b, g]	148 HV10[b, g]

[a]minimum for annealed plate
[b]annealed
[c]annealed hot-rolled plate
[d]annealed plate
[e]state of Škoda delivery as referred at Ignatiev et al. (2008)
[f]Rockwell
[g]Vickers
[h]Brinnel

4.5. Inconel 600

Inconel 600 (UNS N06600, W. Nr. 2.4816), sometimes referred to as Nickelvac 600 or Ferrochronin 600, is a nickel-based alloy with a high percentage of chromium and iron. Inconel 600 is a nonmagnetic, high-temperature alloy with a great resistivity to many corrosive materials. It has excellent mechanical properties, high strength, and good hot and cold workability. On the other hand, Inconel 600 is vulnerable to sulfur attack and is not recommended to use in oxidizing sulfur, reducing sulfur, or molten metal (Cu, Zn, or Mg) environment.

A common use of Inconel 600 alloy includes furnace trays, mufflers, hangers, heaters, stills, bubble towers, vegetable and fatty acid vessels, soap manufacture, engine and airframe components in aeronautics, nuclear reactors, and more. For the nuclear reactors purposes, the Inconel 600T specification has been developed ("Inconel 600 Tech Data," n.d.; "Inconel 600, UNS N06600," n.d.; "Inconel alloy 600," n.d.).

4.6. Inconel 625

Inconel 625 (UNS N06625, W. Nr. 2.4856), also known as Chornin 625, Altemp 625, or Nickelvac 625, is a nickel-based alloy with a high percentage of chromium, molybdenum, and iron. Inconel 625 possesses similar properties as above mentioned Inconel 600, such as high-temperature resistance and chloride ions stress-corrosion cracking resistance.

Inconel 625 alloy is commonly used as heat shields, furnace hardware, chemical plant hardware, aircraft thrust-reverser systems, electrical cable connectors and fasteners, reactor-core and control-rod components in nuclear reactors, in gas turbines, submarines, and other special seawater applications ("Inconel 625 Tech Data," n.d.; "Inconel alloy 625," n.d.; "Premium Grade Inconel 625," n.d.).

Table 4

Chemical composition of chosen alloys as referred in the literature ("316/316L Stainless Steel," *n.d.*; *Ignatiev et al., 2008;* "Incoloy 800 Advanced Nickel Alloy," *n.d.;* "Inconel alloy 600," *n.d.;* "Inconel alloy 625," *n.d.; Podany et al., n.d.; Yvon, 2017).*

	316L	EUROFER 97	Incoloy 800HT	Inconel 600	Inconel 625	MoNiCr	HN80MTY
Fe	min 62	89	min 39.5	6 - 10	max 5	2.32	0.15
Ni	10 - 14	-	30 - 35	min 72	min 58	75	82
Cr	16 - 18	8.86	19 - 23	14 - 17	20 - 23	6.82	6.81
Mo	2 - 3	-	-	-	8 - 10	15.81	13.2
C	max 0.03	-	0.05 - 0.1	max 0.15	max 0.1	-	max 0.025
Mn	max 2	0.470	-	max 1	max 0.5	0.04	0.013
Cu	-	0.110	-	max 0.5	-	-	0.02
Si	max 0.75	0.16	-	max 0.5	max 0.5	-	0.04
S	max 0.03	-	-	max 0.015	max 0.015	-	-
Nb	-	-	-	-	3.15 - 4.15	0.01	0.01
Al	-	0.11	0.15 - 0.6	-	max 0.4	0.26	1.12
Ti	-	-	0.15 - 0.6	-	max 0.4	0.03	0.93
P	max 0.04	-	-	-	max 0.015	-	-
Co	-	-	-	-	max 1	-	-
W	-	1.08	-	-	-	0.06	0.072
V	-	0.21	-	-	-	-	-
Ta	-	0.32	-	-	-	-	-
N	max 0.1	-	-	-	-	-	-

4.7.Hastelloy N

Hastelloy N (UNSN10003), also known as INOR-8, is a nickel-based superalloy developed for containing molten salts. Originally, Hastelloy N was invented at ORNL during the molten salt reactor program in the 1960s. More information about MSRE can be found in chapter 2.1. Many other alloys developed for molten salts, such as Czech MoNiCr, Chinese GH3535, or Russian HN80MTY, are also based on Hastelloy N and are described in the following subchapters.

Hastelloy N has an excellent oxidation resistance in the environment of molten fluoride salts in up to 900 °C. It also shows good oxidation resistance in the air up to 1000 °C. It is the baseline for corrosion resistance measurements in molten salt environments for all the other alloys. Besides its oxidation resistance, Hastelloy N has good weldability and can be easily forged and formed. However, solution heat-treatment is recommended after hot or cold working ("Hastelloy N alloy," 2017; "Super Alloy Hastelloy N," 2013).

4.8.MoNiCr

MoNiCr, the nickel-based superalloy developed in the Czech Republic by COMTES FHT Inc. in collaboration with ŠKODA VÝZKUM, is the Czech version of high-temperature corrosion-resistant alloy for molten fluoride salt applications. The chemical composition is shown in Table 4, and it differs from Hastelloy N mainly by the amount of Fe, Mo, Mn, and Al with Ti.

The development of MoNiCr started in the year 2001, and since then, the main focus has been put on the activation of recrystallization processes in the cast structure and formability. Moreover, the technology for the manufacturing of basic shapes, such as ingots, sheets, wires, tubes, and profiles, has been proven. Similarly to Hastelloy N, MoNiCr superalloy shows good weldability, creep resistance, and oxidation resistance in the air and the environment of molten fluoride salts in high temperatures (up to 900 °C) (Koukolikova et al., 2018; Novy et al., 2011, 2015).

4.9.HN80MTY

HN80MTY, or by the other name K-50, is a Russian Ni-based alloy purposefully developed for molten salt reactors. It is based on the HN80MT alloy, which is a Russian version of Hastelloy N. The development from HN80MT aimed mainly to increase Te corrosion resistance and to increase resistance against selective Cr corrosion; therefore, HN80MTY is modified by Ti and Al (Ignatiev et al., 2016; Krejčí, 2017). The research and development of this superalloy has been conducted in the Kurchatov Institute, which is a leading Russian organization of nuclear research, based in Moscow.

4.10. GH3535

GH3535 nickel-based superalloy developed on the basis of Hastelloy N is the Chinese construction material for advanced reactor designs with molten salts. In 2011, GH3535 was chosen as the candidate material of TMSR in the "Advanced Nuclear Fission Energy" by the Chinese Academy of Sciences. The high alloying degree of GH3535 results in poor processability; however, the proper forming processes for hot extrusion, cold processing, heat treatment, and more have already been developed. Currently, this superalloy is used as the main construction material in the Chinese TMSR program (more in chapter 2.3.1) (Wang, M. et al., 2018; Wang, Y. et al., 2015 & 2018; Yvon, 2017).

5. Corrosion Mechanisms in Molten Salts

The corrosion is a great challenge in all high-temperature environments, and molten salts are not an exception; however, there is a difference in how to achieve corrosion resistance. In many other cases, the corrosion resistance is ensured by an oxidation layer on the surface of materials (Khanna, 2004). Unfortunately, any protective oxidation film is unstable and dissolved in molten salt systems.

The main driving forces for corrosion in molten salts are impurities in salts themselves such, as water and oxides; temperature gradient; and galvanic corrosion (Devan, 1969). Therefore, corrosion resistance in molten salt environments is achieved by carefully chosen structural materials, high-purity of construction materials, and strict control of molten salt composition.

As far as the literature suggests, molten salts are radiolytically stable, and the expected effect of radiolysis on corrosion is insignificant (Ignatiev & Surenkov, 2013; Sohal et al., 2013). However, the transmutation of Li and F can possibly produce H and O, which could increase the oxidation potential of the salt (Lantelme & Groult, 2013).

5.1. Thermodynamically-driven Corrosion

Thermodynamically-driven corrosion has a major impact on construction materials, especially at the beginning of the operation. It is driven by the difference of free energy of the alloying materials and salt constituents. Therefore, those elements with the higher free energy of new molecules formation are more affected. After some time, molten salt and structural materials should reach an equilibrium, which would result in no further corrosion based on thermodynamics.

In this paragraph, the example of fluoride salts is described. Free energies of some fluoride compound formations are listed in Table 5. As can be seen, fluorides used in the most common salts, such as $NaBF_4$, LiF, NaF, KF, and BeF_2, are at the top of the list. Alloying elements that are the most prone to attack follow, and they are Al, Mn, and Cr (Misra & Whittenberger, 1987). Mo, W, and Ni are most to the right of the table as the best elements to use, which is in the correspondence with compositions of some prior mentioned superalloys, namely Inconel 600/625, MoNiCr, Hastelloy N, GH3535, and HN80MTY.

Table 5

Gibbs free energies of formation of common fluoride compounds of salts and structural materials at temperature 1000 K (Forsberg, 2004; Wagman, 1981).

	$NaBF_4$	LiF	LiF	NaF	NaF	KF	KF	BeF_2	ZrF_4	AlF3	CrF_2	FeF_2	HF	WF_6	NiF_2	MoF_3
-ΔG [kcal/mol]	418[a]	147[a]	125	137[a]	112	135[a]	109	104	94	90	74	66	66	56	55	50

[a]at the temperature of 298 K

5.2. Impurity-driven Corrosion

Impurity-driven corrosion is another mechanism that plays a significant role in molten salt systems, mainly at the beginning of the operation. The most impactful impurities, which might be found in salts, are moisture, oxides, hydroxides, and metallic impurities. Corrosion caused by impurities has a major impact at the beginning, and later it is losing its importance with the depletion of impurities.

From impurities in the molten salts, the moisture is recognized as the most damaging. It reacts with constituents of molten salt (MeF) according to reactions:

$MeF\ (l) + H_2O\ (g) \rightarrow MeOH\ (l) + HF\ (g)$,

$2MeF\ (l) + H_2O\ (g) \rightarrow Me_2O\ (l) + 2HF\ (g)$,

forming a highly corrosive hydrofluoric acid, which attacks alloying elements (M) of construction materials:

$xM + yHF \rightarrow MxFy + y/2\ H_2$.

The way that metallic impurities, such as Fe, Ni, and Co, contained in the molten salt cause corrosion is that they deplete chromium, alloying element used in the most high-temperature corrosion-resistant alloys, via reaction:

$FeF_2 + Cr \rightarrow CrF_2 + Fe$,

and similarly with other elements. The experimental study has been performed in ORNL by Koger (1972a) to show this effect by adding FeF_2 to the molten salt.

In order to reduce impurity-driven corrosion, several techniques and treatments need to be incorporated. The purification process usually consists of several steps: a vacuum-drying to remove moisture; hydrofluorination to remove moisture, oxides, halides, and sulfur; and active metal treatment to reduce the oxidation potential of the salt, and remove hydrofluoric acid, moisture, and hydroxides (Anderson et al., 2015).

5.3. Thermal Gradient-driven Corrosion

Thermal gradient-driven corrosion is the most significant corrosion type in the later stages of any molten salt coolant system. The mechanism is based on the solubility difference of corrosion products at different temperatures; in higher temperatures, solubility is greater than in lower temperatures. Therefore, the corrosion products dissolved in hotter sections of the system are transported with the salt flow, and consequently, the dissolved corrosion products are deposited in the cooler section.

Extensive research has been done on this topic in ORNL (Koger, 1972a), such as nine years-long exposure of Hastelloy N in the thermal convection loop. The loop operated with $LiF\text{-}BeF_2\text{-}ZrF_4\text{-}UF_4\text{-}ThF_4$ (70-23-5-1-1 mol%) salt and temperatures of 700 °C in the hottest place and 560 °C in the coldest place. The results of this experiment show Cr and Fe mass transport according to the temperature gradient. (Koger, 1972b) Current research on corrosion driven by thermal gradient is conducted by the University of Wisconsin-Madison on their Natural Circulation Flibe Loop, which is in Figure 34 (Britsch et al., 2019).

Figure 34

Picture of the University of Wisconsin-Madison's Natural Circulation Flibe Loop. Adapted from "Natural Circulation Flibe Loop" (n.d.).

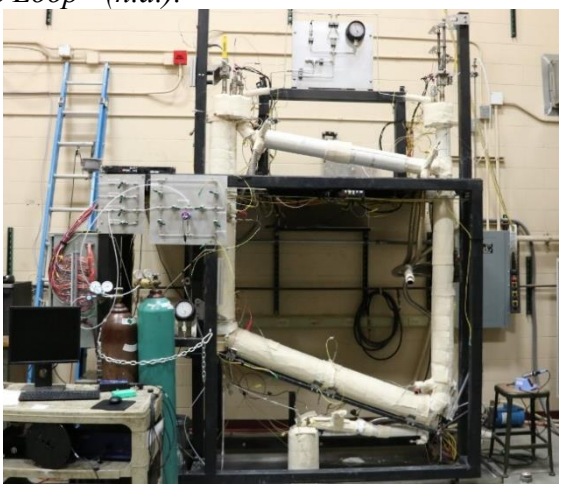

5.4. Activity-driven Corrosion

Activity-driven corrosion, also referred to as galvanic corrosion, is possible only if two or more different construction materials with the different activity of the dissolved species are present in the system. In that situation, dissolved species migrate from the material with higher activity to the material with lower activity. The most prone combinations of structural materials to this corrosion are those, where the low-activity material has a chemical affinity to dissolved species and can form thermodynamically favorable compounds.

However, the necessity for combinations of multiple construction materials in molten salt nuclear reactors is considerable; therefore, extensive research on this topic is ongoing. For example, Sellers (2012) shows dissolving of chromium from either stainless steel 316 or Hastelloy N specimens to LiF-NaF-KF (46.5-11.5-42 mol%) molten salt is followed by a formation of chrome carbide compounds on graphite. In another experiment, Sellers (2012) also finds, that stainless steel 316 and Hastelloy N in the same system with molten salt results in zirconium depletion in stainless steel 316 and consequential zirconium plating on Hastelloy N. Moreover, galvanic rankings for metals in molten salts have not been identified yet, in contrary with galvanic rankings in water and seawater systems, and further research is necessary (Lantelme & Groult, 2013).

6. Corrosion Tests

According to the current development status of Energy Well reactor design, when important neutronic, hydraulic, and thermal calculations of the primary circuit were done, construction material research is one of the priorities. The main focus has been heading towards materials for the primary loop, as described in the Master's thesis by Vlach (2019); however, the importance of materials for the intermediate loop is also recognized. Vlach's work is the predecessor of this Master's thesis and is an important source that guarantees continuity and standardized analysis, enabling future comparison.

Experimental setup and methods build on long experience of molten salt research within Fluoride salts research group of Research Centre Řež. As it is mentioned in chapter 2.3.12, the chosen salt for the intermediate circuit is NaF-$NaBF_4$. The NaF-$NaBF_4$ salt is not as well researched as FLiBe, and its corrosion effects need to be defined.

When choosing construction materials for corrosion test, these considerations were taken into account:

- which group particular alloy belongs to (stainless steels; Ni-based alloy with a higher concentration of Fe, or Ni-based superalloy with a low concentration of Fe);
- alloy development status (on-shelf alloy, alloy in development, or experimental alloy);
- alloy predisposition as described in the literature (high-temperature corrosion resistance, high corrosion resistance within the molten salt environment, and more);
- alloy availability.

The following alloys were chosen for tests:

1. Stainless steel 316L;
2. Stainless steel EUROFER 97;
3. Incoloy 800HT;
4. Inconel 600;
5. Inconel 625;
6. MoNiCr batch 17;
7. MoNiCr batch 18 sheet;
8. HN80MTY batch 17.

The MoNiCr and HN80MTY are experimental alloys or alloys in development and were supplied by COMTES FHT. They are also main adepts for construction materials of primary and secondary loops of the Energy Well project.

6.1.Specimens Preparation

The specimens of each alloy were prepared with the same methods ensuring minimal influence on experimental results. First, the specimens were obtained by cutting bigger pieces into similar samples with dimensions of approximately 30 x 15 x 1 mm. For cutting, the Struers Accutom-100 precise cutter with Aluminium oxide Cut-off Wheel 50A15, which is recommended for hard ferrous metals (HV 500 - 800 or lower), was used. The cutting speed was set up to 0.015 - 0.030 mm/s, depending on the material, with a rotation speed of 2500 rpm.

Afterward, specimens were ground using Struers Gekko PSA wet grinder with SiC Foil #500. SiC Foil #500 with a roughness of 500 particles per square millimeter is recommended for materials with a hardness of HV 30 - 800.

Before the beginning of an experiment, each specimen was measured twice in each dimension with Mitutoyo Digimatic caliper with a precision of ± 0.02 mm. The average dimensions, surface, and volume of each specimen were calculated (Appendix A: Dimensions, Volumes, and Surface Areas of Specimens.). Moreover, weight measurements were made with Precisa 125A scales (Appendix B: The Weight of Specimens) with a precision of ± 0.001 g.

Figure 35

Pictures of specimens and experiment preparation: a) Precisa 125A precise scales; b) ampules full of solidified NaF-$NaBF_4$ salt with specimens covered and prepared for a test; c) test glove box; and d) ampule after 720 h / 550 °C with leaked salt visible.

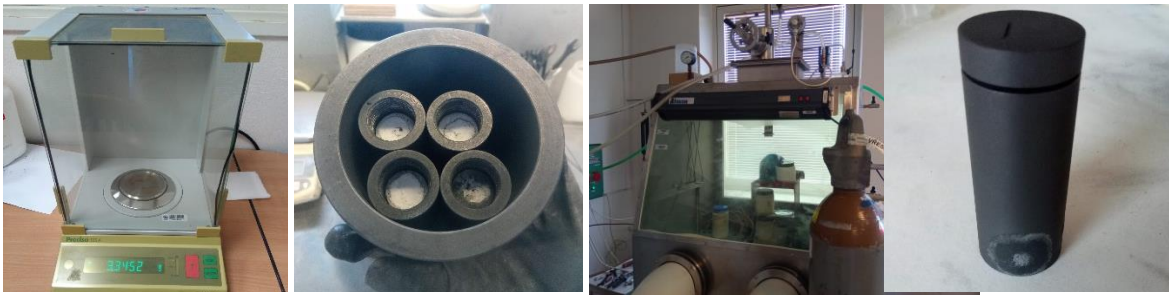

a) b) c) d)

6.2.Experimental Setup

In order to perform a test, firstly, the NaF-$NaBF_4$ salt was prepared by combining the exact amount of crystalline NaF (3 wt%) and crystalline $NaBF_4$ (97 wt%) to obtain the eutectic mixture. Approximately 250 g of the eutectic mixture was contained in a graphite crucible and put into CLARE 4.0 electric furnace at a temperature of 500 °C. After four hours, the NaF-$NabF_4$ eutectic mixture was melted and ready to be poured into ampules with specimens.

Into each graphite ampule (Figure 35), containing one specimen, approximately 30 g of molten salt was poured in order to cover the specimen completely. Afterward, ampules were let to cool down to room temperature. When cooled down, each ampule was inspected for a salt leakage, the level of salt, and any irregularities. Inspected ampules were closed and in groups of four put into a bigger crucible (Figure 35). The main purpose of the crucible is to catch molten salt during the

experiment in case of ampule salt leakage. Lastly, two crucibles with four ampules each were put into the electric furnace. The whole preparation, and consequently the test itself, was performed within the glove box with a nitrogen atmosphere.

Three tests were performed: 720 hours long test at a temperature of 550 °C (720 h / 550 °C), 720 hours long test at a temperature of 700 °C (720 h / 700 °C), and 2160 hours long test at a temperature of 550 °C (2160 h / 550 °C).

6.3. Specimens Cleaning

After the end of the experiment, the heating was turned down, and all the specimens with salt and ampules were let to cool down at the place. This cooling down to room temperature took approximately 48 hours. After cooling down, the ampules with specimens and solidified salt were taken out of the inert box.

Consequently, the specimens were taken out of the graphite ampules. Due to the uneven solidification of the salt within the ampules, some of the ampules were destroyed during the removing of specimens and salt. $NaBF_4$ salt did not stick to specimens as much as FLiBe salt; therefore, the specimens cleaning was rather easy and straightforward. Most of the salt was carefully separated from the specimen by hand or using brushes and scalps. The last cleaning step was ultrasound cleaning in demineralized water for approximately twenty-four hours. Cleaned and dried specimens were prepared for the first analysis.

6.4. Weight Measurement and Visual Inspection

As well as before the experiment, all the specimens were weighted, and pictures were taken. Weight measurements were made with Precisa 125A scales with a precision of ± 0.001 g (Appendix B: The Weight of Specimens). With before and after the experiment weight measurements and with size measurements done prior to the experiment, weight loss and weight loss per area were calculated (Appendix B: The Weight of Specimens and Corrosion Mass Losses). Visual inspection and comparison of specimens were performed, and pictures of all specimens were taken with a Cubot X19 phone camera to get an overall idea. For smaller details, specimens were inspected under the Leica DM 2700 M microscope with 5 Mpix camera and pictures with 4x zoom were taken. All the results are in Appendix D: Specimens Overview Pictures and Appendix E: Detailed Pictures of Specimens Taken with Microscope.

6.5. XRF Analysis

For the general chemical surface composition of specimens, Energy Dispersive X-ray Fluorescence analysis (XRF) was done using Thermo Scientific ARL QUANT'X spectrometer. Specimens were held by 4 μm thick proline thin-film (cat. no. 416) with typical impurities of Ca, P, Fe, Zn, Cu, Zr, Ti, Al. The chosen spectrometer setup was 8.8 mm collimator, eight different filters assuring range from Mg to Es, and factory-ready Kappa list template "MetalAir". For each specimen, the measurement was done for both sides and 60 seconds for each out of eight filters.

Software used for data acquisition was Acquisition Manager by Thermo Fisher Scientific Inc. (Version 10.2.0.57), for data analysis it was UniQuant Quant`X ED 6.25 by Thermo Fisher Scientific Inc. and Spectrum Viewer by Thermo Fisher Scientific Inc. (Version 10.2.0.57).

From each measurement, all the elements and their respective concentrations were acquired and can be found in Appendix C: Chemical Compositions Obtained from XRF Measurements. Two sets of data from both sides of each specimen were averaged and normalized; however, for further analysis and comparison, some of the elements were omitted. The minimum concentration

limit for an element to be taken into consideration was set to 100 ppm since many elements had concentrations of tens of ppm or smaller and were either varying greatly in each measurement or sometimes missing at all. Moreover, some of the results were dismissed due to elements spectra interferences. Examples of rejected elements and compounds are sulfates, phosphates, Potassium, Calcium, Arsenic, Thallium, and Thorium.

6.5.1. Energy Dispersive X-ray Spectroscopy

Energy Dispersive X-ray Spectroscopy is a non-destructive analytical method for chemical composition analysis based on the difference of the electromagnetic emission spectrum of each element. In order to get a characteristic spectrum, the X-ray beam is focused on the sample, which excites an electron in an inner shell creating an electron hole. An electron from a higher-energy shell fills the hole, and the energy difference is released in the form of an X-ray. The energy of the X-rays emitted is measured by an energy-dispersive spectrometer, which allows to assign energies to specific elements and, consequently, to define the elemental composition of the sample (Beckhoff et al., 2006; Grieken & Markowicz, 2002).

6.6. Specimens Preparation for SEM Analysis

SEM analysis requires specific preparation of samples. The first step of preparing specimens for SEM analysis was cutting each specimen into two pieces. The specimens were cut by Struers Accutom-100 precise cutter (Figure 36) with Aluminium oxide Cut-off Wheel 50A15 which is recommended for hard ferrous metals (HV 500 - 800 or lower). The cutting speed was set up to 0.015 - 0.030 mm/s, depending on the material, with a rotation speed of 2500 rpm. All specimens were cut in half (Figure 36) to get two pieces with approximate dimensions of 15 x 15 x 1 mm. One piece of each specimen was stored for additional analysis, and one piece was used for SEM analysis.

Figure 36

Pictures of specimens preparation for SEM analysis: a) Struers Accutom-100 precise cutter; b) cutting wheel and holder with a specimen; c) Struers CitoPress 30; and d) a half of a specimen with copper tape ready for casting.

a) b) c) d)

The next step after cutting was casting the sample into a bakelite matrix. As can be seen in Figure 36, the copper tape was used in order to hold a specimen and enable analysis in a cross-section direction. For the casting itself, the Struers CitoPress 30 (Figure 36) was used to apply PolyFast – black bakelite hot mounting resin with carbon filler. CitoPress PolyFast method was used as a setting with an applied temperature of 180 °C and pressure of 250 bar for 3.5 min. The cooling process was 1.5 min.

The next steps in preparation were grinding, polishing, and etching (final polishing) of the sample. These steps were performed using Struers Tegramin-25 grinding and polishing machine (Figure 37). Either four- or five-step process was chosen for nickel alloys and stainless steels, respectively, with intermediate steps of washing specimens with water using Struers Lavamin automatic-cleaning machine (Figure 37) and visual inspection with a microscope. In cases where visual inspection showed insufficient progress, the previous step was reapplied.

Figure 37

Pictures of specimens preparation for SEM analysis: a) a sample in casted bakelite matrix ready for grinding; b) Struers Tegramin-25 grinding and polishing machine; c) Struers Lavamin automatic-cleaning machine; and d) GT SONIC-S series ultrasonic cleaner.

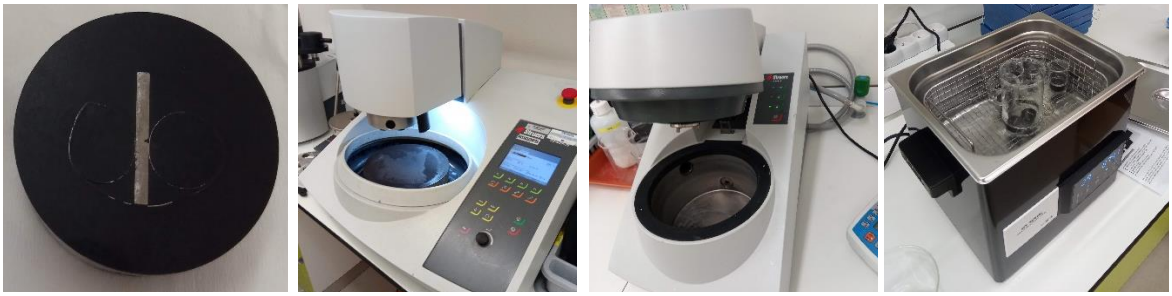

a) b) c) d)

Grinding and polishing steps for nickel alloys (Inconel 800HT, Inconel 600, Inconel 625, MoNiCr, and HN80MTY) are shown in Table 6, steps for stainless steels (316L and EUROFER 97) are shown in Table 7. Description of grinding and polishing materials is in the next subchapter.

Table 6

Grinding and polishing steps used for nickel alloys.

Step	Foil or Disc	Suspension	Speed [rpm]	Force per sample [N]	Time [min]
Grinding	SiC Foil 220	Water	300	40	3:00
Grinding	MD-Largo	DiaPro Allegro / Largo 9 µm	150	30	3:00
Polishing	MD-Dac	DiaPro Dac 3 µm	150	30	3:00
Polishing	MD-Chem	OP-S 0.04 µm	150	15	2:00

Table 7

Grinding and polishing steps used for stainless steels.

Step	Foil or Disc	Suspension	Speed [rpm]	Force per sample [N]	Time [min]
Grinding	SiC Foil 220	Water	300	20	2:00
Grinding	MD-Largo	DiaPro Allegro / Largo 9 µm	150	30	5:00
Polishing	MD-Dac	DiaPro Dac 3 µm	150	25	4:00
Polishing	MD-Nap	DiaPro Nap B 1 µm	150	20	1:30
Polishing	MD-Chem	OP-S 0.04 µm	150	10	1:00

Following the last polishing and water cleaning, all the specimens were cleaned in ethanol bath with ultrasonic waves and no heating for 15 minutes using the GT SONIC-S series ultrasonic cleaner (Figure 37). After the bath, specimens were carefully dried and put into a sample storing box with a low vacuum.

6.6.1. Description of Grinding and Polishing Materials

Consumable materials such as grinding foil, grinding and polishing discs, and grinding and polishing suspensions that were used for SEM specimens preparation and are listed in Table 6 and Table 7 are described in the following lines:

- SiC Foil 320 (220) is Silicon Carbide grinding paper with a grit of 320 (220) particles per square millimeter that is for wet grinding of materials with a hardness of HV 30 - 800.
- MD-Largo is a composite disc for fine grinding of materials with hardness higher than HV 40, using diamond suspension or spray.
- MD-Dac is a polishing cloth made of woven acetate for the polishing of all materials with the use of diamond suspensions.
- MD-Nap is a polishing cloth made of short synthetic naps for the polishing of all materials.
- MD-Chem is a polishing cloth made of porous neoprene for the final polishing of all materials.
- DiaPro Allegro/Largo 9 µm is a stable diamond suspension containing a mixture of 9 µm diamond crystals and a cooling lubricant for materialographic fine grinding on MD-Allegro and MD-Largo.
- DiaPro Dac 3 µm is a stable water-based diamond suspension containing a mixture of 3 µm diamond crystals and a cooling lubricant for materialographic polishing on MD-Dac and DP-Dac.
- DiaPro Nap B 1 µm is a stable water-based diamond suspension containing a mixture of 1 µm diamond crystals and cooling lubricant for materialographic polishing of hard materials (with hardness greater than 150 HV) on MD-Nap and DP-Nap.
- OP-S, 0.04 µm is standard colloidal silica suspension with 0.04 µm crystals for final polishing.

6.7.Scanning Electron Microscope Analysis

Specimens after the tests and non-tested specimens casted into a bakelite matrix were analyzed using a TESCAN LYRA3 scanning electron microscope (Figure 38). Information about specimen topography was obtained using secondary electrons (SE), and morphological data were acquired using back-scattered electrons (BSE) and energy-dispersive X-ray spectroscopy detectors.

For each specimen, a topographical picture and maps of chemical composition were taken; moreover, a line scan analysis was performed. Topographical pictures and chemical maps give an idea about the overall surface and structural changes; whereas, line scan analysis provides information about the changes at the surface layer and the depth of corrosion layer.

For data acquisition and data analysis the AZtecSteel, AZtecSynergy, and other AZtec software by the Oxford Instruments were used. Topographical pictures and chemical maps are presented in the following chapter, while line scan analysis was used to calculate the depth of the affected surface layer.

6.7.1. Scanning Electron Microscope

A scanning electron microscope (SEM) is a type of microscope that uses a focused beam of electrons to produces images of a sample's surface. The interaction between the sample and the electron beam produces different signals. Those signals can be detected and used to infer various information about the sample, such as its' surface topography or composition. These signals include secondary electrons (SE), back-scattered electrons (BSE), characteristic X-rays, absorbed current, and more.

Secondary electrons (SE) are used to collect images of the sample surface with a very high resolution (below 1 nm). This resolution is possible due to low energies (~ 50 eV) of SE, and the fact that the signal from SE is highly localized at the point of impact of the primary electron beam.

Back-scattered electrons (BSE) are often used in analytical SEM, along with the spectra made from the characteristic X-rays. This analysis method is based on the relation of the intensity of the BSE and the atomic number (Z) of the specimen. BSE themselves are beam electrons that are reflected from the sample by elastic scattering.

Characteristic X-rays can be measured by Energy-dispersive X-ray spectroscopy (more in chapter 6.5.1) or Wavelength-dispersive X-ray spectroscopy and are used to identify elements present in the sample (Chandler & Roberson, 2009; Joy, 2003; Khursheed, 2011).

Figure 38

TESCAN LYRA3 scanning electron microscope. Adapted from LYRA3. (n.d.).

7. Results

In the following pages, the results of corrosion tests itself, and all analyses performed are presented and discussed. Note that most of the data acquired during specimens' measurements and analyses are in full length in appendixes.

7.1. Structural Heterogeneities of Tested Materials

For most tested and untested specimens, the topographical and morphological analyses were done. Chemical composition maps are in Appendix F: Chemical Composition Maps and topological pictures are in Appendix G: Topographical Pictures Obtained by Scanning Electron Microscope.

From the chemical composition maps, topographical pictures, and other morphological analyses, some interesting findings have been made on specimens prior to corrosion test:

- EUROFER 97 specimens before any test show vanadium oxides precipitates;
- Incoloy 800HT specimens before any test show titanium clusters;
- MoNiCr specimens before any test show chromium oxides precipitates;
- HN80MTY specimens before any test show titanium carbides precipitates;
- MoNiCr sheet specimens before any test show cracks and material deformation, as can be seen in Figure 39.

Any additional findings on specimens after the tests, except those listed above, were aluminum-chromium oxides within MoNiCr specimens. Due to chromium oxides precipitates findings in untested MoNiCr specimens, it is probable that these $AlCrO_x$ precipitates found after the test are not corrosion-induced.

Figure 39

Picture of MoNiCr sheet specimens before the test from scanning electron microscope with 738x zoom (1.5 mm x 1.5 mm). An example of topographical analysis. More images are in Appendix G: Topographical Pictures Obtained by Scanning Electron Microscope.

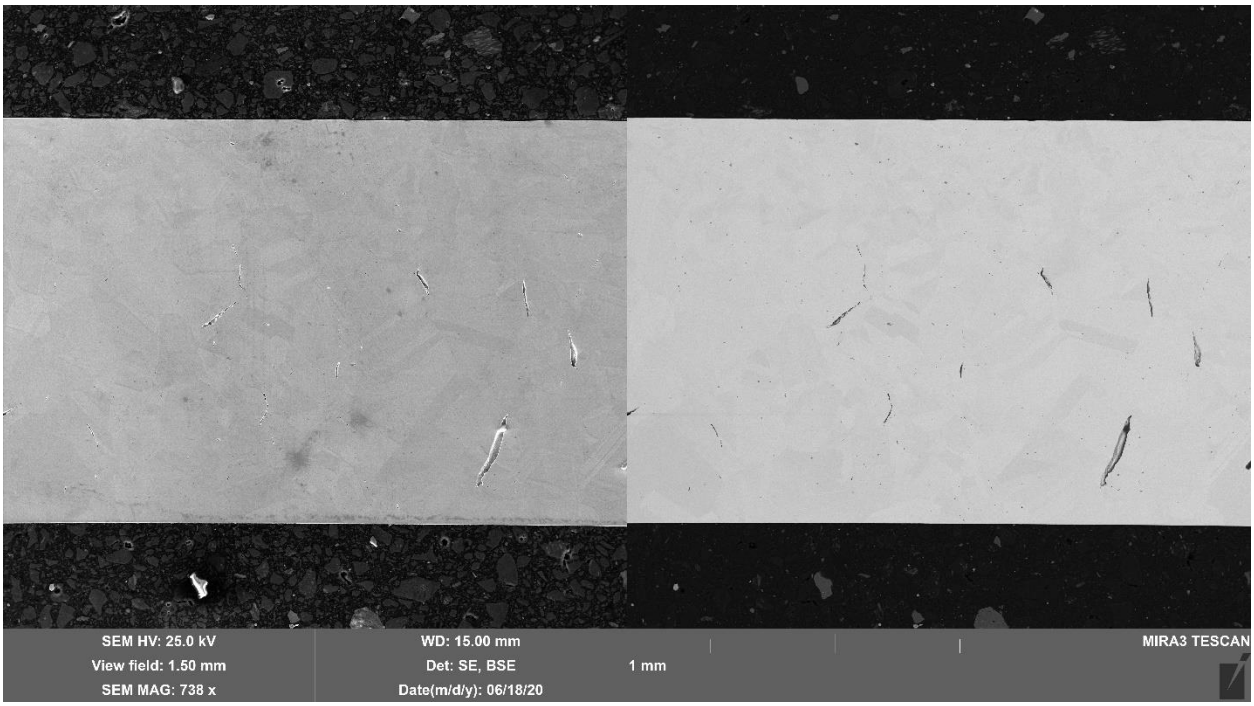

7.2. Visual Changes of Specimens' Surfaces

In the Appendix D: Specimens Overview Pictures, the overall pictures of specimens can be found. The pictures of EUROFER 97 specimens (Figure D2) show the most significant change in the color of all specimens into a very dark surface. Pictures of most of the other specimens show patterns of smaller or larger spots on the surface. As an example of these patters, there are pictures of HN80MTY specimens in Figure 40. Note that the 316L specimen after 720 h / 550 °C test has a long bruise across the one side.

Figure 40

Pictures of HN80MTY specimens: a) before 720 h / 550 °C test, b) after 720 h / 550 °C test, c) after 720 h / 700 °C test, and d) after 2160 h / 550 °C test. Pictures of other specimens are in Appendix D: Specimens Overview Pictures.

a) b) c) d)

Detailed pictures taken with a microscope are provided in Appendix E: Detailed Pictures of Specimens Taken with Microscope. Some of the Inconel 625 and nickel-based superalloy specimens after tests show a pattern of spots with a severely damaged center and almost undamaged surroundings within the lightly damaged surface. An example of these circles is on HN80MTY specimen after 2160 h / 550 °C test in Figure 41.

Figure 41

Pictures of HN80MTY specimens under the microscope with 4x zoom (1670 µm x 1670 µm): a) before 720 h / 550 °C test, b) after 720 h / 550 °C test, c) after 720 h / 700 °C test, and d) after 2160 h / 550 °C test. Pictures of other specimens are in Appendix E: Detailed Pictures of Specimens Taken with Microscope.

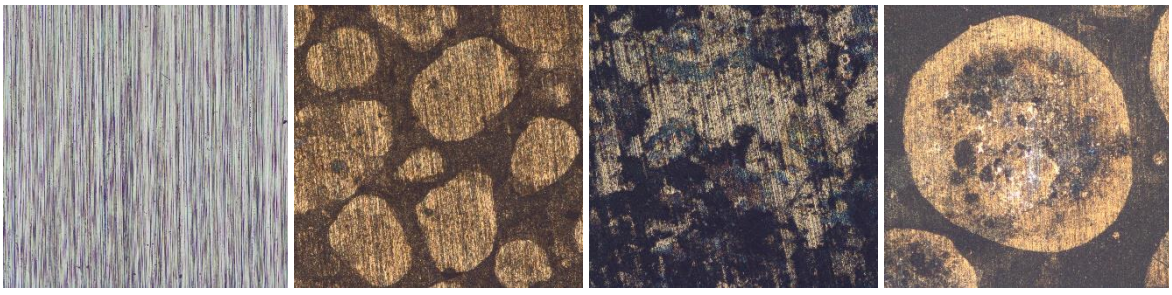

a) b) c) d)

7.3. Corrosion Mass Losses

The graph of corrosion mass losses is in Figure 42 with error bars of one σ standard error based on weight measurement precision of ± 0.001 g, the dimensions measurement precision of ± 0.02 mm, and specimen dimensions deviation from average. The following findings can be inferred from corrosion mass losses results:

- MoNiCr and HN80MTY are generally the best performing alloys out of tested according to corrosion mass losses;
- EUROFER 97 is by far the worst-performing alloy out of tested according to corrosion mass losses;
- for most of the alloys, the results after 2160 h / 550 °C test are better than after 720 h / 700 °C test; therefore, it is concluded that the higher temperature has more severe effect than longer exposure of lower temperature;
- MoNiCr sheet performed surprisingly bad after 720 h / 700 °C test and especially after 2160 h / 550 °C test, which could be due to either batch composition (batch T-18, different than MoNiCr specimens T-17) or by structural changes induced by rolling as mentioned in chapter 7.1.

Figure 42

Corrosion mass losses per area after 720 h / 550 °C test, after 720 h / 700 °C test, and after 2160 h / 550 °C test with error bars of 1 σ.

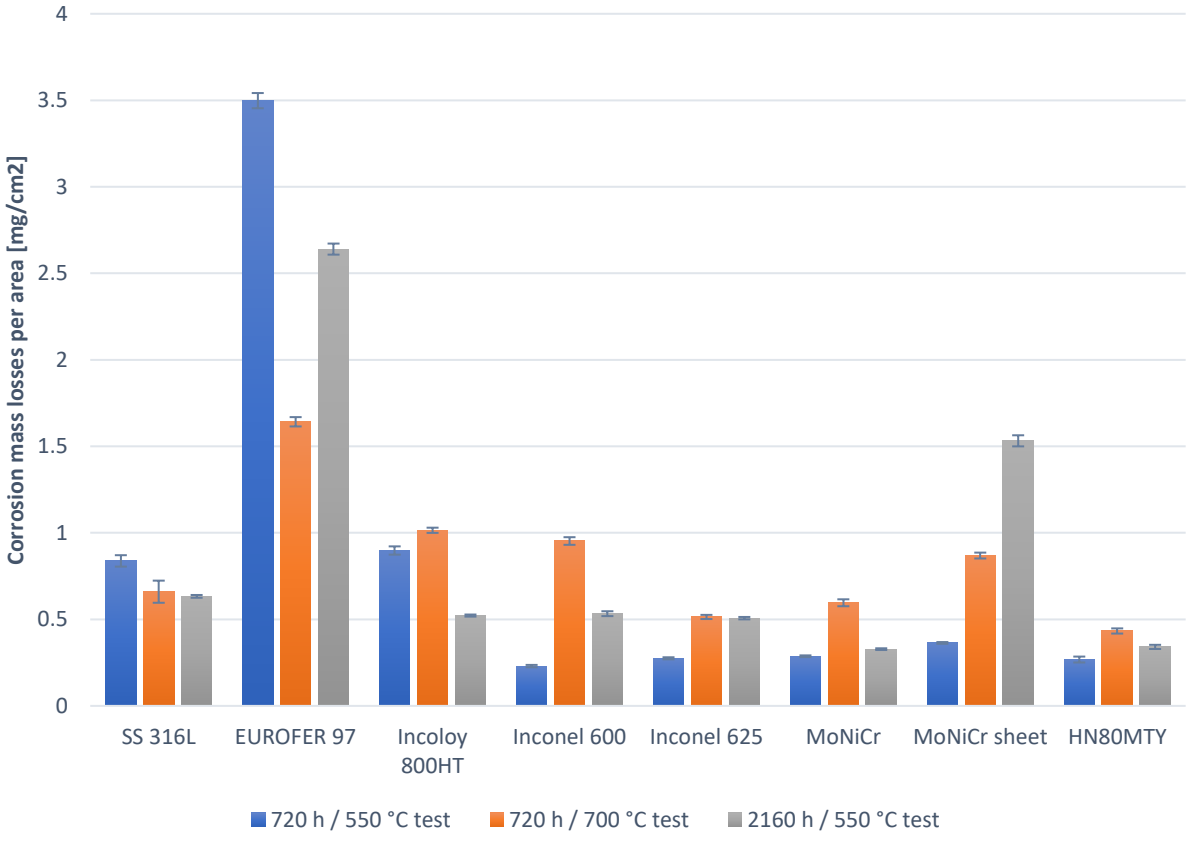

7.4. Chromium Depletion

Results of relative chromium depletion are presented in Figure 43 as calculated from XRF measurements data (Appendix C: Chemical Compositions Obtained from XRF Measurements). The chromium (and manganese) depletion is noticeable on chemical maps from SEM measurements, as seen in Figure 44 and Appendix F: Chemical Composition Maps. The following conclusions are made based on the results:

- There is no apparent convergent point of chromium concentration similar to all alloys and stainless steels visible from data obtained by the XRF method;
- there might be a trend of chromium depletion after 720 h / 700 °C test and after 2160 h / 550 °C test with most of the tested specimens relative decrease of more or less around 30 %;
- MoNiCr sheet results of chromium depletion after 2160 h / 550 °C test are surprisingly low and in contrary to its high corrosion mass losses.

Figure 43

The relative decrease of chromium quantity measured by XRF method after 720 h / 550 °C test, after 720 h / 700 °C test, and after 2160 h / 550 °C test with error bars of 1 σ.

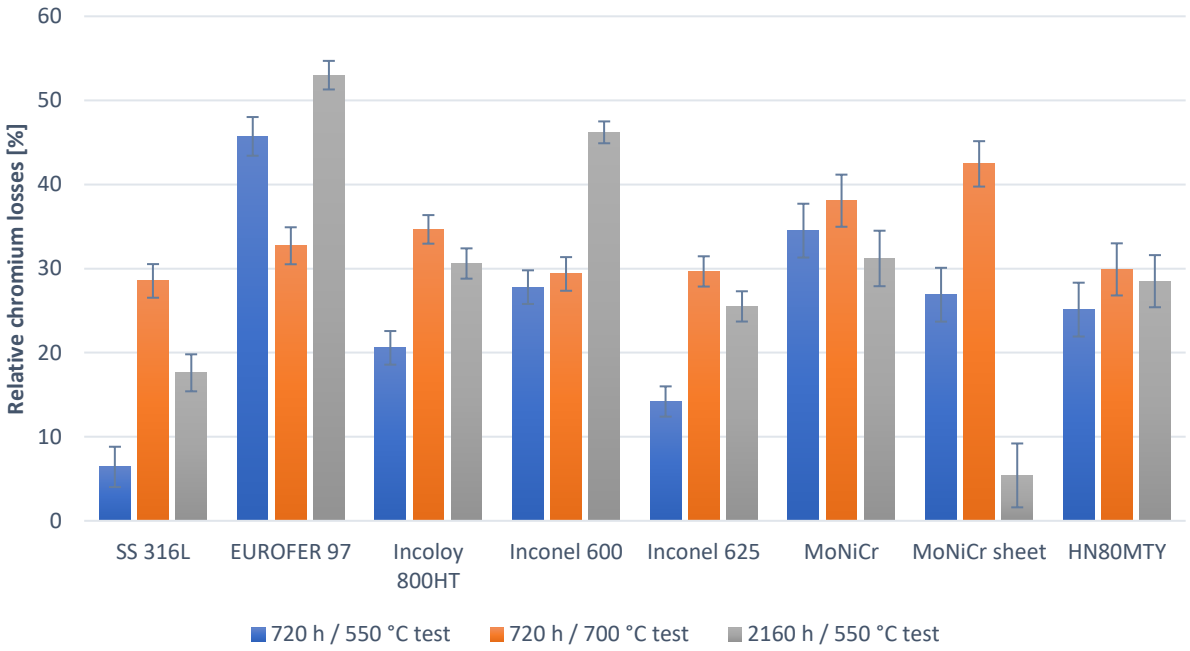

Figure 44

Chemical composition maps of Inconel 600 after 720 h / 700 °C test. Chemical maps of other specimens are in Appendix F: Chemical Composition Maps.

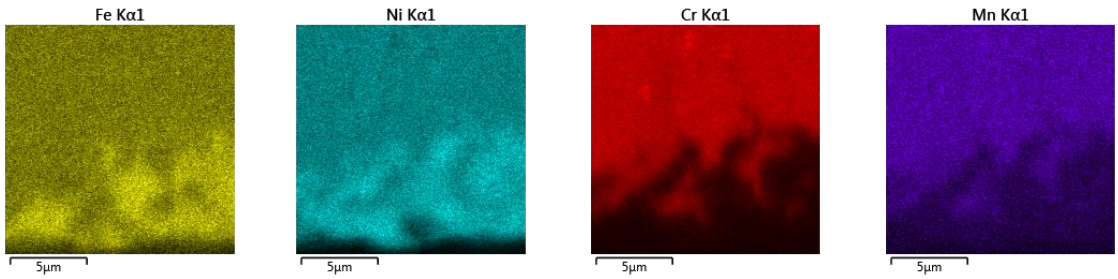

7.5.Depth of Corrosion Layer

As it is mentioned in chapter 5, there is usually no passivation oxide layer created in the molten salt environment; however, it is still possible to measure the depth of the corrosion layer. In this Master's thesis, the change of chromium concentration with depth was used to identify the depth of the corrosion layer.

The graph of the corrosion layer depths is in Figure 45. The best performing specimens are MoNiCr and MoNiCr sheet, followed by HN80MTY and Inconel 625. The results for the MoNiCr sheet after 720 h / 700 °C test are surprisingly better than after 720 h / 550 °C test and contrary to corrosion mass losses results.

Figure 45

Graph of corrosion layer depth after 720 h / 550 °C test, after 720 h / 700 °C test, and after 2160 h / 550 °C test with error bars of 1 σ.

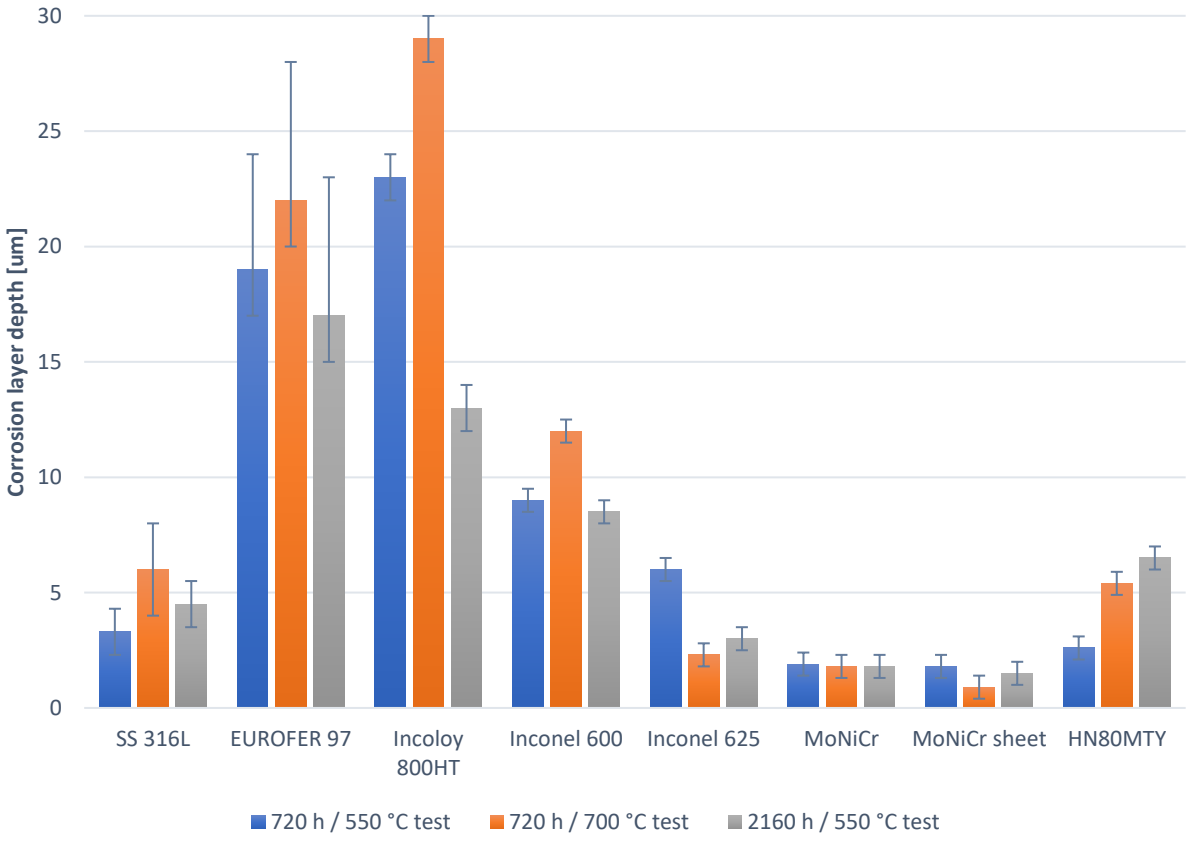

8. Conclusions

In the first two chapters, the introduction to current and future perspectives of nuclear power plants, introduction to molten salt reactors, their history, and an overview of currently proposed designs is given. Next, in chapters 3, 4, and 5, the basic information on molten salts, possible construction materials for MSRs, and corrosion mechanisms are presented. Corrosion experiments that were performed are described in chapter 6, with results given in chapter 7.

The main findings of corrosion experiments are the following:

- Increased temperature has more severe impacts than longer exposure to a lower temperature;
- stainless steels 316L and EUROFER 97, Incoloy 800HT, and both Inconels shows severe disturbance in a structure near the surface;
- stainless steel 316L specifically, but also EUROFER 97, Incoloy 800HT, and both Inconels are dominantly attacked by corrosion along the grain boundaries;
- bad results of stainless steel 316L after 720 h / 550 °C test might be caused by specimen anomaly (long bruise find, Figure D1)
- there are no new carbides or other precipitates found in any alloy after the tests;
- there are no correlations found or conclusions made based on chromium depletion measurements.

The final evaluation of tested alloys as concluded on all the results and measurements is as listed:

- MoNiCr and HN80MTY are the best performing alloys;
- stainless steel 316L performed well and could be considered for future research;
- Inconel 625 performance is decent and superior to Inconel 600; therefore, Inconel 625 might be considered for future research;
- EUROFER 97 and Incoloy 800HT performed poorly and are not recommended for any further research or application in molten salts;
- MoNiCr sheet specimens performed worse than expected, which could be explained by cracks within the material; therefore, further research is ongoing.

All the results will be used in research articles and reports for ongoing research projects. Moreover, outputs of this work will help the development of Energy Well design and choice of structural materials and coolant salts. However, note that performed corrosion tests have their limitations, such as no irradiation and no thermal gradient; therefore, any decision on which material will be used for Energy Well project or any other application cannot be made based only upon presented results. Further research in an environment with a neutron flux and tests in molten salt circulating loop with a thermal gradient need to be performed. Besides, the research of corrosion resistance of different structural materials within molten salts continues with the focus on corrosion resistance dependency on material preparation way, mainly additive manufacturing.

9. References

316/316L Stainless Steel. (n.d.). Penn Stainless Products. Retrieved November 15, 2019, from http://www.pennstainless.com/stainless-grades/300-series-stainless-steel/316l-stainless-steel/

Alloy 400 Tech Data. (n.d.). High Temp Metals. Retrieved November 25, 2019, from https://www.hightempmetals.com/techdata/hitempMonel400data.php

Alloy 800H/HT. (n.d.). Corrosion Materials. Retrieved November 25, 2019, from https://www.corrosionmaterials.com/documents/dataSheet/alloy800DataSheet.pdf

Anderson, M., Sridharan, K., Morgan, D., Peterson, P., Calderoni, P., Scheele, R., … Mcnamara, B. (2015). *Heat Transfer Salts for Nuclear Reactor Systems - Chemistry Control, Corrosion Mitigation, and Modeling*. doi: 10.2172/1169921

Andreades, C., Cisneros, A. T., Choi, J. K., Chong, A. Y. K., Fratoni, M., Hong, S., … Peterson, P. F. (2014, September). *Mark-1 PB-FHR Technical Description.* Berkeley, CA: University of California, Berkeley. Retrieved December 2, 2019, from http://fhr.nuc.berkeley.edu/wp-content/uploads/2014/10/14-002-PB-FHR_Design_Report_Final.pdf

Andreades, C., Cisneros, A. T., Choi, J. K., Chong, A. Y. K., Fratoni, M., Hong, S., … Zweibau, N. (2016). Design Summary of the Mark-I Pebble-Bed, Fluoride Salt–Cooled, High-Temperature Reactor Commercial Power Plant. *Nuclear Technology, 195*(3), 223–238. doi: 10.13182/nt16-2

Beckhoff, B., Kanngießer, B., Langhoff, N., Wedell, R., & Wolff, H. (2006). *Handbook of Practical X-Ray Fluorescence Analysis*. Berlin, Germany: Springer.

Bell, T. (2019, November 14). *Properties of Type 316 and 316L Stainless Steels.* The Balance. Retrieved November 15, 2019, from https://www.thebalance.com/type-316-and-316l-stainless-steel-2340262

Bettis, E. S., & Ergen, W. K. (1958). Aircraft Reactor Experiment. In *Fluid fuel reactors* (pp. 673–680). Boston, MA: Addison-Wesley Pub. Co. Available from: http://moltensalt.org/references/static/downloads/pdf/FFR_chap16.pdf

Brähler, G., Froschauer, K., & Welbers, P. (2008). *The PBMR Fuel Plant*. 4th Topical Meeting on High temperature Reactor Technology, Washington.

Britsch, K., Anderson, M., Brooks, P., & Sridharan, K. (2019). Natural circulation FLiBe loop overview. *International Journal of Heat and Mass Transfer, 134*, 970–983. doi: 10.1016/j.ijheatmasstransfer.2018.12.180

Cantor, S., Cooke, J. W., Dworkin, A. S., Robbins, G. D., Thoma, R. E., & Watson, G. M. (1968). *Physical Properties of Molten-Salt Reactor Fuel, Coolant, and Flush Salts.* (S. Cantor, Ed.). ORNL-TM-2316. Oak Ridge, TN: Oak Ridge National Laboratory.

Centrum výzkumu Řež. (n.d.). *Energy Well - produktový list.* Retrieved December 4, 2019, from https://www.ujv.cz/file/edee/2018/04/ew_pl_cz.pdf

Chandler, D. E., & Roberson, R. W. (2009). *Bioimaging: current concepts in light and electron microscopy*. Sudbury, MA: Jones and Bartlett Publishers. ISBN 9780763738747.

Cornwell, K. (1971). The thermal conductivity of molten salts. *Journal of Physics D: Applied Physics, 4*(3), 441–445. doi: 10.1088/0022-3727/4/3/313

Cul, G. D. D., Spencer, B. B., Forsberg, C. W., Collins, E. D., & Rickman, W. S. (2002). *TRISO-Coated Fuel Processing to Support High Temperature Gas-Cooled Reactors*. ORNL-TM-2002/156. Oak Ridge, TN: Oak Ridge National Laboratory. doi: 10.2172/814326

Devan, J. H. (1969). *Effect of alloying additions on corrosion behavior of nickel-molybdenum alloys in fused fluoride mixtures*. ORNL-TM-2021. Oak Ridge, TN: Oak Ridge National Laboratory. doi: 10.2172/4789147

Dolan, T. J. (Ed.). (2017). *Molten salt reactors and thorium energy*. Oxford, UK: Woodhead Publishing.

Duarte, J. P., Oliva, J. de J. R., & Melo, P. F. F. F. (2013). *Generation IV Nuclear Systems: State of the Art and Current Trends with Emphasis on Safety and Security Features.* IntechOpen, DOI: 10.5772/53140. Available from: https://www.intechopen.com/books/current-research-in-nuclear-reactor-technology-in-brazil-and-worldwide/generation-iv-nuclear-systems-state-of-the-art-and-current-trends-with-emphasis-on-safety-and-securi

Engineering the Future of Energy. (n.d.). Copenhagen Atomics. Retrieved January 7, 2020, from https://www.copenhagenatomics.com/

Flibe Energy, Inc. (n.d.). Flibe Energy, Inc. Retrieved November 29, 2019, from https://flibe-energy.com/

Forsberg, C. W. (2004). *Reactors with Molten Salts: Options and Missions*. Frederic Joliot & Otto Han Summer School on Nuclear Reactors, Physics, Fuels, and Systems, Cadarache, France. Available from: http://moltensalt.org/references/static/downloads/pdf/MoltenSaltOptions.pdf

Generations of nuclear reactors. (2018, November 22). Foro Nuclear. Retrieved November 14, 2019, from https://www.foronuclear.org/en/press-room/infographics/124340-generations-of-nuclear-reactors

Grieken, R. van, & Markowicz, A. (2002). *Handbook of X-ray spectrometry*. New York, NY: Marcel Dekker.

Hastelloy N alloy, Principle Features. (2017). Haynes International. Retrieved December 16, 2019, from http://haynesintl.com/docs/default-source/pdfs/new-alloy-brochures/corrosion-resistant-alloys/brochures/n-brochure.pdf?sfvrsn=18

Hastings, P. (2018). *Design Overview of the Kairos Power Fluoride Salt-Cooled, High Temperature Reactor (KP-NRC-1811-002, Project No. 99902069).* Washington, DC: US Nuclear Regulatory Commission.

Heuer, D., Merle-Lucotte, E., Allibert, M., Brovchenko, M., Ghetta, V., & Rubiolo, P. (2014). Towards the Thorium Fuel Cycle with Molten Salt Fast Reactors. *Annals of Nuclear Energy 64*, 421–429

Holcomb, D. E., & Cetiner, S. M. (2010). *An Overview of Liquid-Fluoride-Salt Heat Transport Systems.* Oak Ridge, Tennessee: Oak Ridge National Laboratory.

Ignatiev, V. V., & Surenkov, A. (2013). Alloys compatibility in molten salt fluorides: Kurchatov Institute related experience. *Journal of Nuclear Materials, 441*(1-3), 592–603. doi: 10.1016/j.jnucmat.2013.05.007

Ignatiev, V. V., Surenkov, A., Gnidoi, I., Fedulov, V., Uglov, V., Afonichkin, V., … Toropov, A. (2008). Compatibility of Selected Ni-Based Alloys in Molten Li,Na,Be/F Salts with PuF3 and Tellurium Additions. *Nuclear Technology, 164*(1), 130–142. doi: 10.13182/nt08-a4014

Ignatiev, V. V., Surenkov, A. I., Gnidoi, I. P., Uglov, V. S., & Konakov, S. A. (2016). Experimental Investigation of Tellurium Corrosion of Nickel-Molybdenum Alloys in Molten Lithium-, Beryllium-, and Uranium-Fluoride Salts. *Atomic Energy, 120*(6), 397–402. doi: 10.1007/s10512-016-0148-1

Incoloy 800 Advanced Nickel Alloy. (n.d.). Magellan Metals. Retrieved November 15, 2019, from https://www.magellanmetals.com/incoloy-800

Incoloy 800H/HT UNS N08810 UNS N08811. (n.d.). High Performance Alloys, Inc.. Retrieved November 25, 2019, from https://www.hpalloy.com/Alloys/descriptions/INCOLOY800H.aspx

Inconel 600, UNS N06600. (n.d.). Magellan Metals. Retrieved November 15, 2019, from https://www.magellanmetals.com/inconel-600

Inconel 600 Tech Data. (n.d.). High Temp Metals. Retrieved November 14, 2019, from https://www.hightempmetals.com/techdata/hitempInconel600data.php

Inconel 625 Tech Data. (n.d.). High Temp Metals. Retrieved November 14, 2019, from https://www.hightempmetals.com/techdata/hitempInconel625data.php

Inconel alloy 600. (n.d.). Special Metals. Retrieved November 14, 2019, from https://www.specialmetals.com/assets/smc/documents/alloys/inconel/inconel-alloy-600.pdf

Inconel alloy 625. (n.d.). Special Metals. Retrieved November 14, 2019, from https://www.specialmetals.com/assets/smc/documents/alloys/inconel/inconel-alloy-625.pdf

International Atomic Energy Agency's Advanced Reactors Information System. (2011). *Status report 70 - Pebble Bed Modular Reactor (PBMR)*. Retrieved March 16, 2020, from https://aris.iaea.org/pdf/pbmr.pdf

International Atomic Energy Agency's Advanced Reactors Information System. (2016a). *Status Report – Mark 1 Pebble-Bed Fluoride-Salt-Cooled High-Temperature Reactor*. Retrieved December 2, 2019, from https://aris.iaea.org/PDF/Mk1%20PB-FHR%20ARIS%20final.pdf

International Atomic Energy Agency's Advanced Reactors Information System. (2016b). *Status Report – IMSR-400*. Retrieved November 27, 2019, from https://aris.iaea.org/PDF/IMSR400.pdf

International Atomic Energy Agency's Advanced Reactors Information System. (2016c). *Status Report – LFTR*. Retrieved November 27, 2019, from https://aris.iaea.org/PDF/LFTR.pdf

International Atomic Energy Agency's Advanced Reactors Information System. (2016d). *Status Report – MSR-FUJI*. Retrieved December 4, 2019, from https://aris.iaea.org/PDF/MSR-FUJI.pdf

International Atomic Energy Agency's Advanced Reactors Information System. (2016e). *Status Report – MSTW*. Retrieved December 4, 2019, from https://aris.iaea.org/PDF/MSTW.pdf

International Atomic Energy Agency's Advanced Reactors Information System. (2016f). *Status Report – ThorCon*. Retrieved January 7, 2020, from https://aris.iaea.org/PDF/ARISThorCon9.pdf

International Atomic Energy Agency's Advanced Reactors Information System. (2018). *Advances in Small Modular Reactor Technology Developments, A* Supplement to: IAEA Advanced Reactors Information System (Aris). Retrieved February 5, 2020, from https://aris.iaea.org/Publications/SMR-Book_2018.pdf

International Atomic Energy Agency's Power Reactor Information System - IAEA's PRIS. (n.d.). Retrieved November 14, 2019, from https://pris.iaea.org/PRIS/home.aspx

The Nuclear Energy Agency. (n.d.). *JEFF Nuclear Data Library*. Retrieved June 10, 2020, from https://www.oecd-nea.org/dbdata/jeff/

Joy, D. C. (2003). Introduction to the Scanning Electron Microscope. *Microscopy and Microanalysis, 9* (S02), 1556–1557. doi: 10.1017/s1431927603447788

Kelmers, A. D., Baes, C. F., Bettis, E. S., Brynestad, J., Cantor, S., Engel, J. R., … Meyer, A. S. (1976). *Evaluation of alternate secondary (and tertiary) coolants for the molten-salt breeder reactor*. doi: 10.2172/7351862

Khanna, A. S. (2004). *Introduction to high temperature oxidation and corrosion*. Materials Park, OH: ASM International.

Khursheed, A. (2011). *Scanning electron microscope optics and spectrometers*. New Jersey, NJ: World Scientific.

Koger, J.W. (1972a). *Effect of FeF2 Addition on Mass Transfer in a Hastelloy N - LiF-BeF2-UF4 Thermal Convection Loop*. ORNL-TM-4188. Oak Ridge, TN: Oak Ridge National Laboratory.

Koger, J. W. (1972b). *Evaluation of Hastelloy N alloys after nine years exposure to both a molten fluoride salt and air at temperatures from 700 to 560 °C*. ORNL-TM-4189. Oak Ridge, TN: Oak Ridge National Laboratory. doi: 10.2172/4468052

Kolektiv ÚJV Řež a.s. a CVŘ. (2018). *Energy Well - Studna energie*. Technologie pro elektrárny a teplárny na tuhá paliva. Medlov 5/2018. Retrieved December 4, 2019, from https://www.tespo-eng.cz/images/zpravy/24-21-rocnik-konference-technologie-pro-elektrarny-a-teplarny-na-tuha-paliva-minulosti/Medlov_FHR_vl.pdf

Koukolikova, M., Slama, P., Dlouhy, J., Cerny, J., & Marecek, M. (2018). Cold/Hot Deformation Induced Recrystallization of Nickel-Based Superalloys for Molten Salt Reactors. *Metals, 8*(7), 477. doi: 10.3390/met8070477

Lantelme, F., & Groult, H. (2013). *Molten salts chemistry: from lab to applications*. Amsterdam, Netherlands: Elsevier.

Losa, E., Harutyunyan, D., Ruščák, M., Mazzini, G., Krivda, M., Pilát, J., … Dostál P. (2017). *Návrh aktivní zóny a studie proveditelnosti malého modulárního reaktoru chlazeného roztavenou solí*. Internal report of Research Centre Řež: unpublished.

Macpherson, H. G. (1985). The Molten Salt Reactor Adventure. *Nuclear Science and Engineering, 90*(4), 374–380. doi: 10.13182/nse90-374

Mathieu, L., Heuer, D., Brissot, D., Le Brun, C., Liatard, E., Loiseaux, J.M., … Walle, E. (2006). The Thorium Molten Salt Reactor: Moving on from the MSBR. *Prog. in Nucl. En., vol 48*, pp. 664-679

Mathieu, L., Heuer, D., Merle-Lucotte, E., Brissot, R., Le Brun, C., Lecarpentier, D., … Nuttin, A. (2009). Possible Configurations for the TMSR and advantages of the Fast Non Moderated Version. *Nuclear Science and Engineering 161*, p. 78–89

Mergia, K., & Boukos, N. (2008). Structural, thermal, electrical and magnetic properties of Eurofer 97 steel. *Journal of Nuclear Materials, 373*(1-3), 1–8. doi: 10.1016/j.jnucmat.2007.03.267

Misra, A. K., & Whittenberger, J. D. (1987). *Fluoride Salts and Container Materials for Thermal Energy Storage Applications in the Temperature Range 973 – 1400 K*. 22nd Intersociety Energy Conversion Engineering Conference. doi: 10.2514/6.1987-9226

Moltex Energy. (2018). *An Introduction to the Moltex Energy Technology Portfolio*. Retrieved January 8, 2020, from https://www.moltexenergy.com/learnmore/An_Introduction_Moltex_Energy_Technology_Portfolio.pdf

Moltex Energy. (2020). Moltex Energy. Retrieved January 8, 2020, from https://www.moltexenergy.com/

Monel 400 - UNS N04400 Advanced Nickel-Copper Alloy. (n.d.). Magellan Metals. Retrieved November 25, 2019, from https://www.magellanmetals.com/monel-400

Monel alloy 400. (n.d.). Special Metals. Retrieved November 25, 2019, from https://www.specialmetals.com/assets/smc/documents/alloys/monel/monel-alloy-400.pdf

Monel Alloy 400 Nickel Alloy. (n.d.). Matmatch. Retrieved November 25, 2019, from https://matmatch.com/materials/come056?utm_term=&utm_medium=ppc&utm_campaign=[SD]+Materials+Suppliers+4&utm_source=adwords&hsa_grp=58081510957&hsa_cam=1524267343&hsa_src=g&hsa_net=adwords&hsa_tgt=dsa-459478932863&hsa_ad=289355519940&hsa_mt=b&hsa_kw=&hsa_ver=3&hsa_acc=2813184419&gclid=EAIaIQobChMIp9Oi8pKF5gIVwprVCh2SWQFCEAAYAyAAEgIzx_D_BwE

MSFR - Laboratory of Subatomic Physics & Cosmology. (2019). IN2P3 (CNRS), Université Grenoble Alpes. Retrieved December 6, 2019, from http://lpsc.in2p3.fr/index.php/en/106-groupes-de-physique/msfr

Natural Circulation Flibe Loop. (n.d.). College of Engineering - University of Wisconsin - Madison. Retrieved March 20, 2020, from https://anderson.ep.wisc.edu/AndersonWebsite/F3.html

Novy, Z., Džugan, J., Motycka, P., Podany, P., & Dlouhy, J. (2011). On Formability of MoNiCr Alloy. *Advanced Materials Research, 295-297*, 1731–1737. doi: 10.4028/www.scientific.net/amr.295-297.1731

Novy, Z., Džugan, J., Wangyao, P., & Kraus, L. (2015). Development of Forming Processes for MoNiCr Alloy. *Key Engineering Materials, 658*, 3–7. doi: 10.4028/www.scientific.net/kem.658.3

NRG irradiates steel alloy for use in ITER. (2019, January 30). world nuclear news. Retrieved November 14, 2019, from http://world-nuclear-news.org/Articles/NRG-irradiates-steel-alloy-for-use-in-ITER

Petroski, R. C. (2008). *Design of a 2400 MW Liquid-Salt Cooled Flexible Conversion Ratio Reactor*. Massachusetts Institute of Technology, Cambridge.

Pioro, I. L. (Ed.). (2016). *Handbook of generation Iv nuclear reactors*. Amsterdam, Netherlands: Elsevier. doi https://doi.org/10.1016/C2014-0-01699-1

Podany, P., Novy, Z., & Dlouhy, J. (n.d.). *Recrystallization Behaviour of Nickel Based Superalloy*. COMTES FHT. Retrieved from https://www.comtesfht.cz/media/document/recrystallization-behavior-of-nickel-based-superalloy.pdf

Powering up our world. (n.d.). ThorCon. Retrieved February 5, 2020, from http://thorconpower.com/

Premium Grade Inconel 625 Nickel Alloy. (n.d.). Magellan Metals. Retrieved November 15, 2019, from https://www.magellanmetals.com/inconel-625

Program on Technology Innovation: Technology Assessment of a Molten Salt Reactor Design: The Liquid-Fluoride Thorium Reactor (LFTR). (2015). EPRI, Palo Alto, CA: 2015. 3002005460.

Rieth, M., Schirra, M., Falkenstein, A., Graf, P., Heger, S., Kempe, H., … Zimmermann, H. (2003). *EUROFER 97 Tensile, Charpy, Creep and Structural tests*. Karlsruhe, Germany: Institut für Materialforschung. Available from https://publikationen.bibliothek.kit.edu/270055720/3814432

Robertson, R. C. (1965). *MSRE design and operations report, Part I: Description of reactor design*. ORNL-TM-728. Oak Ridge, TN: Oak Ridge National Laboratory. Available from http://moltensalt.org/references/static/downloads/pdf/ORNL-TM-0728.pdf

Rosenthal, M. W., Briggs, R. B., & Kasten, P. R. (1969). *Molten-salt reactor program: Semiannual progress report for period ending February 28, 1969*. ORNL-4396. Oak Ridge, TN: Oak Ridge National Laboratory. Available from http://moltensalt.org/references/static/downloads/pdf/ORNL-4396.pdf

Rubbia, C. (2010), New Energies for the Future of Mankind. *Nuclear Disarmament, Non-Proliferation and Development.* Vatican City, Vatican City: Pontifical Academy of Sciences. Available from: http://www.pas.va/content/dam/accademia/pdf/sv115/sv115-rubbia.pdf

Ruscak, M. (2019). *Energy Well - Conceptual Design of a Molten Salt Cooled Small Modular Reactor.* SMR 2019, Prague. Retrieved December 4, 2019, from http://malereaktory.cz/en/

Ruscak, M. (2020). *Energy Well project of UJV Group.* SMR 2020, Prague. Retrieved March 6, 2020, from http://malereaktory.cz/en/

Schiffer, H. W. (2016). *World Energy Resources.* The World Energy Council. Retrieved from https://www.worldenergy.org/assets/images/imported/2016/10/World-Energy-Resources-Full-report-2016.10.03.pdf

Seaborg Technologies. (n.d.). Seaborg Technologies. Retrieved December 4, 2019, from https://www.seaborg.co/

Sellers, R. S. (2012). *Impact of Reduction-Oxidation Agents on the High Temperature Corrosion of Materials in LiF-NaF-KF*. Madison, WI: University of Wisconsin-Madison. Available from http://rstevesellers.com/lit/Thesis_RS_Sellers_FINAL_small.pdf

Serp, J., Allibert, M., Beneš, O., Delpech, S., Feynberg, O., Ghetta, V., … Zhimin, D. (2014). The molten salt reactor (MSR) in generation IV: Overview and perspectives. *Progress in Nuclear Energy, 77*, 308–319. doi: 10.1016/j.pnucene.2014.02.014

Shanghai Institute of Applied Physics. (n.d.). Shanghai Institute of Applied Physics Chinese Academy Of Sciences. Retrieved February 4, 2020, from http://english.sinap.cas.cn/

Small Nuclear Power Reactors. (2019, December). World Nuclear Association. Retrieved February 5, 2020, from https://www.world-nuclear.org/information-library/nuclear-fuel-cycle/nuclear-power-reactors/small-nuclear-power-reactors.aspx

Sohal, M. S., Ebner, M. A., Sabharwall, P., & Sharpe, P. (2013). *Engineering Database of Liquid Salt Thermophysical and Thermochemical Properties.* Idaho Falls, ID: Idaho National Laboratory. Available from https://inldigitallibrary.inl.gov/sites/STI/STI/5698704.pdf

Sorensen, K. (2018). *Reimagining Nuclear Energy with Molten-Salt Technology - Flibe Energy*. Thorium Energy Conference 2018, Brussels. Retrieved March 21, 2020, from http://www.thoriumenergyworld.com/uploads/6/9/8/7/69878937/flibe_energy_thec18_slides.pdf

Sorensen, K. (n.d.a). Two-Fluid MSBR Core Designs. *Energy from Thorium* Retrieved March 21, 2020, from https://energyfromthorium.com/history/msbr-design-two-fluid-core/

Sorensen, K. (n.d.b). One-Fluid MSBR Core Designs. *Energy from Thorium* Retrieved February 21, 2020, from https://energyfromthorium.com/history/msbr-design-one-fluid-core/

Specification Sheet: Alloy 800H/800HT. (n.d.). Sandmeyer Steel Company. Retrieved November 25, 2019, from https://www.sandmeyersteel.com/images/Alloy800H-800HT-APR2013.pdf

Stainless 316, 316L, 317, 317L. (n.d.). UPMet.com. Retrieved November 25, 2019, from https://www.upmet.com/sites/default/files/datasheets/316-316l.pdf

Stefaniak, A. B. (2011). Comment on Strupp Papers on Beryllium Metal Toxicity. *The Annals of Occupational Hygiene, 55*(5), 556–557. doi: 10.1093/annhyg/mer030

Strupp, C. (2011a). Beryllium Metal I. Experimental Results on Acute Oral Toxicity, Local Skin and Eye Effects, and Genotoxicity. *The Annals of Occupational Hygiene, 55*(1), 30–42. doi: 10.1093/annhyg/meq071

Strupp, C. (2011b). Beryllium Metal II. A Review of the Available Toxicity Data. *The Annals of Occupational Hygiene, 55*(1), 43–56. doi: 10.1093/annhyg/meq073

Super Alloy Hastelloy N (UNS N10003). (2013, June 11). AZo Materials. Retrieved December 16, 2019, from https://www.azom.com/article.aspx?ArticleID=7832

Super Alloy Incoloy 800HT (UNS N08811). (2012, November 15). AZo Materials. Retrieved November 25, 2019, from https://www.azom.com/article.aspx?ArticleID=7742

Terrestrial Energy Inc. (n.d.). Terrestrial Energy Inc. Retrieved November 27, 2019, from https://www.terrestrialenergy.com/

LYRA3. (n.d.). TESCAN Korea. Retrieved July 11, 2020, from http://www.tescan.co.kr/product/em/em04

The Future of Nuclear Power. (n.d.). Kairos Power. Retrieved November 25, 2019, from https://kairospower.com/

The Generation IV International Forum. (n.d.). Retrieved June 8, 2020, from https://www.gen-4.org/gif/

The Mark 1 Pebble-Bed Fluoride High Temperature Reactor. (n.d.). The University of California Berkeley. Retrieved November 29, 2019, from https://fhr.nuc.berkeley.edu/

The ThorCon Team. (2018). *ThorCon: The Do-able Molten Salt Reactor* (1.24 ed.). Stevenson, WA: ThorCon USA Inc. Available from http://thorconpower.com/docs/domsr20180119.pdf

Thorium Molten Salt Reactor (TMSR), China. (n.d.). Thorium Energy World. Retrieved February 1, 2020, from http://www.thoriumenergyworld.com/china.html#

Uhlíř, J. (2007). Chemistry and technology of Molten Salt Reactors - history and perspectives. *Journal of Nuclear Materials*, *360*(1), 6–11. doi: https://doi.org/10.1016/j.jnucmat.2006.08.008

Vergnes, J., Lecarpentier, D., Garzenne, C., Mouney, H., Ritter, G., Valade, M., …Loiseaux, J.M. (2000). *The AMSTER concept (Actinide Molten Salt TransmutER).* Physor 2000 Conference, Pittsburgh, PA, USA. Available from https://www.oecd-nea.org/pt/docs/iem/madrid00/Proceedings/Paper17.pdf

Vlach, J. (2019). *Technology of Molten Salt Reactor and testing corrosion-resistant materials in fluoride salt FLiBe*. Prague, Czech Republic: CTU in Prague.

Wagman, D. D., Evand, W. H., Parker, V. B., Schumm, R. H., & Nuttall, R. L. (1981). *Selected Values of Chemical Thermodynamic Properties Compounds of Uranium, Protactinium, Thorium, Actinium, and the Alkali Metals*. Washington, DC: National Bureau of Standards. Available from https://nvlpubs.nist.gov/nistpubs/Legacy/TN/nbstechnicalnote270-8.pdf

Wang, M., Nai, Q., Qiu, J., Wang, B., Yang, C., Su, C., & Liang, J. (2018). Development of GH3535 Alloy for Thorium Molten Salt Reactor. *Springer Proceedings in Energy Advances in Energy and Environmental Materials*, 137–147. doi: 10.1007/978-981-13-0158-2_16

Wang, Y., Liu, H., Yu, G., Hou, J., & Zeng, C. (2015). Electrochemical study of the corrosion of a Ni-based alloy GH3535 in molten (Li,Na,K)F at 700°C. *Journal of Fluorine Chemistry, 178*, 14–22. doi: 10.1016/j.jfluchem.2015.06.014

Wang, Y., Zhang, S., Zeng, C., & Li, W. (2018). Weld corrosion of GH3535 in molten (Li,Na,K)F. *International Journal of Electrochemical Science, 13*, 2577–2584. doi: 10.20964/2018.03.65

Williams, D. F. (2006a). Assessment of Candidate Molten Salt Coolants for the Advanced High Temperature Reactor (AHTR). ORNL/TM-2006/12 doi: 10.2172/885975

Williams, D. F. (2006b). Assessment of Candidate Molten Salt Coolants for the NGNP/NHI Heat-Transfer Loop. ORNL/TM-2006/69 doi: 10.2172/1360677

Xu, H. (2017, January). S*tatus and Perspective of TMSR in China*, PSI, Switzerland. Retrieved January 24, 2020, from https://www.gen-4.org/gif/upload/docs/application/pdf/2017-05/03_hongjie_xu_china.pdf

Yvon, P. (Ed.). (2017). *Structural materials for generation IV nuclear reactors.* Duxford, the United Kingdom: Woodhead Publishing. doi: https://doi.org/10.1016/C2014-0-03589-7

Zou, Y. (2019, July). *Research Progress of TMSR design*, SAMOFAR Final Meeting, Delft, Netherlands. Retrieved January 23, 2020, from http://samofar.eu/wp-content/uploads/2019/07/2019-TMSR-SAMOFAR%E2%80%94%E2%80%94Yang-ZOU-PDF-version-1.pdf

10. The List of Appendixes